Physiological Mechanisms Behind High Photosynthetic Capacity Ludovico Caracciolo 2024

Physiological Mechanisms Behind High Photosynthetic Capacity

Ludovico Caracciolo

Propositions

1. Decreasing the functional antenna size of photosystem II increases the F_v/F_m parameter.
   (this thesis)

2. Variation in chloroplast size plays a role in photosynthetic adaptation.
   (this thesis)

3. Sci-hub is not the solution to overcome limited access to information, but an illegal step in the right direction.

4. The significance of results obtained from an instrument depends on the knowledge of the experimentalist.

5. The cheese slicer is the most versatile tool in the kitchen.

6. Changes in dietary habits have a bigger impact on food security than improvement in crop yield.

Propositions belonging to the thesis, entitled

Physiological Mechanisms Behind High Photosynthetic Capacity

Ludovico Caracciolo
Wageningen, 12 November 2024

Physiological Mechanisms Behind High Photosynthetic Capacity

Ludovico Caracciolo

Thesis committee

Promotor:
Prof. Dr. Herbert van Amerongen
Laboratory of Biophysics
Wageningen University & Research

Co-promotor:
Dr. Jeremy Harbinson
Associate Professor, Laboratory of Biophysics
Wageningen University & Research

Other members:
Prof. Dr. Ute Armbruster, Heinrich-Heine-University Düsseldorf, Düsseldorf, Germany
Prof. Dr. Tomas Morosinotto, Università di Padova, Padova, Italy
Prof. Dr. Alexander V. Ruban, Queen Mary University of London, London, UK
Prof. Dr. Ir. Paul C. Struik, Wageningen University & Research, Wageningen, The Netherlands

This research was conducted under the auspices of
the Graduate School of Experimental Plant Sciences

Physiological Mechanisms Behind High Photosynthetic Capacity

Ludovico Caracciolo

Thesis
submitted in fulfilment of the requirements for the degree of doctor
at Wageningen University
by the authority of the Rector Magnificus
Prof. Dr. Carolien Kroeze,
in the presence of the
Thesis Committee appointed by the Academic Board
to be defended in public
on Tuesday 12 November 2024
at 15:30 in the Omnia Auditorium.

Ludovico Caracciolo
Physiological Mechanisms Behind High Photosynthetic Capacity
153 pages

PhD thesis, Wageningen University, Wageningen, The Netherlands (2024)
With references, with summary in English and Dutch

DOI: 10.18174/674973

Contents

List of abbreviations

σ_f(PSII): relative functional antenna size of PSII
σ(PSII): PSII optical cross-section
Φ_{CS}(PSII): PSII maximum quantum yield for charge separation
AC: Alternated Current
CCR: Constant Current Regulation
DC: Direct Current
DCMU: 3-(3,4-dichloropheny1)-1,1-dimethylurea
ETC: Electron Transport Chain
FFP: Fast Fluorescence Protocol
FI: Fluorescence Induction
F_o: Minimum fluorescence intensity in condition of open-reaction centers
F_j: Fluorescence intensity of the fluorescence at step J of a fluorescence induction
F_i: Fluorescence intensity of the fluorescence at step I of a fluorescence induction
F_m: Maximum fluorescence intensity of a fluorescence induction, condition of closed reaction center
F_s: Any fluorescence intensity measured between the F_o and F_m step
F_v: Difference in fluorescence intensity between the points F_m and F_o (F_m-F_o)
F_{vj}: Difference in fluorescence intensity between the points F_j and F_o (F_{vj}=F_j-F_o)
I/O: Input/output
IRF: Instrument Response Function
LDR: Light Dependent Resistor
LED: Light Emitting Diode
MCU: Microcontroller Unit
NPQ: Non-Photochemical Quenching
O, J, I and M: different stages of a fluorescence induction
PPFD: Photosynthetic Photon Flux Density

PSI: Photosystem 1
PSII: Photosystem 2
PWM: Pulse Width Modulation
RC: Reaction Center
VCCS: Voltage Controlled Current Source

Chapter 1

General Introduction

1.1 Preamble

Oxygenic photosynthesis, hereafter referred to as photosynthesis, is the metabolic process that uses light energy to convert inorganic matter, such as CO_2 or NH_3, into energy-rich organic matter as sugars and amino acids. Since photosynthesis provides all the required molecules for biomass accumulation, it is expected that improving the rate of photosynthesis of crops may lead to improved yield of biomass production [1]. The maximum rate of photosynthesis is referred to as photosynthetic capacity and it is expressed as molecules of CO_2 fixated per time per unit area of photosynthetic material (µmol m^{-2} s^{-1}) [2]. Despite the limited genetic variability of the enzymes involved in the transduction of light energy into energy-rich molecules [3, 4], species or ecotypes (i.e. genetically distinct geographic varieties) grown under the same conditions can show a wide variability in their photosynthetic capacity (see Faralli & Lawson [5] and references therein). Finding the physiological mechanisms and the genes responsible for increased photosynthetic capacity could be the keystone to durably improve agricultural yield.

The work reported in this thesis was part of a broader multidisciplinary effort aiming to find the physiological causes and involved genes behind the high photosynthetic capacity observed in some Brassicaceae when grown under high light. A high photosynthetic capacity at saturating irradiance reflects a higher light-use efficiency (LUE), intended as the ratio of the rates of photosynthesis measured at a certain irradiance. These Brassicaceae were selected because they are phylogenetically close to the model plant *Arabidopsis thaliana* [6], do not have any carbon concentration metabolism (i.e. C3 plants) and when grown at high light (up to 1800 µmol m^{-2} s^{-1}) they exhibit photosynthetic capacity almost double than a "normal C3 plant" (respectively, 50 and 30 µmol m^{-2} s^{-1} of CO_2 fixation). The works detailed in this thesis aimed to find possible physiological mechanisms related to the light reactions that could explain mechanistically how some of the Brassicaceae maintain a high photosynthetic capacity at high irradiance. The Brassicaceae studied were *Hirschfeldia incana*, a species displaying high light-use efficiency [7]; *Brassica nigra* and *Brassica rapa*, two crops known for their fast growth and economical importance [8, 9]; and *Arabidopsis thaliana* a model organism in plant science, with lower light-use efficiency compared to the above mentioned species [10]. The possible physiological adaptation that could explain the higher light-use efficiency of some Brassicaceae were studied by the mean of different spectroscopic techniques (e.g. fluorescence lifetime, fluorescence induction, multiphoton microscopy). Additionally, two novel methodologies useful for the field of photosynthesis research were developed, such as a light controller to generate user defined irradiance patterns and a flexible modulated

spectrophotometer to measure absorbance and fluorescence changes in illuminated samples.

1.2 Photosynthetic organization and function

1.2.1 The chloroplasts

In higher plants, photosynthesis takes place mostly in leaves within specialized organelles, the chloroplasts. Chloroplasts are composed of a double-layer membrane, the chloroplast envelope, and an additional inner membrane, the thylakoid membrane. The thylakoid membrane is a complex lamellar system, which separates the inner lumen from the outer stroma, and contains a large part of the photosynthetic machinery. A characteristic of the thylakoid membrane is its ability to stack to form the so-called grana thylakoids. The grana are interconnected to each other by a continuous and unstacked network of thylakoid membranes referred to as stroma lamellae [11]. The thylakoid membrane has remarkable structural flexibility and can change the number of grana or the number of granum lamellae per grana in response to different factors, in particular light intensity [12, 13].

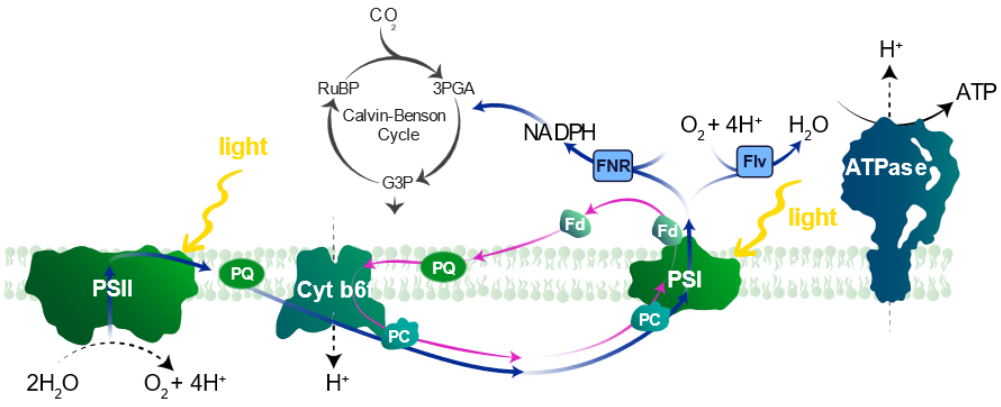

Figure 1.1. *Schematic representation of the photochemical reactions taking place in and around the thylakoid membrane. PSII, photosystem II; PQ, plastoquinone pool; Cyt b_6f, cytochrome b_6f; PC, plastocyanin; PSI, photosystem I; Fd, ferredoxin; Flv, flavodiiron protein; FNR, ferredoxin NADP oxidoreductase; ATPase, ATP synthase. Solid black arrows indicate chemical reactions. Solid blue arrow, Linear Electron Flow (LEF). Solid pink arrow, Cyclic Electron Flow (CEF). Credits: Daria Chrobok for the Jan Ingenhousz Institute.*

1.2.2 The photochemical and electrochemical reactions

At the level of the thylakoid membrane takes place an ensemble of chemical reactions that use light energy to (re)generate energetically rich molecules such as adenosine triphosphate (ATP) and nicotinamide-adenine-dinucleotide phosphate (NADPH). The formed energetic molecules (e.g. ATP, NADPH, ferredoxin etc..) are used to support the metabolism of the phototrophic organism such as carbon fixation (**Figure 1.1**). The photochemical and electrochemical reactions driving photosynthesis are explained in considerable detail in Chapter 5 and are covered here only in a summary form.

Photochemistry is initiated by the absorption of photons by the light-harvesting complexes (LHCs), pigment-proteins complexes that increase the optical cross-section of the photosystems. The absorption results in the formation of a chlorophyll excited state (Chl*) which energy is transferred to the reaction centers (RCs) of the photosystems within ten to hundreds of picoseconds. There are two types of photosystems, I and II (respectively PSI and PSII), located within the thylakoid membrane. Once the excitation reaches the PSII reaction center, the RC gets into an excited state and one of its chlorophyll *a* donate an electron leading to the formation of $P680^{\bullet+}$. The radical cation has a redox potential $\sim$1.2 V, generating a strong oxidative power used by the oxygen-evolving-complex (OEC) to strip electrons from water molecules resulting in the formation of oxygen, protons, and free electrons [14]. For every two molecules of water split, one molecule of dioxygen, four electrons, and four protons are evolved. The electrons are transferred from PSII to PSI along the electron transport chain (ETC). The ETC is composed of different electron carriers (i.e. plastoquinol pool, cytochrome b_6f, plastocyanin) which for each transferred electron pumps one additional H^+ into the lumenal side of the thylakoid membrane (i.e. Q cycle, [15]).

The accumulation of protons in the lumenal side creates a proton motive force (*pmf*) which is used by the ATP-synthase to (re) phosphorylate ADP to ATP. At the level of PSI, light energy is used to bring the primary electron donor of PSI RC into an excited state (P700*), which has a potential of -1.2 V [16]. The strong reducing power is used in combination with the electron provided by the ETC to reduce the primary stable electron acceptor, ferredoxin. The flow of electrons along the so-called "Z scheme" resulting from the antagonistic redox reactions of the two photosystems (i.e. formation of oxidative and reductive power) is at the base of the energy transduction in photosynthesis: it generates reducing power (e.g. ferredoxin, NADPH) and forms the *pmf* used by the ATP-synthase.

1.3 Measuring photosynthesis

The rate at which photosynthesis occurs (i.e. the rate of photosynthesis) has been widely assessed by measuring either the rate O_2 evolution (e.g. via oxygen electrode) or the rate of CO_2 fixation (e.g. via infrared gas-analysis). Leaf photosynthesis is usually evaluated by measuring the rate of CO_2 fixation, normally expressed in μmol m^{-2} s^{-1}. The use of CO_2 fixation rather than the measurement of O_2 evolution was preferred due to the practicality of measuring small change in gas concentration when dealing with the small background signal of atmospheric carbon dioxide (0.042%) compared to that of oxygen (21%).

The rate of carbon fixation, henceforth referred to as the rate of photosynthesis, is commonly measured using differential infrared gas analyzers and is reported as the rate at which CO_2 is absorbed per unit leaf area per unit time (μmol m^{-2} s^{-1}), with higher rates of carbon assimilation being associated with "better" photosynthesis.

Photosynthesis occurs alongside respiration and therefore the rate of photosynthesis can be referred to as either gross, which consider respiration losses, or net rate; all the photosynthetic rates referred to in this thesis are net unless specifically mentioned. On a side note, in higher plants the rate of photosynthesis is usually measured at the leaf level. However, there is a growing interest in photosynthesis in non-foliar tissue that could participate in the positive energy balance of the plant by "recycling" of CO_2 emitted by respiration [17, 18].

1.4 Achieving high photosynthetic capacity

In C3 plants, achieving a high photosynthetic capacity per unit area of leaf requires the optimization of different processes at different scales [19].The quantity of photosynthetic components per unit leaf area certainly plays a role. For example, plants grown under high irradiance usually have thicker leaves and more chloroplasts per cell compared to plants grown under lower irradiance; having more photosynthetic enzymes leads to higher photosynthetic capacity expressed on an area basis [20, 21]. However, more photosynthetic material does not directly imply higher photosynthetic capacity at the leaf level.

A high photosynthetic capacity involves a series of different structural and molecular adjustments because it requires higher rates of "many things". For example, thicker leaves have a stronger interleaf irradiance gradient [22]; without optimizing light penetration

or light harvesting, the chloroplasts located on the abaxial (bottom) leaf side would have insufficient irradiance to drive photosynthesis to a significant extent [23, 24]. A thicker leaf means also that CO_2 might need to diffuse on longer distances reducing the [CO_2] at the site of carboxylation. Therefore, thicker leaves with high rates of photosynthesis are likely "pressured" to adjust their morphology to reduce the resistance to CO_2 diffusion to the site of carboxylation (usually expressed as its inverse, the conductance, see Lawson *et al.* [25]) by increasing the stomatal (g_s) and/or the mesophyll conductance (g_m) [26, 27].

1.5 Maintaining high photosynthetic rate at high light

Assuming a high [CO_2] can be provided at the site of carboxylation and there is a sufficient amount of RUBISCO, a high rate of photosynthesis will depend on there being an adequate rate of electron and proton transport to generate the necessary reducing power and nucleotide phosphates (e.g. reduced ferredoxin and NADPH, and ATP) to meet the needs of those photosynthetic metabolic processes taking place in the mesophyll. In a normally photosynthesizing leaf this metabolic demand for ATP and reducing power is dominated by the activity of the Calvin–Benson–Bassham (CBB) cycle, which form sugar phosphates, including ribulose-1,5-bisphosphate. The ATP/NADPH demand of the CBB functioning in this way is 3:2 [28]. Other metabolic processes, however, take place in the chloroplasts, and these have different demands for ATP and reducing power so photosynthetic electron transport must not only make ATP and reducing power but make ATP and reducing power in the correct ratio to meet the needs of metabolism. An increase in the rate of carbon assimilation and other photosynthetic metabolic processes will require an increase in the rate of formation of NADPH and ATP, which requires an increase in irradiance.

With increasing irradiance the rate of carbon assimilation displays a characteristic curvilinear response where at low irradiances assimilation has a low rate but a high light-use efficiency (**Figure 1.2**, part a), while with increasing irradiance the assimilation carbon assimilation increases but with a decreasing light-use efficiency (**Figure 1.2**, part b. This progressively decreasing light-use efficiency, or quantum yield of photosynthesis, results in the overall light-saturation of the light response curve (**Figure 1.2**, part b).

To maintain a high light-use efficiency of photosynthesis with increasing irradiance, the rate of charge separation therefore needs to be matched with the capacity for electron and proton transport capacity. It is possible to measure the rate constant of

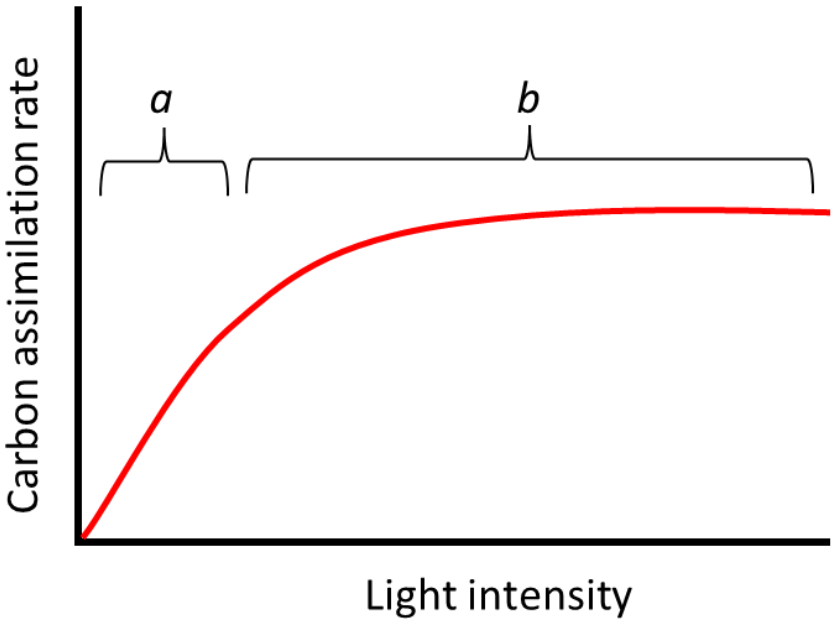

Figure 1.2. *Schematic of the evolution of the rate of carbon assimilation versus an increasing light intensity (i.e. light-response curve). The light-response curve can be divided into two parts: a) the light-limited part, and b) the curvilinear phase in which light-use efficiency decreases with increasing irradiance.*

the plastoquinol/ cytochrome b_6f electron transfer step, which is thought to be the kinetically limiting step for electron transport, using the 820 nm light induced absorbance change [29]. Electron transport is also subject to regulation via a mechanism termed photosynthetic control [30–32] that adjusts the overall rate of electron transport to match the demand of metabolism if the latter should be limiting. Photosynthetic control depends on lumen acidification. Electron transport is coupled to the translocation of H^+ into the thylakoid lumen. The acidification of the lumen plays an important role in the regulation of photosynthesis. First, decreases in lumen pH decreases the light-use of efficiency for electron transport by PSII via activation of the qE mechanism, and, second, lumen acidification will impose a kinetic limitation at the plastoquinol/cytochrome b_6f electron transfer step (i.e. photosynthetic control).Light-saturated rates of carbon fixation are species-specific (and can vary even within ecotypes), indicating that plants adapt their photosynthetic machinery to maximize (or minimize) their rates of carbon fixation according to their ecological niche [5, 33, 34].

1.6 Photosynthesis and crop yield

The history of agriculture has been one of improvements either in the crops that are grown or the means available to manage the land and cultivate the crops. The last phase of agricultural improvement, sometimes seen as the industrialization of agriculture, began in the late 50's, and resulted in a more than doubling of average crop yields. Improved agronomical practices, such use of pesticides, irrigation, and fertilization, have strongly reduced abiotic and biotic stressors. Under these optimal conditions, above ground crop yield (Yp, g m^{-2}) tends to linearly correlate with the amount of light absorbed and used to photosynthesize [35–37] and can be modeled as:

$$Y_p = \frac{s_t \cdot \eta \cdot \epsilon_c \cdot \epsilon_i}{k} \tag{1.1}$$

Here S_t is the integrated incident photosynthetic active radiation across the growing period (MJ m^{-2}), η the fraction of that absorbed light-energy allocated to the harvested part of the crop (e.g. seeds), ε_i the efficiency of light interception by the canopy, ε_c the energy conversion efficiency of the harvested light energy into biomass, and k the energy content of the plant biomass (MJ g^{-1}). While η and ε_i are now believed to be close to their maximum values (at least for major crops) thanks to breeding in the last 70 years (e.g. use of dwarfing genes in wheat) and optimized spacing of the plants in the field, it is expected that ε_c can still be improved to increase yields in agricultural field [38–40].

It should be stressed that improving ε_c to increase crop yield can only be a viable

solution for well-managed agricultural fields. For example, while the theoretical maximum ε_c is expected to lie between 4.6% and 6% depending on the type of carbon metabolism (i.e. C3 or C4) [41, 42], the estimated ε_c of worldwide ecosystems ranges between 0.4% and 1.1% [43]. The discrepancy is unlikely to be due to inefficiencies in the photosynthetic processes but rather results from the limitation in the supply of resources other than light. For example, maintaining high rates of carbon fixation requires nitrogen rich soils [44], or in environments where water availability is limited, reduced transpiration rates result in lower amounts of CO_2 being fixed [43]. It is noteworthy that multiple limitation can occur concurrently. A good demonstration of this can be observed when measuring the rates of carbon fixations in a light limiting conditions, either an increase in light intensity or a decrease of $[O_2]$ will lead to higher rates of carbon fixation.

Recently different approaches based on genetic modification (GM) showed that it is possible to increase biomass accumulation by targeting photosynthetic inefficiencies at different levels such as PSII functional antenna size [45], relaxation kinetics of light-induced photo-protection mechanisms [46, 47] or regeneration kinetics of the CBB cycle [48]. However, similar approaches implemented in other crop species [49, 50] or in successive growing seasons [46] did not result in yield increase. The difficulty in finding a set of genes that would universally improve yield is most likely due to the complexity of photosynthesis and our relatively limited understanding of photosynthetic regulation at different scales in the field. Additionally, in some countries (e.g. European Union countries), the legislative framework is rather restrictive regarding the use of GM, thereby limiting the possible use of genetically engineered crops anyway. Nonetheless considerable variation in light-saturated photosynthetic capacity (Pmax) exists [19] and while this is not the only photosynthetic property that is likely to be important in improving photosynthesis as a route to improving crop yields it is likely to relevant to this goal. Understanding the genetics and physiology of this important but complex trait is surely an important ambition.

1.7 Outlook of the thesis

During the project detailed in this thesis, I studied a group of plant species belonging to the Brassicaceae family: *Hirschfeldia incana*, *Brassica nigra*, and *Brassica rapa* which have been reported to have photosynthetic capacity almost twice as high than normal C3 plants (50 µmol m^{-2} s^{-1} compared to 30 µmol m^{-2} s^{-1}) [7, 10, 51]. Maintaining high photosynthetic capacity at high light requires maintaining high efficiency of the underlining processes (e.g. rate of charge separation, rate of electron transport). Two

possible physiological mechanisms were investigated that could explain how some Brassicaceae maintain high photosynthetic capacity when grown under high light. The first physiological mechanisms was at the level of the thylakoid membrane and is detailed in Chapter 3, and the second at the leaf level and is discussed in Chapter 4. In Chapters 2 and 5 are described two methodologies that were developed to enable further research.

In Chapter 2 is described the development of an electronic circuit used to control dimmable light fixtures, enabling the growth of plants under two different irradiances. The photosynthetic capacity observed in a plant species tightly depends on the light intensity [23, 52]. By using two different levels of irradiance, it easier to disentangle the effects of the environment (i.e. light intensity) on the photosynthetic capacity from the genetic effects. In the experiments reported in this thesis, the light controller was used exclusively to generate constant high light and low light under which the plants were grown. However, the light controller was designed to generate intricate light patterns (e.g. sinusoid, fluctuation) to test the response of photosynthesis to it. Additionally, the circuit can be used to mimic in controlled environment the diurnal variation of light intensity, enabling to separate the effects of irradiance fluctuations from other effects (e.g. biotic stressors, nutrients, etc..). The design of the electronic circuit was released as open-source so that it could benefit the research community, and some studies, in which I was involved, already made use of it [53–55].

In Chapter 3 the PSII functional antenna size, σ_f(PSII), was measured on the different Brassicaceae grown under two different light intensities; the σ_f(PSII) was measured on both sides of the leaf (i.e. adaxial, abaxial). The σ_f(PSII) was measured *in folio* using two independent spectroscopic techniques in two independent experiments. The first experiment was executed at the BIAM-CEA (France), the σ_f(PSII) was measured using a custom-made fluorometer to record chlorophyll's fluorescence rise induced by a flash of light. The irradiance of the flash was strong enough to induce the rise of the fluorescence within microseconds, which allowed to measure the σ_f(PSII) without relying on the chemical photoinhibition of PSII. The second experiment was executed at Wageningen University and Research (The Netherlands), the σ_f(PSII) was measured using a streak-camera to resolve spectrally the lifetime of chlorophyll's fluorescence decay in the ps-ns range in condition of open reaction centers (F_o). The spectrally and kinetically resolved fluorescence lifetime allowed to disentangle the PSII fluorescence component from the PSI fluorescence. The chloroplasts located on the adaxial side of the leaf had a smaller σ_f(PSII) compared to the ones located on the abaxial side of the same leaf, exhibiting a light-and-shade-adaptation. The size of the σ_f(PSII) scaled with

the light-use efficiencies reported in [10], with smaller σ_f(PSII) associated with higher light-use efficiencies. Interestingly, the smaller σ_f(PSII) correlated with an increased PSII maximum quantum yield (i.e. F_v/F_m parameter). The correlation could be caused either by an improved trapping efficiency of the reduced optical cross-section (i.e. higher RC/LHCs ratio), or results from a high intensity quenching taking place in the PSII antenna.

Chapter 4 details the investigation of whether chloroplast size within the leaf section could explain the higher light-use efficiency observed in some members of the Brassicaceae. The distribution of chloroplasts were imaged *in vivo* for different plant species grown under two growth irradiances (250 and 1600 µmol m^{-2} s^{-1}) using a multiphoton microscope. I trained a convolutional neural network designed to detect round-shape objects [56, 57] and used it to detect thousands (n= 1260) of individual chloroplasts in 3D; for each single detected chloroplast, the volume and surface area were calculated. To assess possible inter-leaf differences, I analyzed separately the chloroplasts located in the palisade or the spongy mesophyll. I observed that the different species tested regulate the chloroplasts' size in different ways. *H. incana* and *A. thaliana* were shown to regulate the chloroplasts' size according to the light treatment (smaller at higher light) and the mesophylls (different size between palisade and spongy). On the other hand, *B. rapa* did not adapt its chloroplast volume, either between the different mesophylls nor across growth irradiance. The possible reasons for the observed natural variability in chloroplast regulation are discussed in the function of the potential physiological trade offs (e.g. light distribution, mesophyll conductance, etc..).

Chapter 5 details the development of an open-source instrument aimed at further investigating the physiological mechanisms behind the high photosynthetic capacity observed in some of the Brassicaceae. The instrument is designed to modulate a light source (i.e. generate flashes with a defined frequency) and measure the amplitude of the light flash after having interacted with a photosynthetic specimen (i.e. inducing fluorescence emission, or changing its transmission), similar to a Joliot's spectrophotometer [58]. The changes in the amplitude of the pulse reflect changes in absorbance or fluorescence. The instrument can measure (i.e. modulate a light source and demodulate the signal) up to five different channels, which means that up to five different light sources (i.e. with different emission wavelengths) can be connected to probe different parts of the photosynthetic machinery. The instrument can measure up to five channels: one channel to measure chlorophyll fluorescence and assess the regulation and operation of photosystem II; two channels to measure absorption changes in the near-infrared (NIR)

and assess the operation and regulation of photosystem I; and the remaining channels used to measure the absorbance changes caused by an electrochromic shift of chlorophyll *b* and carotenoids located in the thylakoid membrane and exposed to the increased electric to assess the *pmf* and its regulation (i.e. proton efflux). The instrument can be connected to a leaf cuvette to complement the spectroscopic measurement with rates of gas exchanges (i.e. CO_2, H_2O) measured by a differential gas analyzer. Due to time constraints, it was not possible to use the instrument for this thesis work and I hope it will be used in follow-up projects.

References

1. Bonner, J. The upper limit of crop yield: this classical problem may be analyzed as one of the photosynthetic efficiency of plants in arrays. *Science* **137,** 11–15 (1962).
2. Emerson, R., Green, L. & Webb, J. L. Relation between quantity of chlorophyll and capacity for photosynthesis. *Plant Physiology* **15,** 311–317 (1940).
3. Oliver, T., Kim, T. D., Trinugroho, J. P., Cordón-Preciado, V., Wijayatilake, N., Bhatia, A., Rutherford, A. W. & Cardona, T. The evolution and evolvability of photosystem II. *Annual Review of Plant Biology* **74,** 225–257 (2023).
4. Shi, T., Bibby, T. S., Jiang, L., Irwin, A. J. & Falkowski, P. G. Protein interactions limit the rate of evolution of photosynthetic genes in cyanobacteria. *Molecular Biology and Evolution* **22,** 2179–2189 (2005).
5. Faralli, M. & Lawson, T. Natural genetic variation in photosynthesis: an untapped resource to increase crop yield potential? *The Plant Journal* **101,** 518–528 (2020).
6. Hoang, N. V., Walden, N., Caracciolo, L., Luoni, S. B., Retta, M., Li, R., Wolters, F. C., Woldu, T., Becker, F. F. M., Verbaarschot, P., Harbinson, J., Driever, S. M., Struik, P. C., Amerongen, H. V., De Ridder, D., Aarts, M. G. & Schranz, M. E. *Expanding the Triangle of U: The genome assembly of Hirschfeldia incana provides insights into chromosomal evolution, phylogenomics and high photosynthesis-related traits* 2024.
7. Canvin, D. T., Berry, J. A., Badger, M. R., Fock, H. & Osmond, C. B. Oxygen exchange in leaves in the light. *Plant Physiology* **66,** 302–307 (1980).
8. Taylor, S. H. & Long, S. P. Slow induction of photosynthesis on shade to sun transitions in wheat may cost at least 21% of productivity. *Philosophical Transactions of the Royal Society B: Biological Sciences* **372,** 20160543 (2017).
9. Vaughan, J. G. & Hemingway, J. S. The utilization of mustards. *Economic Botany* **13,** 196–204 (1959).
10. Garassino, F., Wijfjes, R. Y., Boesten, R., Reyes Marquez, F., Becker, F. F. M., Clapero, V., Van Den Hatert, I., Holmer, R., Schranz, M. E., Harbinson, J., De Ridder, D., Smit, S. & Aarts, M. G. M. The genome sequence of *Hirschfeldia incana* , a new Brassicaceae model to improve photosynthetic light-use efficiency. *The Plant Journal* **112,** 1298–1315 (2022).
11. Pribil, M., Labs, M. & Leister, D. Structure and dynamics of thylakoids in land plants. *Journal of Experimental Botany* **65,** 1955–1972 (2014).
12. Anderson, J. M. Photoregulation of the composition, function, and structure of thylakoid membranes. *Annual Review of Plant Physiology* **37,** 93–136 (1986).
13. Herbstová, M., Tietz, S., Kinzel, C., Turkina, M. V. & Kirchhoff, H. Architectural switch in plant photosynthetic membranes induced by light stress. *Proceedings of the National Academy of Sciences* **109,** 20130–20135 (2012).
14. Barber, J. *Photosystem II: redox and protein components* in *Encyclopedia of Biological Chemistry* 512–519 (Elsevier, 2013).
15. Mitchell, P. The protonmotive Q cycle: A general formulation. *FEBS Letters* **59,** 137–139 (1975).
16. Webber, A. N. & Lubitz, W. P700: the primary electron donor of photosystem I. *Biochimica et Biophysica Acta (BBA) - Bioenergetics* **1507,** 61–79 (2001).
17. Aschan, G. & Pfanz, H. Non-foliar photosynthesis – a strategy of additional carbon acquisition. *Flora - Morphology, Distribution, Functional Ecology of Plants* **198,** 81–97 (2003).
18. Simkin, A. J., Faralli, M., Ramamoorthy, S. & Lawson, T. Photosynthesis in non-foliar tissues: implications for yield. *The Plant Journal* **101,** 1001–1015 (2020).
19. Harbinson, J., Kaiser, E. & Morales, A. S. *Integrating the stages of photosynthesis* in *Photosynthesis in Action* 195–242 (Elsevier, 2022).
20. Terashima, I., Miyazawa, S.-I. & Hanba, Y. T. Why are sun leaves thicker than shade leaves? — consideration based on analyses of CO2 diffusion in the leaf. *Journal of Plant Research* **114,** 93–105 (2001).
21. Wild, A. & Wolf, G. The effect of different light intensities on the frequency and size of stomata, the size of cells, the number, size and chlorophyll content of chloroplasts in the mesophyll and the guard cells during the ontogeny of primary leaves of Sinapis alba. *Zeitschrift für Pflanzenphysiologie* **97,** 325–342 (1980).
22. Terashima, I. & Inoue, Y. Palisade tissue chloroplasts and spongy tissue chloroplasts in spinach: biochemical and ultrastructural differences. *Plant and Cell Physiology* (1985).
23. Evans, J. Carbon fixation profiles do reflect light absorption profiles in leaves. *Functional Plant Biology* **22,** 865 (1995).
24. Slattery, R. A. & Ort, D. R. Perspectives on improving light distribution and light use efficiency in crop canopies. *Plant Physiology* **185,** 34–48 (2021).
25. Lawson, T., Emmerson, R., Battle, M., Pullin, J., Wall, S. & Hofmann, T. A. *Carbon fixation* in *Photosynthesis in Action* 31–58 (Elsevier, 2022).
26. Wong, S. C., Cowan, I. R. & Farquhar, G. D. Stomatal conductance correlates with photosynthetic capacity. *Nature* **282,** 424–426 (1979).

27. Wong, S. C., Cowan, I. R. & Farquhar, G. D. Leaf conductance in relation to rate of CO_2 assimilation: Influence of nitrogen nutrition, phosphorus nutrition, photon flux density, and ambient partial pressure of CO_2 during ontogeny. *Plant Physiology* **78,** 821–825 (1985).
28. Edwards, G. & Walker, D. *C3, C4: mechanisms and cellular and environmental regulation, of photosynthesis* (University of California Press, Berkeley, Calif, 1983).
29. Harbinson, J. & Woodward, F. I. Field measurements of the gas exchange of woody plant species in simulated sunflecks. *Annals of Botany* **53,** 841–851 (1984).
30. Foyer, C., Furbank, R., Harbinson, J. & Horton, P. The mechanisms contributing to photosynthetic control of electron transport by carbon assimilation in leaves. *Photosynthesis Research* **25,** 83–100 (1990).
31. Kanazawa, A. & Kramer, D. M. *In vivo* modulation of nonphotochemical exciton quenching (NPQ) by regulation of the chloroplast ATP synthase. *Proceedings of the National Academy of Sciences* **99,** 12789–12794 (2002).
32. Genty, B. & Harbinson, J. *Regulation of light utilization for photosynthetic electron transport* in *Photosynthesis and the Environment* (ed Baker, N. R.) 67–99 (Kluwer Academic Publishers, Dordrecht, 1996).
33. Flood, P. J., Harbinson, J. & Aarts, M. G. Natural genetic variation in plant photosynthesis. *Trends in Plant Science* **16,** 327–335 (2011).
34. Theeuwen, T. P. J. M., Logie, L. L., Harbinson, J. & Aarts, M. G. M. Genetics as a key to improving crop photosynthesis. *Journal of Experimental Botany* **73** (ed Kromdijk, J.) 3122–3137 (2022).
35. Monteith, J. L. Climate and the efficiency of crop production in Britain. *Philosophical Transactions of the Royal Society of London. B, Biological Sciences* **281,** 277–294 (1977).
36. Wells, R., Meredith, W. R. & Williford, J. R. Canopy photosynthesis and Its relationship to plant productivity in near-isogenic cotton lines differing in leaf morphology. *Plant Physiology* **82,** 635–640 (1986).
37. Zhu, X.-G., Long, S. P. & Ort, D. R. Improving photosynthetic efficiency for greater yield. *Annual Review of Plant Biology* **61,** 235–261 (2010).
38. Croce, R., Carmo-Silva, E., Cho, Y. B., Ermakova, M., Harbinson, J., Lawson, T., McCormick, A. J., Niyogi, K. K., Ort, D. R., Patel-Tupper, D., Pesaresi, P., Raines, C., Weber, A. P. M. & Zhu, X.-G. Perspectives on improving photosynthesis to increase crop yield. *The Plant Cell,* koae132 (2024).
39. Long, S. P., Zhu, X.-G., Naidu, S. L. & Ort, D. R. Can improvement in photosynthesis increase crop yields? *Plant, Cell & Environment* **29,** 315–330 (2006).
40. Parry, M. A. J., Reynolds, M., Salvucci, M. E., Raines, C., Andralojc, P. J., Zhu, X.-G., Price, G. D., Condon, A. G. & Furbank, R. T. Raising yield potential of wheat. II. Increasing photosynthetic capacity and efficiency. *Journal of Experimental Botany* **62,** 453–467 (2011).
41. Beadle, C. & Long, S. Photosynthesis — is it limiting to biomass production? *Biomass* **8,** 119–168 (1985).
42. Zhu, X.-G., Long, S. P. & Ort, D. R. What is the maximum efficiency with which photosynthesis can convert solar energy into biomass? *Current Opinion in Biotechnology* **19,** 153–159 (2008).
43. Kleidon, A. What limits photosynthesis? Identifying the thermodynamic constraints of the terrestrial biosphere within the Earth system. *Biochimica et Biophysica Acta (BBA) - Bioenergetics* **1862,** 148303 (2021).
44. Garnier, E. & Vancaeyzeele, S. Carbon and nitrogen content of congeneric annual and perennial grass species: relationships with growth. *Plant, Cell & Environment* **17,** 399–407 (1994).
45. Kirst, H., Gabilly, S. T., Niyogi, K. K., Lemaux, P. G. & Melis, A. Photosynthetic antenna engineering to improve crop yields. *Planta* **245,** 1009–1020 (2017).
46. De Souza, A. P., Burgess, S. J., Doran, L., Hansen, J., Manukyan, L., Maryn, N., Gotarkar, D., Leonelli, L., Niyogi, K. K. & Long, S. P. Soybean photosynthesis and crop yield are improved by accelerating recovery from photoprotection. *Science* **377,** 851–854 (2022).
47. Kromdijk, J., Głowacka, K., Leonelli, L., Gabilly, S. T., Iwai, M., Niyogi, K. K. & Long, S. P. Improving photosynthesis and crop productivity by accelerating recovery from photoprotection. *Science* **354,** 857–861 (2016).
48. Lefebvre, S., Lawson, T., Fryer, M., Zakhleniuk, O. V., Lloyd, J. C. & Raines, C. A. Increased sedoheptulose-1,7-bisphosphatase activity in transgenic tobacco plants stimulates photosynthesis and growth from an early stage in development. *Plant Physiology* **138,** 451–460 (2005).
49. Garcia-Molina, A. & Leister, D. Accelerated relaxation of photoprotection impairs biomass accumulation in Arabidopsis. *Nature Plants* **6,** 9–12 (2020).
50. Suzuki, Y., Wada, S., Kondo, E., Yamori, W. & Makino, A. Effects of co-overproduction of sedoheptulose-1,7-bisphosphatase and Rubisco on photosynthesis in rice. *Soil Science and Plant Nutrition* **65,** 36–40 (2019).
51. Taylor, S. H., Orr, D. J., Carmo-Silva, E. & Long, S. P. During photosynthetic induction, biochemical and stomatal limitations differ between *Brassica* crops. *Plant, Cell & Environment* **43,** 2623–2636 (2020).

52. Poorter, H., Niinemets, Ü., Ntagkas, N., Siebenkäs, A., Mäenpää, M., Matsubara, S. & Pons, T. A meta-analysis of plant responses to light intensity for 70 traits ranging from molecules to whole plant performance. *New Phytologist* **223,** 1073–1105 (2019).
53. Schiphorst, C., Koeman, C., Caracciolo, L., Staring, K., Theeuwen, T. P. J. M., Driever, S. M., Harbinson, J. & Wientjes, E. The effects of different daily irradiance profiles on Arabidopsis growth, with special attention to the role of PsbS. *Frontiers in Plant Science* **14,** 1070218 (2023).
54. Theeuwen, T. P., Lawson, A. W., Tijink, D., Fornaguera, F., Becker, F. F., Caracciolo, L., Fisher, N., Kramer, D. M., Wijnker, E., Harbinson, J. & Aarts, M. G. *The NDH complex reveals a trade-off that constrains maximising photosynthesis in Arabidopsis thaliana* preprint (2022).
55. Theeuwen, T. P., Logie, L. L., Put, S., Bagheri, H., Łosiński, K., Drouault, J., Flood, P. J., Hanhart, C., Becker, F. F., Wijfjes, R., Hall, D., Kramer, D. M., Harbinson, J. & Aarts, M. G. *Plethora of QTLs found in Arabidopsis thaliana reveals complexity of genetic variation for photosynthesis in dynamic light conditions* preprint (2022).
56. Schmidt, U., Weigert, M., Broaddus, C. & Myers, G. *Cell Detection with star-convex polygons* in *Medical Image Computing and Computer Assisted Intervention – MICCAI 2018* (eds Frangi, A. F., Schnabel, J. A., Davatzikos, C., Alberola-López, C. & Fichtinger, G.) 265–273 (Springer International Publishing, Cham, 2018).
57. Weigert, M., Schmidt, U., Haase, R., Sugawara, K. & Myers, G. *Star-convex polyhedra for 3D object detection and segmentation in microscopy* in *2020 IEEE Winter Conference on Applications of Computer Vision (WACV)* (IEEE, Snowmass Village, CO, USA, 2020), 3655–3662.
58. Joliot, P., Beal, D. & Frilley, B. Une nouvelle méthode spectrophotométrique destinée à l'étude des réactions photosynthétiques. *Journal de Chimie Physique* **77,** 209–216 (1980).

Chapter 2

An open-source controller to build a dynamic light intensity setup

A version of this chapter has been published as:

Ludovico Caracciolo, John Philippi, Tom P. J. M. Theeuwen, Herbert van Amerongen and Jeremy Harbinson. An open-source controller to build a dynamic light intensity setup. *Plant Methods* **20**, 35 (2024).

Abstract

The development and physiology of plants are influenced by light intensity and its changes. Despite the significance of this phenomenon, there is a lack of understanding regarding the processes light regulates. This lack of understanding is partly due to the complexity of plant's responses, but also due to the limited availability of light setups capable of producing specific light patterns. While unraveling the complexities of plant responses will require further studies, this research proposes a simple method to implement dynamic light setups. In this study, we introduce two distinct electronic circuits that are cost-effective and enable the control of a dimmable power supply. This method enables the generation of intricate light patterns and rapid intensity fluctuations, providing a means to investigate how plants respond and develop when exposed to dynamic light conditions.

2.1 Introduction

Light intensity is an important parameter that shapes the physiology and development of plants [1–3] and an aspect of intensity are fluctuations in intensity. Plants respond to the fluctuation of light intensity through physiological changes ranging from short-term responses to longer-term adaptation. For example, the fluctuation of light intensity can induce changes in the chlorophyll a/b ratio, leaf thickness, and plant biomass [4–6]. To reproducibly study plant physiological processes, plants are often grown in controlled conditions. The light intensity in these controlled environment spaces is typically kept constant during the photoperiod. However, in nature irradiance can vary significantly within seconds, due to factors such as shading from other leaves or passing clouds, so account should be taken of plant responses to fluctuating irradiances (e.g. in Harbinson & Woodward [7]). This difference between controlled environment systems and nature cause certain discrepancies between the observations made on plants grown in field and in controlled conditions [8]. To better understand how plants might operate in nature, it is desirable to mimic the natural dynamic light regime when growing plants under artificial irradiance. The effect of fluctuating irradiance on plant physiology, and most conspicuously on photosynthesis, has been recognized as a major knowledge gap in our understanding of plant/environment interactions as well as a path to crop yield improvement.

Many photosynthetic processes are affected by fluctuating irradiance. For example, when exposed to an increase in irradiance that results in carbon assimilation being no longer wholly light-limited, plants and other photosynthetic organisms can activate photoprotective mechanisms called non-photochemical quenching (NPQ). NPQ safely dissipates some of the excess excited states of chlorophyll formed in photosystem II (PSII) as heat. This dissipation is expected to lower photodamage in PSII [9]. Some components of NPQ relax when the light intensity decreases but this response can be relatively slow compared to the rate of decrease of irradiance. This results in PSII light-use efficiency becoming limiting for photosynthesis and, consequently, reduced CO2 fixation and biomass productivity. Knowledge of the underlying physiology and genes coding for proteins (including enzymes) connected with the formation and relaxation of NPQ allowed acceleration of the relaxation kinetics of NPQ via up-regulation of a set of these genes. This resulted in a 15% increase in dry biomass of field-grown tobacco [10] and up to 33% increased yield of soybean seeds [11]. However, increasing the kinetics of NPQ relaxation may not always be the silver bullet to improve crop yield in the field; the same approach led to a decrease in biomass accumulation in *Arabidopsis*

thaliana grown in fluctuating light conditions [12]. A deeper understanding of the effect of fluctuating light on photosynthetic performance is therefore needed to improve crop yield.

Field experiments will always be required to confirm the extent to which a potentially adaptive aspect of plant physiology has an impact under field conditions. However, our understanding of the underlying mechanisms of these adaptive features of plant function of plant biology can be accelerated by conducting initial trials where other potentially affecting parameters can be controlled (i.e. temperature, watering, competition). Therefore, there is an increased need to have a fluctuating irradiance in controlled environment spaces. The ease with which the light intensity can be controlled in indoor experiments has improved tremendously over the last 30 years. This improvement can be attributed first to the introduction of dimmable ballasts for fluorescent tubes and high-pressure sodium lamps, and then more recently to the introduction of dimmable LED lighting systems. However, there remain limitations in the options and extent of control of irradiance that can be routinely achieved in typical controlled environment rooms. One approach is to switch the light on and off to vary between two different light intensities [13–15]. This approach is simple to implement and cost effective although it does not allow mimicking of the more complex fluctuations obtained in nature. Another solution is to use commercial systems that can change the light intensity according to a schedule set by the user. This allows the growth of plants under simulated natural daylight conditions, at least as far as the maximum irradiance and the emission spectrum of the system permits [2, 6, 16]. Nonetheless, this flexibility comes at a price that is not always affordable. A cheaper alternative is to design a dimmable LED power supply that can dynamically adjust the light intensity (e.g. in Wu [17]). However, many plant scientists do not have enough knowledge of electronics to implement an approach of this kind.

A workaround is to exploit the ability of some commercial lighting systems to be dimmed by an external signal and to home-build only the circuit required to produce this controlling signal. Dimmable power supplies are available for most LED or fluorescence tube fixtures [18], allowing a simple and easy implementation of a fluctuating irradiance system that can be retrofitted to an existing controlled environment space. We have developed two circuits that can be used with dimmable power supplies for LEDs or fluorescent lamps to produce a dynamic light system. The objective of this work is to provide individuals who are not always comfortable with electronics with the essential knowledge to build a simple light controller that can be connected to an existing dimmable lighting system. This is accomplished by offering comprehensive

explanations, open-source code, and a practical example of how to build a small and low-cost programmable lightning setup. Moreover, this setup can adjust light intensity within milliseconds, which is substantially faster than the 20 seconds reported recently [19].

2.2 Materials and methods

The proposed dynamic light system is composed of a dimmable power supply, a light source, and a controller circuit. The type of power supply needed depends on the light source that needs to be driven (fluorescence, LED, etc.). Dimmable power supplies exist for a whole variety of lamps. In this work, we implemented a dynamic lighting system based on LEDs because of their wide availability and decreasing cost. Nonetheless, the same approach can also be used with other types of light sources if their power supply is dimmable.

The wide-scale use of LEDs as a light source in controlled environments for plant research is relatively new. To avoid confusion over terminology and the way LEDs function, a short overview on how LEDs work is provided hereafter. As light sources, LEDs need to be powered using direct current (DC) applied using the correct polarity. The power supply therefore converts alternating current (AC) supplied from the mains socket to DC. Within the operating limits of the device, the brightness or radiation output of an LED is almost linearly correlated to the current flowing through it. LEDs can be dimmed in two ways; first by controlling the current flowing through the LED or, second, by driving them with a current pulsed at a fixed frequency (usually >3kHz) but with a variable duty-cycle (i.e. the ratio between the on and off time of the pulses). The first method is referred to as Constant Current Reduction (CCR) while the latter is generally referred to as Pulse Width Modulation (PWM). The frequency of the PWM modulation is usually well above that for the human perception of flicker (which is about 25 Hz) and the perceived brightness depends on the duty-cycle. While PWM is often used in illumination engineering it is not suited for plant growth; some studies indicate that using PWM to control irradiance can induce physiological responses [20]. Therefore, the use of CCR is preferred to control irradiance in plant research unless the aim is to provide irradiance in the form of repetitive pulses. It is worth noting that the power supplies dimmable using CCR might use PWM as a control signal (i.e. the amplitude of the constant current is adjusted through a PWM control signal). In the method presented here, we will use a PWM only as a control signal so dimming of irradiance will always be achieved by reducing the current provided to the LEDs.

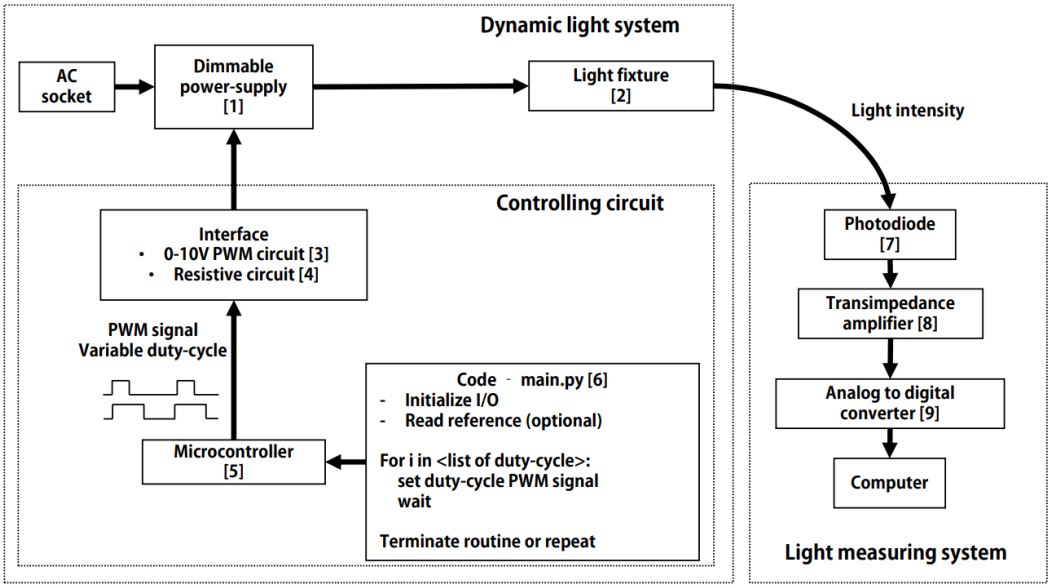

Figure 2.1. *Overview of the dynamic light setup and light measuring system. LCM-60, Mean Well® (1); L2C5-30HG1203E0900, Lumiled® (2); the interfaces (3,4) are reported in figure 2.2 and 2.4; RP2040, Raspberry Pi Foundation (5); example code in supplementary material (6); LI-COR® quantum sensor (7); DLPCA-200, Femto(8); PICOLOG 1216, Pico Technology (9).*

2.2.1 Overview of the setup

Figure 2.1 summarizes the dynamic light setup presented in this work. Commercial dimmable power suppliers have their dimming percentage usually controlled through the so-called 0-10V protocol. These power supplies have two control pins from which a 10V voltage is sourced. There are two commonly used ways of controlling the dimming percentage of a 0-10V dimmable power supply. One is to modulate the 10V on the power supply side in a PWM fashion way, the second is by changing an external resistance between the controlling pins [21]. **Figure 2.2** and **Figure 2.4** show, respectively, the interfacing circuits for a 0-10V PWM control and a resistive control. In both cases, the controlling signal is generated by a microcontroller (MCU) and is PWM modulated at a constant frequency (in the kHz range) with a variable duty-cycle. The percentage of the duty-cycle controls the current dimming of the power supply. In our case, an RP2040 (Raspberry Pi Foundation) was chosen as the MCU because of its low price and its use of Micropython, which is a dialect of Python designed for microcontrollers. Python is an easy to use and widely taught programming language. Any other MCU, however, that is able to generate a PWM output could have been used (e.g. an Arduino). To achieve dynamic

fluctuations, the microcontroller follows an algorithm outlined in the main application code uploaded to the MCU (**Figure 2.1**-[6], "main.py"). This program typically involves reading a value from an array or text file, changing the PWM duty-cycle based on the read value, and waiting for a specified duration before repeating the process. For complex fluctuations with thousands of different dimming percentages (i.e. while mimicking a natural light profile), the duty-cycle's values can be saved on an external drive (e.g. an SD card). Both interface circuits use optically coupled components to electrically isolate the MCU from the power supply to allow communication between different voltage levels and to increase the safety of the system by largely isolating the low voltage home-built circuit from the mains voltage dimmable power supply (i.e 3.3V and 10V).

2.2.2 Interface circuits

2.2.2.1 0-10V PWM interface

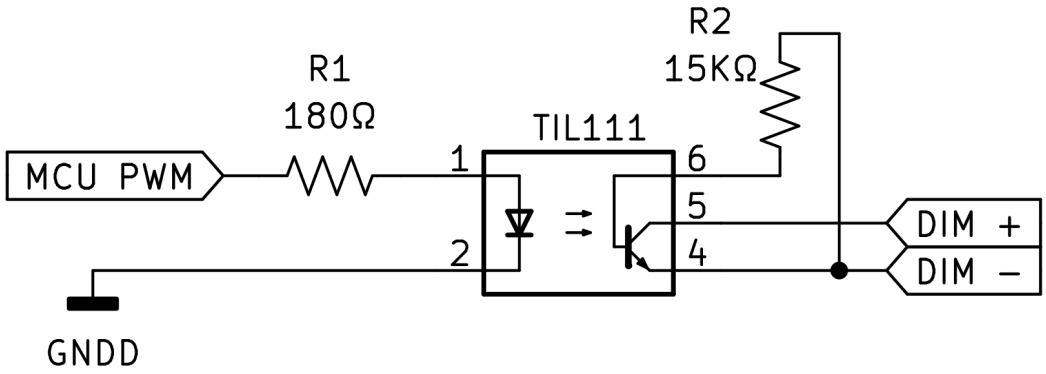

Figure 2.2. *Circuit diagram of the 0-10V PWM circuit. R_x, resistors; TILL111, optocoupler.*

Figure 2.2 shows the circuit for the 0-10V PWM interface (see **Figure 2.1**-[3]). It is composed of two resistors and one optocoupled transistor (TIL111, ON Semiconductor / Fairchild). The dimming percentage of the power supply linearly depends on the voltage sensed between its control pin, averaged over time. The control pins of the power supply (DIM+, DIM-) are connected to the transistor side of the optocoupler. The base of the transistor (**Figure 2.2**, TIL111 pin 6) is connected through a pull-down resistor to the emitter (**Figure 2.2**, TIL111 pin 4), to decrease the fall time of the modulated pulse. The value of R1 was chosen according to the datasheet of the TIL111 to produce a 10mA current running through the optocoupler. **Figure 2.3** shows the voltage measured on the

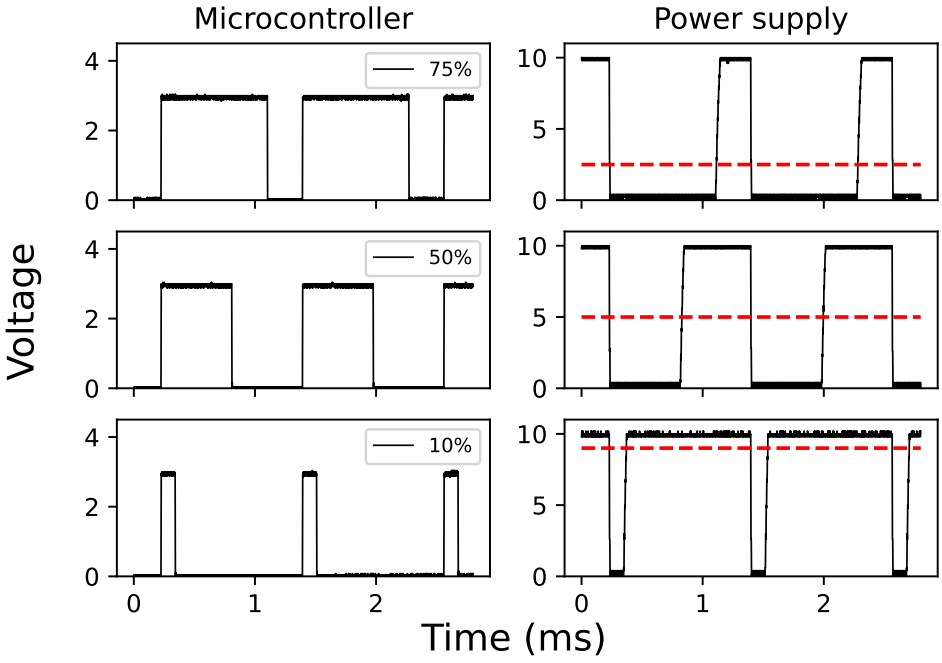

Figure 2.3. *Oscilloscope measurement of the PWM signal on the microcontroller and power supply side. The dashed line indicates the average voltage sensed on the power supply control pins.*

microcontroller side (**Figure 2.2**, TIL111 pins 1 and 2) and on the power supply controlling pin side (**Figure 2.2**, TIL111 pins 4 and 5).

2.2.2.2 Resistive interface

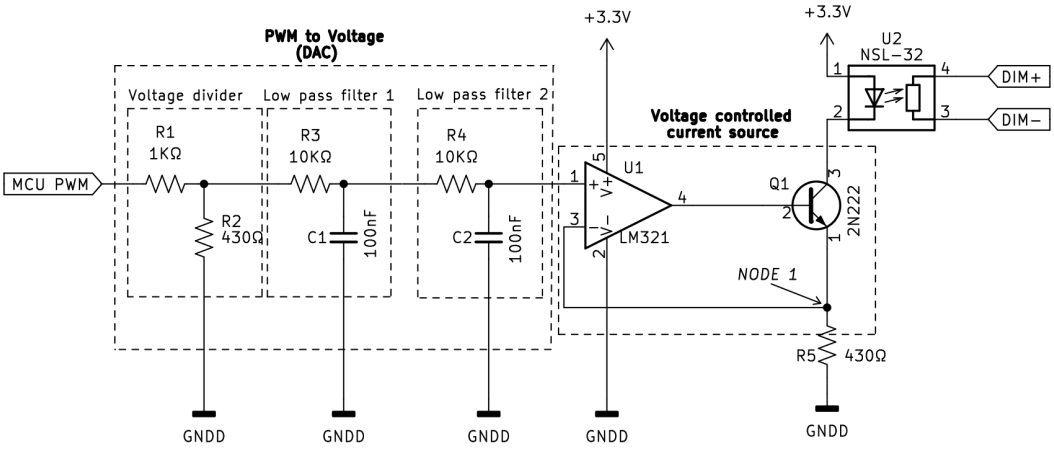

Figure 2.4. *Circuit diagram of the resistive circuit. R_x, resistors; C_x, capacitors; U1, opamp; U2, optocoupled LDR; Q1, transistor*

Figure 2.4 shows the circuit for a resistive interface (see **Figure 2.1**-[4]). The circuit is composed of five resistors, two capacitors, one operational amplifier (LM321, Texas Instrument), one NPN transistor (2N222, ON Semiconductor), and one optocoupled light-dependent resistor (NSL-32-R2, Advanced Photonix). While the 0-10V PWM interface is easy to implement, some dimmable power supplies might have an unstable output when controlled by the 0-10V PWM interface. The resistive interface controls the dimmable power supply output by changing the resistance between the power supply's control pins.

As resistance increases, the dimming percentage decreases. An optocoupled light-dependent resistor (optocoupled-LDR) was chosen as variable resistance. An LDR is a component that changes its resistance in response to the light intensity. This component has an LED and an LDR enclosed in a single package. When the LED is powered, the light intensity logarithmically decreases the resistance of the LDR. A Voltage Controlled Current Source (VCCS) is used in the circuit to drive at a constant current the LED in the optocoupled LDR. The VCCS is composed of an operational amplifier (U2), a transistor (Q1), and a resistance (R5). See the appendix for an explanation on how the VCCS works.

A Digital to Analog Converter (DAC) is needed to provide a digitally controlled variable voltage. Since the RP2040 does not have an onboard DAC, we converted

the high-resolution PWM (16bit) to a constant voltage by using two low-pass filters. Simulation made in LTspice® (Analog Device) shows the operation of the circuits (**Figure 2.5** and **Figure 2.6**). To avoid saturating the operational amplifier, the 3.3V amplitude of the PWM (**Figure 2.5**-A), is reduced to 1 V through a voltage divider (**Figure 2.5**-B). The two first-order low-pass filters put in series smooth the square waves to a close-to stable voltage (**Figure 2.5**-C,D). In this way, we can generate an adjustable current flowing through the LDR that depends on the duty-cycle of the PWM (**Figure 2.6**).

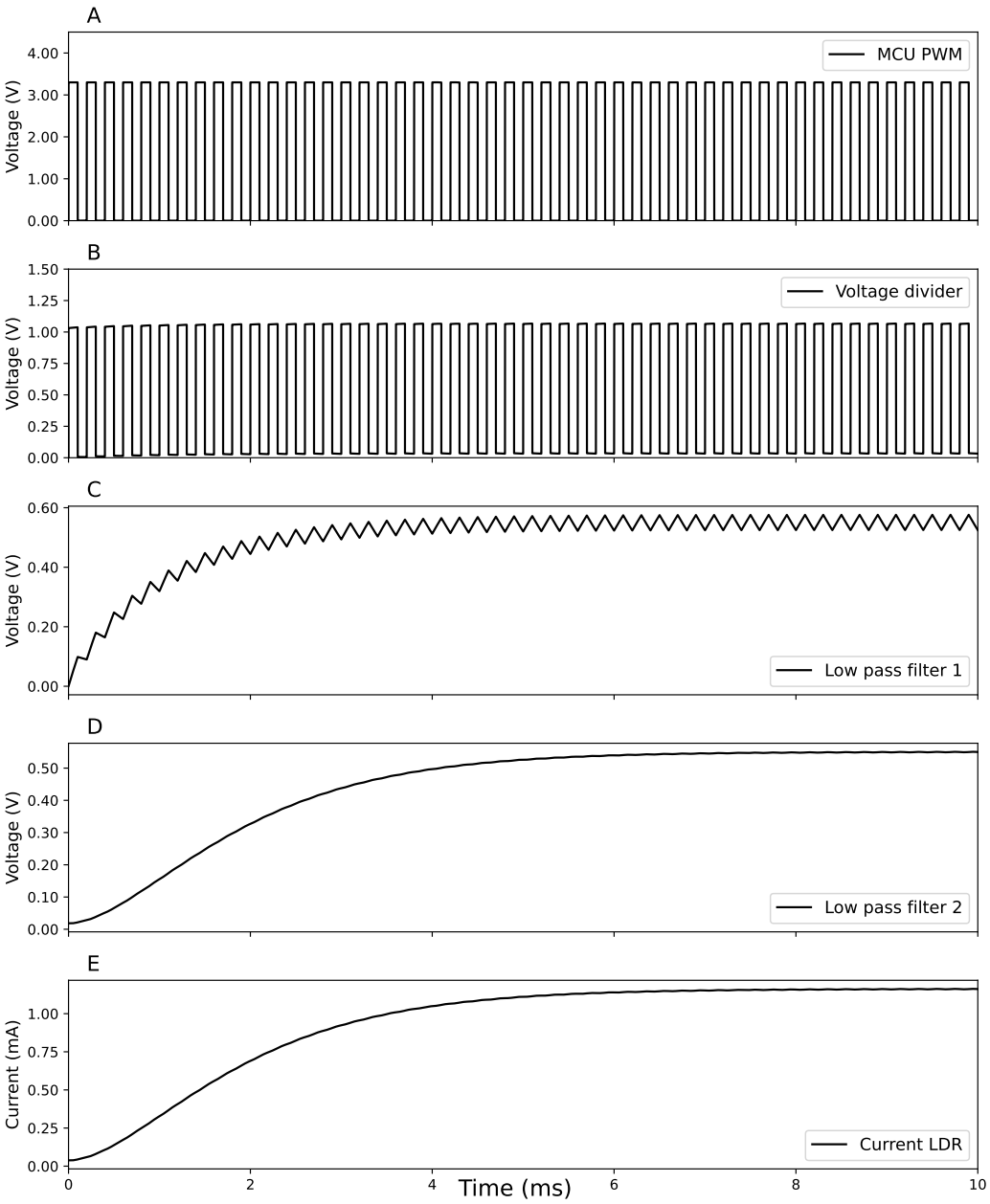

Figure 2.5. *Difference in voltage/current in the different parts of the resistive circuit. At the output of the MCU (A). After the voltage divider (B). After the first LP filter (C). After the second LP filter (D). The current flowing on NODE 1 (E)*

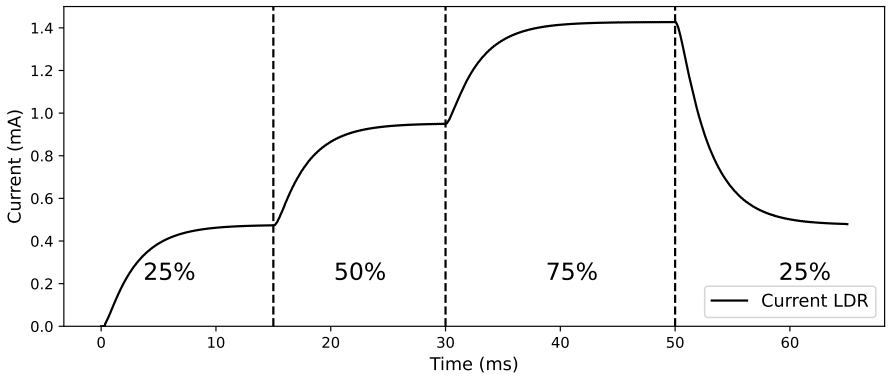

Figure 2.6. *Current flowing through NODE 1 after a change of the PWM duty-cycle (in percentage*

2.2.3 Coding the MCU

In this work, the MCU uses a MicroPython program as firmware. When a MicroPython device starts up, it automatically looks for a file named "main.py" on its file system and executes the code within that file. Developers often write their main application logic in the "main.py" file, including initializing hardware components, configuring settings, and implementing the desired functionality. The Thonny IDE [22] was used to upload to the RP2040 the main application and, in some cases, the desired dimming values were stored in an additional text file saved in the MCU's memory. The MCU is programmed to initialize the I/O and generate a PWM signal at a fixed frequency. The duty cycle of PWM is adjusted based on predefined values, each of which is followed by a specific time delay before the process is repeated (for an example, see Code 1 in the supplementary, Listing 2.1). Due to the limited number of functions and libraries available by default in MicroPython, more complex fluctuations, such as a sinusoidal modulated irradiance, are best obtained by calculating the dimming steps on a computer and then providing them as a text file to MCU (see Code 2 and 3 in the supplementary, Listing 2.2, Listing 2.3). When generating a complex light profile with thousands of points (i.e. when mimicking diurnal light intensity), it is also easier to upload them to the MCU as an additional text file and then read them sequentially (see Code 4 in the supplementary, Listing 2.4). If the external text file is too large to fit the onboard memory of the MCU, an external memory device can be used (i.e. an SD card). Examples demonstrating SD card setup and reading in MicroPython for RP2040 microcontroller can easily be found online.

2.2.4 Calibrating the setup

To achieve specific light intensities, often required in photosynthetic photon flux density (PPFD), it is necessary to calibrate the control circuits. The approach to calibration depends on the type of interface used and involves utilizing a photosynthetic active radiation (PAR) sensor, (e.g. Li-250, LI-COR Inc). In the case of the 0-10V PWM interface (**Figure 2.2**), the duty cycle generated by the MCU is inversely equal to the dimming percentage of the power supply; for example, if the duty-cycle of the PWM generated by the MCU is 25%, the dimming percentage of the power supply will be 75%. In the case of the resistive interface (**Figure 2.4**), a calibration table is required. A calibration table is made by sequentially changing the duty-cycle of the PWM generated by the MCU and noting the corresponding PPFD produced by the power supply. The relation between duty-cycle and dimming percentage is non-linear due to the characteristic of the optocoupled LDR (**Figure 2.4**-U2).

2.2.5 Light setup

The light control unit was used to control one high-power and one low-power light setup, respectively 3800W and 25W power output (**Figure 2.1**-[1]). The high-power setup was composed of 6 Vypr V2 modules (Fluence), used in controlled environment rooms and greenhouses as light source. The low-power setup was comprised of a single LED (L2C5-30HG1203E0900, Lumiled) powered by a dimmable power supply (LCM40, Mean Well), which was used as an actinic light source in laboratory experiments.

2.2.6 Light measurement

The irradiance profiles generated by the controlling circuit were measured using a light-measuring setup made of off-the-shelf components (Figure 1-[7] to [9]). A Li-Cor® quantum sensor was connected to a commercial transimpedance amplifier (DLPCA-200, Femto), which has an output socket and also has a faster frequency response than the Li-Cor PAR meter (Li-250, LI-COR, Inc). The output was recorded using a datalogger with a sampling frequency of 1kHz (PICOLOG 1216 - Pico Technology). The Li-Cor® sensor/Femto pair were calibrated using the same sensor with a Li-Cor readout meter (Li-250, LI-COR, Inc). The same off-the-shelf photodiode, transimpedance amplifier, and datalogger were used to measure a profile of natural irradiance from a north-facing window (coordinates 51.984620, 5.661515) with a sampling frequency of 1,5Hz (see supplementary material).

2.3 Results

2.3.1 Generating different patterns of light

The presented method was used to generate 3 different light patterns (**Figure 2.7**) using a benchtop light setup composed of a white light LED and a 60W dimmable power supply. The power supply accepted a 0-10V PWM dimming protocol and was therefore controlled using the circuit of **Figure 2.2**.

The first light pattern was a series of step-wise irradiance changes (**Figure 2.7**-A). The light setup was controlled to achieve 6 different intensities, respectively 100%, 50%, 10%, 75%, 10%, and 90% of its maximum output. The MCU was programmed to change the duty-cycle of the PWM control signal 6 times with a delay of 20 seconds between each change (see Code 1 in the supplementary, Listing 2.1). A step-wise change of light intensity of this kind can be used in a growing environment to produce a steady light intensity or to expose plants to a sudden change of irradiance to assess the kinetics of a physiological response (e.g. changes in carbon assimilation rates, changes in quantum efficiency of photosystem II, etc.).

The second light pattern generated was a 4Hz sinusoidal fluctuation (**Figure 2.7**-B). When used as an actinic light pattern it can be used to study the frequency response of plant's photosynthesis through chlorophyll fluorescence or photoacoustic signal [23, 24]. For this more complex pattern, the microcontroller was programmed (see Code 3 in the supplementary, Listing 2.3) to iterate repetitively through an array of values encoding duty-cycles changing as one period of a sinusoid. The array of values encoding the duty-cycle was first generated on a PC using a Python script (see Code 2 in the supplementary, Listing 2.2). The frequency of the sinusoidal output depends on the delays coded between each change of duty-cycle. It is worth noting that while the circuit supports change of duty-cycles in less than milliseconds, the maximum achievable light fluctuation frequency mostly depends on the response time of the power supply (see controlling light setup section).

The last light pattern mimicked a natural irradiance recorded during a day (**Figure 2.7**-C). This light pattern has therefore a profile of the kind to which a plant could be exposed in nature. Because of the high number of values in the light intensity dataset (above 43000 points), the dataset was supplied to the microcontroller memory as an additional text file along with the main program (see Code 4 in supplementary, Listing 2.4).

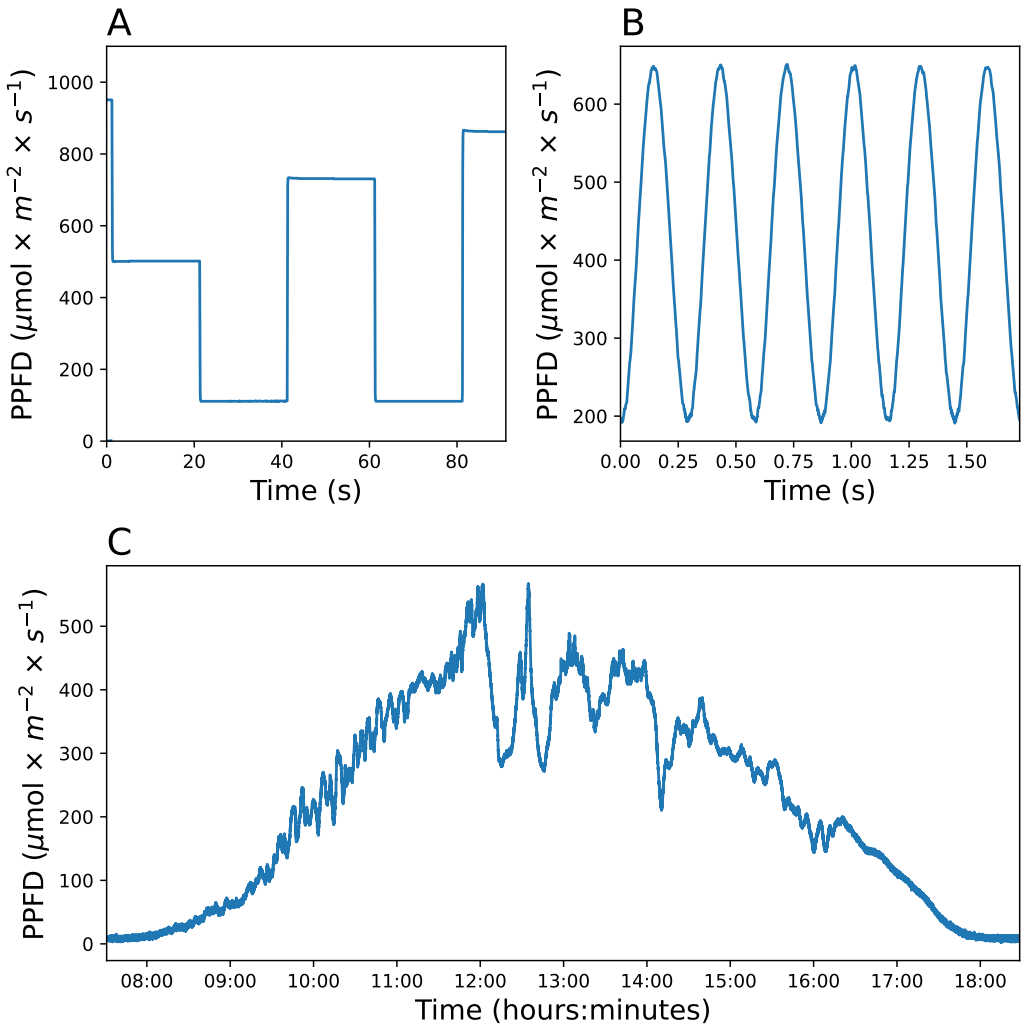

Figure 2.7. *Different light patterns generated with the 0-10V PWM interface controlling a benchtop light setup. Stepwise change in irradiance (A); sinusoidal fluctuation (B); mimicked natural light fluctuation (C)*

2.3.2 Controlling different light setup

The flexibility of the system was assessed by controlling two light setups with different power outputs; a low-power setup (30W) used as a laboratory light source, and a high-power setup (3600W) used in a growth chamber. The low-power light setup was the one used to generate the light pattern in **Figure 2.7**. The high-power light setup consisted of six LED arrays powered by six power supplies (Vypr V2 modules, Fluence). We tested both light setups using the 0-10V PWM circuit (**Figure 2.2**) programmed to generate a light pattern with sequential step-wise fluctuation (see Code 1 in the supplementary, Listing 2.1).

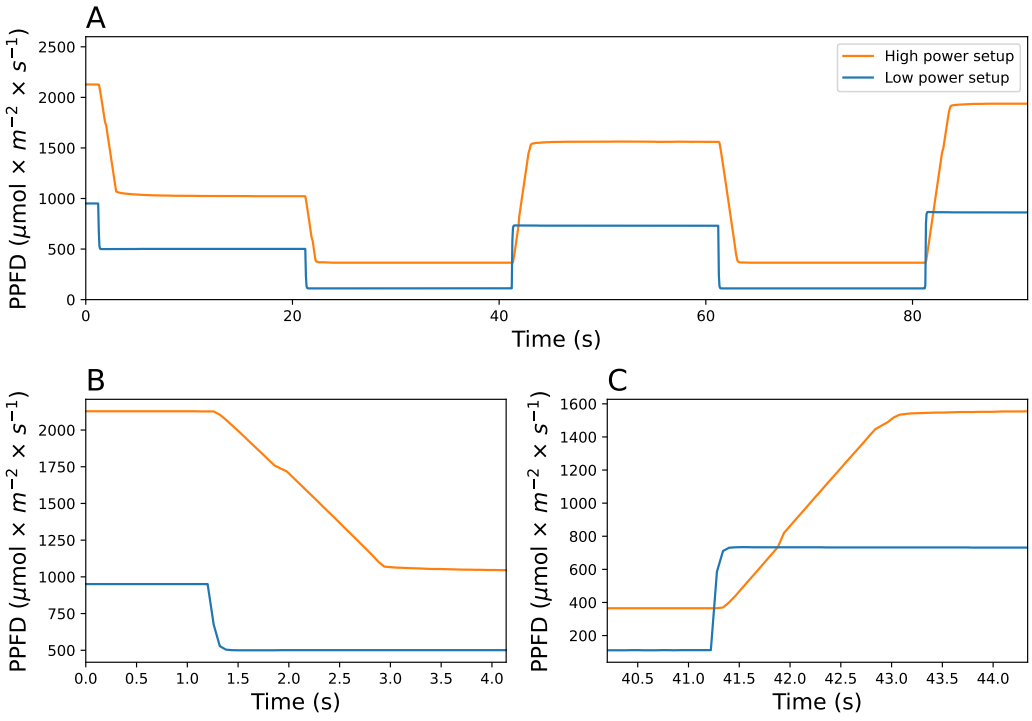

Figure 2.8. *Step-wise pattern generated with a high power and low power light setup controlled by the 0-10V PWM interface (a). Close-up view of the descent time during the transition from 100% to 50% dimming percentage (b). Close-up view of the ascent time during the transition from 10% to 75% dimming percentage (c).*

There is a noticeable difference in the time response of the irradiance changes between the high-power and low-power configurations (**Figure 2.8**), although the control circuit used was the same for both. A longer time response limits the speed at which a change

in irradiance of a certain amplitude can be achieved. The response time for changes to the irradiance output of the high-power setup was longer when compared to the low-power setup. The longer response time depends on the electrical design of the power supply rather than the controller. Some power supplies, especially those made to drive large loads in electrically noisy environments, are designed to prevent rapid or sudden fluctuations in the output current by damping the response of the power supply [25]. Note, that power supply with a longer time response still offers the capability of achieving rapid fluctuations, albeit with a smaller amplitude.

2.4 Discussion

In plant research, understanding and controlling light intensity is crucial for gaining insights into plant growth, development, and responses to environmental cues. However, there is a gap between the limited commercial options available for controlling light intensity and the actual requirements of plant research. To bridge this gap, in the last years, several inexpensive laboratory-built dynamic lighting systems have been developed. While these systems offer affordable solutions, they often prioritize simplicity over the ability to create a complex irradiance profile. For example, some systems were designed to produce step changes between two limiting (maximum and minimum) irradiances [14]. In contrast, our method enables an almost continuous dimming of the light (with a 16-bit resolution in our current design), opening the possibility of generating a wealth of different light profiles. Other approaches directly switch the current flowing through the LED on and off using a PWM signal, resulting in a dynamic but pulsed control of the light intensity [26]. Employing such pulsed control for growing or studying plants is problematic as it may impact the physiological processes of the plants [20]. While our method also uses PWM, it is only used as control feedback for the power supply and the current to the LED is kept constant. Note, however, that some power supplies may flicker at a dimming percentage below 10% due to instability of the regulation of the power supply.

In nature, most light flecks take place in less than 2 seconds, but there is a lack of studies on how plants respond to fluctuations shorter than 20 seconds [19]. Therefore, achieving rapid fluctuations was a requirement in the design of our method. The 0-10V PWM circuit (**Figure 2.2**) and the resistive circuit (**Figure 2.4**) exhibit different response times when changing the controlling signal. The 0-10V PWM circuit can, in principle, switch between two control signals within microseconds, while the resistive circuit requires approximately 10-15ms to stabilize to a new signal (**Figure 2.6**). However, the main limitation to achieving fast fluctuations depends on the electrical design of

the power supply (**Figure 2.8**); some power supplies are designed to damp changes of irradiance to avoid fluctuations that could be undesirable in certain environments as offices or domestic lightning. On the other hand, even with these power-supply design limitations, the fluctuations below one second are easily achievable with the method we use. An additional strength of the method we have developed lies in its ability to control a wide range of power supplies including those with very different wattages. The electrical isolation between the control circuit and the power supply enables its integration into light setups found in greenhouses or climate chambers. The primary limitation in the implementation of our method is the requirement for a dimmable power supply. Fortunately, the majority of existing light setups can be externally dimmed.

The systems we have developed can be particularly useful in photosynthesis research, where there is a growing interest in understanding the effects of fluctuating light on photosynthesis. To date the method described in this study has been used in three distinct research projects in which changes in growth light pattern were shown to affect photosynthesis and plant development [27–29]. In the first investigation, differing profiles of irradiance, each providing the same daily integral of irradiance, were compared. Three different light growth conditions, one sinusoidal, one square wave, and one fluctuating were tested on a panel of different *Arabidopsis thaliana* genotypes. The sinusoidal light regime was shown to improve shoot biomass in comparison to square wave light regimes [27]. In the other two projects, the effect of specific allelic variation in different environmental conditions was assessed using *Arabidopsis thaliana* genotypes grown in a range of constant and fluctuating light conditions. One light regime included large fluctuations every 100ms, which resulted in significant biomass differences in plants with allelic variation for an NDH subunit. This finding was essential to reveal the possible relevance of the NDH complex in field conditions [28]. Altogether, this shows how our method can be useful to reveal novel physiological insights as well as reveal relevant genetic variants that can be used for crop improvements. Finally, our method could be used in modulating the irradiance in systems to measure the frequency-dependent photosynthetic responses (**Figure 2.7**-B).

In conclusion, our work provides an outline of how to build a fluctuating light setup along with the open-source code needed for its control. We expect that this will simplify the implementation of a dynamic light system for researchers. Programmable light setups that generate reproducible and complex patterns of light intensity are necessary for experiments aimed at disentangling the effects of the multiple mechanisms affecting the rates of carbon assimilation. However, light intensity is not the only variable

parameter to affect plant physiology in nature. Fluctuations in CO_2 mole fraction or, water vapor mole fraction between a leaf and the surrounding air, or fluctuations in temperature or light spectrum are all factors that also affect carbon assimilation [30]. To fully understand plant's physiological response to fluctuations in natural settings more studies are required in controlled environments with realistic dynamic environmental parameters.

References

1. Alter, P., Dreissen, A., Luo, F.-L. & Matsubara, S. Acclimatory responses of Arabidopsis to fluctuating light environment: comparison of different sunfleck regimes and accessions. *Photosynthesis Research* **113,** 221–237 (2012).
2. Matthews, J. S., Vialet-Chabrand, S. & Lawson, T. Acclimation to fluctuating light impacts the rapidity of response and diurnal rhythm of stomatal conductance. *Plant Physiology* **176,** 1939–1951 (2018).
3. Slattery, R. A., Walker, B. J., Weber, A. P. M. & Ort, D. R. The impacts of fluctuating light on crop performance. *Plant Physiology* **176,** 990–1003 (2018).
4. Kaiser, E., Morales, A. & Harbinson, J. Fluctuating light takes crop photosynthesis on a rollercoaster ride. *Plant Physiology* **176,** 977–989 (2018).
5. Murchie, E. H., Kefauver, S., Araus, J. L., Muller, O., Rascher, U., Flood, P. J. & Lawson, T. Measuring the dynamic photosynthome. *Annals of Botany* **122,** 207–220 (2018).
6. Vialet-Chabrand, S., Matthews, J. S., Simkin, A. J., Raines, C. A. & Lawson, T. Importance of fluctuations in light on plant photosynthetic acclimation. *Plant Physiology* **173,** 2163–2179 (2017).
7. Harbinson, J. & Woodward, F. I. Field measurements of the gas exchange of woody plant species in simulated sunflecks. *Annals of Botany* **53,** 841–851 (1984).
8. Poorter, H., Fiorani, F., Pieruschka, R., Wojciechowski, T., Van Der Putten, W. H., Kleyer, M., Schurr, U. & Postma, J. Pampered inside, pestered outside? Differences and similarities between plants growing in controlled conditions and in the field. *New Phytologist* **212,** 838–855 (2016).
9. Townsend, A. J., Ware, M. A. & Ruban, A. V. Dynamic interplay between photodamage and photoprotection in photosystem II. *Plant, Cell & Environment* **41,** 1098–1112 (2018).
10. Kromdijk, J., Głowacka, K., Leonelli, L., Gabilly, S. T., Iwai, M., Niyogi, K. K. & Long, S. P. Improving photosynthesis and crop productivity by accelerating recovery from photoprotection. *Science* **354,** 857–861 (2016).
11. De Souza, A. P., Burgess, S. J., Doran, L., Hansen, J., Manukyan, L., Maryn, N., Gotarkar, D., Leonelli, L., Niyogi, K. K. & Long, S. P. Soybean photosynthesis and crop yield are improved by accelerating recovery from photoprotection. *Science* **377,** 851–854 (2022).
12. Garcia-Molina, A. & Leister, D. Accelerated relaxation of photoprotection impairs biomass accumulation in Arabidopsis. *Nature Plants* **6,** 9–12 (2020).
13. Kubásek, J., Urban, O. & Šantrůček, J. C $_4$ plants use fluctuating light less efficiently than do C $_3$ plants: a study of growth, photosynthesis and carbon isotope discrimination. *Physiologia Plantarum* **149,** 528–539 (2013).
14. Leakey, A. D. B., Press, M. C., Scholes, J. D. & Watling, J. R. Relative enhancement of photosynthesis and growth at elevated CO_2 is greater under sunflecks than uniform irradiance in a tropical rain forest tree seedling. *Plant, Cell & Environment* **25,** 1701–1714 (2002).
15. Schneider, D., Lopez, L. S., Li, M., Crawford, J. D., Kirchhoff, H. & Kunz, H.-H. Fluctuating light experiments and semi-automated plant phenotyping enabled by self-built growth racks and simple upgrades to the IMAGING-PAM. *Plant Methods* **15,** 156 (2019).
16. Annunziata, M. G., Apelt, F., Carillo, P., Krause, U., Feil, R., Mengin, V., Lauxmann, M. A., Köhl, K., Nikoloski, Z., Stitt, M. & Lunn, J. E. Getting back to nature: a reality check for experiments in controlled environments. *Journal of Experimental Botany* **68,** 4463–4477 (2017).
17. Wu, Y.-E. Design and implementation of an LED automatic lighting system for plant factories. *IEEE Photonics Journal* **13,** 1–9 (2021).
18. Of North America, I. E. S. *Lighting control protocols* (2011).
19. Morales, A. & Kaiser, E. Photosynthetic Acclimation to Fluctuating Irradiance in Plants. *Frontiers in Plant Science* **11,** 268 (2020).
20. Kanechi, M. *Growth and photosynthesis under pulsed lighting* in *Photosynthesis - From Its Evolution to Future Improvements in Photosynthetic Efficiency Using Nanomaterials* (eds Cañedo, J. C. G. & Lizárraga, G. L. L.) (InTech, 2018).
21. Lutron. *0-10V Lutron Application Note 587* 2021.
22. Annamaa, A. *Introducing Thonny, a Python IDE for learning programming* in *Proceedings of the 15th Koli Calling Conference on Computing Education Research* (ACM, Koli Finland, 2015), 117–121.
23. Dau, H. Molecular mechanisms and quantitative models of variable photosystem II fluorescence. *Photochemistry and Photobiology* **60,** 1–23 (1994).
24. Nedbal, L., Březina, V., Červený, J. & Trtílek, M. Photosynthesis in dynamic light: systems biology of unconventional chlorophyll fluorescence transients in Synechocystis sp. PCC 6803. *Photosynthesis Research* **84,** 99–106 (2005).
25. Instrument, T. *Power Management Guide 2018* 2018.

26. Almeida, C. C., Almeida, P. S., Pinto, M. F., Valle, R. L., Martins, C. H. N. & Braga, H. A. C. *A fast dynamics and PWM-dimmable LED driver for accurate control of illumination in plants physiology experiments* in *2014 11th IEEE/IAS International Conference on Industry Applications* (IEEE, Juiz de Fora, Brazil, 2014), 1–5.
27. Schiphorst, C., Koeman, C., Caracciolo, L., Staring, K., Theeuwen, T. P. J. M., Driever, S. M., Harbinson, J. & Wientjes, E. The effects of different daily irradiance profiles on Arabidopsis growth, with special attention to the role of PsbS. *Frontiers in Plant Science* **14,** 1070218 (2023).
28. Theeuwen, T. P., Lawson, A. W., Tijink, D., Fornaguera, F., Becker, F. F., Caracciolo, L., Fisher, N., Kramer, D. M., Wijnker, E., Harbinson, J. & Aarts, M. G. *The NDH complex reveals a trade-off that constrains maximising photosynthesis in Arabidopsis thaliana* preprint (2022).
29. Theeuwen, T. P., Logie, L. L., Put, S., Bagheri, H., Łosiński, K., Drouault, J., Flood, P. J., Hanhart, C., Becker, F. F., Wijfjes, R., Hall, D., Kramer, D. M., Harbinson, J. & Aarts, M. G. *Plethora of QTLs found in Arabidopsis thaliana reveals complexity of genetic variation for photosynthesis in dynamic light conditions* preprint (2022).
30. Kaiser, E., Morales, A., Harbinson, J., Kromdijk, J., Heuvelink, E. & Marcelis, L. F. M. Dynamic photosynthesis in different environmental conditions. *Journal of Experimental Botany* **66,** 2415–2426 (2015).

2.5 Supplementary

2.5.1 Way of working of VCCS

The operational amplifier in the VCCS endeavors to keep the same voltage between its inverting pin (the '-' pin, number 3, **Figure 2.4**) and its non-inverting pin (the '+' pin, number 1, **Figure 2.4**). If 800mV is applied to the non-inverting input, the operational amplifier (U2) will adjust the current flowing through Q1 so that the inverting input will reach 800mV. This also means that on node 1 (**Figure 2.4**) there will be 800mV. The current flowing through R5, and therefore through U2 will be:

$$I_{optoLDR} = \frac{V_{Node1}}{R_{R5}} = \frac{V_{800mV}}{430\Omega} \approx 2mA \tag{2.1}$$

According the NSL-32-SR2 datasheet, when the LED's side is driven with 2mA, the LDR resistance will be roughly 80Ω.

2.5.2 Python code

Listing 2.1. Code 1 – MCU micropython code to generate step-wise switch light pattern

```
from machine import Pin # import library required for the script
import time

pin15 = machine.Pin(15, machine.Pin.OUT) # initialize pin 15 as output
pin15 = machine.PWM(pin15) # set the initialized pin as PWM output
pin15.freq(1000)           # set the frequency of the PWM signal to 1KHz
delay = 20                 # time delay
values = [0, 32768, 58982, 16384, 58982, 6554] # duty-cycle values
for value in values:
    pin15.duty_u16(value)  # set the PWM duty-cycle
    time.sleep(delay)      # sleep for 20 seconds
```

Code 1 exemplify the steps followed by the MCU to create a 6 steps light fluctuation. The I/O on pin15 is first initialized and set to generate a PWM signal at a 1kHz frequency. The MCU iterates through 6 values, set the PWM's duty-cycle to that value through the

command `gpio.duty_u16()` and wait for a predefined amount of time. The variable value is a number that sets the duty-cycle, which ranges from 0 to 65535 (unsigned 16bit). The values 0 and 65535 stands for a duty-cycle of 0% and 100% respectively. As a practical example, to encode a duty-cycle of 75% the value should be set to 49151 (65535 * 0.75 = 49151, rounded to the closest integer).

Listing 2.2. Code 2 –Python code to generate values of duty-cycle encoding for a sine-wave shaped light profile

```
import numpy as np
from math import pi, sin
pwm_max = 65535 # desired maximum PWM duty-cycle value
pwm_min = 32768 # desired minimum PWM duty-cycle value
x = np.arange(0, 2*pi, 0.1) # generate numbers ranging between 0 and 2pi
                            # with a 0.1 steps

y = [sin(i) for i in x]     # generate one values for sine period
y = (y - np.min(y)) / (np.max(y) - np.min(y)) # normalize y between 0
                                              # and 1

y *= pwm_max - pwm_min # normalize the values of the sine wave
                       # in the  duty-cycle range
y += pwm_min
```

Listing 2.3. Code 3 – MCU micropython code use the array generated in code 2 to produce periodic sinewave-shaped light profile

```
from machine import Pin
import time
pin15 = machine.Pin(15, machine.Pin.OUT)
pin15 = machine.PWM(pin15)
pin15.freq(1000)
y = [x1,x2,x3, ect..]       # array previously generated using code 2
delay = 0.050
while True:
    for value in y:
        pin15.duty_u16(value)  # set the duty-cycle
        time.sleep(delay)      # sleep
```

Listing 2.4. Code 4 – MCU micropython code to generate a sinusoid light pattern

```
from machine import Pin
import time
pin15 = machine.Pin(15, machine.Pin.OUT)
pwm15 = machine.PWM(pin15)
pwm15.freq(1000)
delay = 1
with open("reference.txt","r") as f:
    for value in f:
        value = int(value)    # convert the read value to integer
        pwm15.duty_u16(value) # set the duty-cycle
        time.sleep(delay)     # sleep
```

Chapter 3

Antenna size and photochemical yield of photosystem II: dependency on growth irradiance

A version of this chapter is in preparation by: Ludovico Caracciolo, Jeremy Harbinson, Léo Martin, Lennart Ramakers, Bernard Genty and Herbert van Amerongen.

3

Abstract

Harvesting light energy and converting it into chemically stored energy poses a significant challenge for higher plants. Capturing excessive energy can lead to photodamage of the photosynthetic apparatus, while insufficient harvesting limits the energy supply for photosynthesis. Striking the right balance is crucial for the optimization of photosynthetic efficiency and durability. At photosystem II (PSII) the amount of harvested light energy depends on absorption cross-section (i.e. antenna size). The greater the number of light-harvesting complexes (LHCs) bound to the PSII reaction centre (RC), the greater the rate of excitation per unit reaction centre. However, theory suggests that the larger the antenna size the lower the quantum yield of charge separation due to the prolonged residence time of the excitation in the LHCs/RC complexes of PSII. By using biophysical methods, such as microsecond-resolved fluorescence induction and picosecond-resolved fluorescence decay *in folio*, PSII antenna size and quantum yield were assessed in different plant species grown under different irradiances. Our results indicated that PSII antenna size is regulated in response to irradiance conditions, even within the same leaf. At the same time we have observed small but significant differences in the maximum quantum yield of PSII (F_v/F_m) on growth irradiance which linearly correlates with PSII antenna size, with a larger antenna size being correlated with only a slightly lower quantum efficiency for PSII charge separation.

3.1 Introduction

Photosynthetic reactions convert light energy into chemical energy fixed in carbohydrates, thereby supporting the energy needs of almost all living organisms and fueling the biosphere. In recent years, a renewed interest has sparked efforts to breed crops with increased photosynthetic efficiency, aiming to increase the biomass production and make agriculture not only the source of our food and feedstock but also a source of raw materials for a sustainable industry. In a growth environment where abiotic and biotic stress are minimized, the dry biomass accumulation is proportional to the intercepted radiation that is used to generate carbohydrates [1]. The ratio between energy output (biomass) and energy input (via radiation) is often called the efficiency or yield of photosynthesis [2], although the exact definition can take different forms. The yield at which a leaf can convert a certain light fluence to biomass is given by the light-use efficiency (LUE), defined as the ratio between net rate of carbon fixation (A_{net}, µmol m^{-2} s^{-1}) and the incident photosynthetic photon flux density (PPFD, µmol m^{-2} s^{-1}). LUE measured at atmospheric CO_2 as a function of increasing PPFD evolves as a growth curve which saturates at a certain maximum value (A_{sat} , µmol m^{-2} s^{-1}). This A_{sat}, or light-saturated assimilation rate, can vary significantly among different genotypes and species. Plants with C4 metabolism usually have higher values of A_{sat} than C3 species due to their special anatomical adaptation which allows them to avoid energy consuming processes that do not lead to carbon assimilation (e.g. photorespiration). Interestingly, marked differences for A_{sat} can also be observed among species with C3 metabolism. Recent works showed that some Brassicaceae possess exceptionally high A_{sat} values (>40 µmol m^{-2} s^{-1}) when grown at high PPFD, almost double the value that is observed for the model plant *A. thaliana* [3].

The efficiency of photochemistry must be maintained to achieve high LUE at saturating irradiance. Photochemistry is the complex cascade of light-driven chemical reactions that involve multiple pigment-protein complexes and electron carriers and generates the energy potential needed for ATP and NADPH production. When the energy generation exceeds the leaf's energy needs, photochemistry is down-regulated to avoid damage to the photosynthetic machinery [4]. For example, at saturating light intensity, the flow of electrons generated by PSII charge separation can exceed the capacity of the electron transport chain (ETC) and/or the metabolic energy needs. The ETC becomes increasingly reduced by accumulation of electrons on the PSII acceptor side, which leads to closure of the PSII reaction centers, and a decrease in PSII quantum efficiency. Additionally, the acidification of the lumen activates various mechanisms of non-photochemical quenching

that dissipate excitation energy as heat, which further decreases the energy available to PSII for charge separation. The energy absorbed by PSII which results in charge separation depends on the PSII relative functional antenna size σ_f(PSII), which is the product of PSII optical cross-section σ(PSII) and its maximum quantum yield for charge separation Φ_{CS}(PSII), both being dependent on the excitation wavelength, as:

$$\sigma_f(PSII) = \sigma(PSII) \cdot \Phi_{CS}(PSII) \tag{3.1}$$

Reducing σ_f(PSII) could help to maintain a high LUE with less energy losses at saturating irradiance and at the same time allowing more light to penetrate the leaf. This can happen during long-term acclimation to high light which involves the reduction of σ_f(PSII) [5, 6]. This in turn reduces the rate of charge separation, avoiding over-reduction of the ETC which would in turn lead to an increased production of reactive oxygen species that can damage the photosynthetic apparatus [4, 7]. Similarly, a decrease of σ_f(PSII) has been reported to correlate with higher LUE under light-saturating conditions [8]. This finding prompted researchers to investigate whether regulating photosystem antenna size could lead to higher LUE [9]. To date, genetic mutations leading to reduced photosystem antenna sizes have yielded contrasting results [10]. This is potentially due to the pleiotropic effects that can result from modifying the light-harvesting system, such as a decrease in the energetic coupling between the photosystem reaction centers (RC) and the LHCs. Although not relevant for our present study it can also lead to a decrease in competitiveness due to increased light availability to potential competitors growing in the under canopy [11].

We explored the regulation of σ_f(PSII) in plants known to achieve high rates of photosynthesis at saturating light intensity to assess if it could be one of the mechanisms responsible for higher-than-usual LUE. We compared σ_f(PSII) for three Brassicaceae species reported to have higher-than-average A_{sat} values; *Hirschfeldia incana*, *Brassica nigra* and *Brassica rapa* and another member of the Brassicaceae family, the model plant *Arabidopsis thaliana*, all grown in low light (LL, 250 µmol m^{-2} s^{-1}) and high light (HL, 1100 µmol m^{-2} s^{-1}). We used independent biochemical and spectroscopic methods to assess the ratio between LHCs and PSII RCs. The results show that at higher light intensity σ_f(PSII) decreases, while plants with high rates of LUE appear to have a smaller σ_f(PSII).

3.2 Materials and methods

Measurements and data collection were performed in two separate periods and places. The first set of measurements was acquired at the BIAM-CEA, Cadarache, France, and consisted of measurements of sub-millisecond and sub-microsecond fluorescence induction kinetics. The second set of measurements was perfprmed at Wageningen University and Research (WUR), Wageningen, the Netherlands and consisted of picosecond and nanosecond fluorescence decay measurements and sub-millisecond fluorescence induction curves. The growth conditions (see section Climate chamber growing conditions) were kept as similar as possible.

3.2.1 Climate chamber growing conditions

Seeds of *Brassica nigra*, *Brassica rapa*, *Arabidopsis thaliana* and *Hirschfeldia incana* were directly sown in 2 L pots filled with peat and supplemented with 2 g/L of slow-release fertilizer. The plants were cultivated in a climate chamber maintained at 24 °C during the day and 21 °C at night. Humidity was consistently maintained at 70%, and the photoperiod was set to 12 hours of light and 12 hours of darkness. Within the climate cell, screens divided the space to accommodate two light regimes: one with low light (LL, 250 µmol m^{-2} s^{-1}) and the other with high light (HL, 1100 µmol m^{-2} s^{-1}). Three to four weeks after sowing, fully expanded leaves were detached just before the lights turned on in the climate cell. The petiole of the detached leaf was kept in demineralized water and brought to the laboratory for the measurements. The leaves were kept in complete darkness until the measurements.

3.2.2 Fluorescence induction measurements

Chlorophyll fluorescence induction curves were recorded with sub-millisecond time resolution using a LI-6800 fluorometer (LI-6800 Portable Photosynthesis System, LI-COR, Inc. Lincoln, NE) at WUR. The fluorescence was induced by light flashes of 600 ms duration. The excitation wavelength was centered at 625 nm, with an intensity of 15.000 µmol m^{-2} s^{-1} and the detection wavelengths were selected with a long-pass filter with a cutoff wavelength at 700 nm. The sampling speed was set to 250 kHz.

3.2.3 Fast fluorescence induction measurements

Chlorophyll fluorescence induction kinetics were measured using a custom-built instrument designed by one of us (BG), named Fast Fluorescence Protocol (FFP) in

Cadarache. The custom-built instrument has sub-microsecond time resolution. The fluorescence of dark-adapted detached leaves was induced using very strong (1 mol m^{-2} s^{-1}) light flashes of 300 µs length. The excitation wavelength was centered at 570 nm (±30 nm) and the detection was at 680 nm (±10 nm) (photosystem II centered), the sampling speed was 10 MHz.

3.2.4 Ultrafast fluorescence decay measurements

A streak-camera (C13440-20C, Hamamatsu) was used to measure spectrally resolved fluorescence decay kinetics with picosecond time resolution at WUR. The excitation was provided using a supercontinuum laser (Leukos Rock, Leukos) with an excitation wavelength of 475 ± 10 nm and a spot size of 100 µm. The laser had a repetition rate of 38.3 MHz and the Instrument Response Function (IRF) of the system was $\sim$ 50 ps. The fluorescence was detected between 650 and 790 nm. The raw streak-camera images were 220x1220 pixels sized, with a wavelength-time resolution of 0.11 nm x 1.25 ps per pixel. Detached leaves were placed in a rotating and translating leaf cuvette functioning as a Lissajous-scanner, as detailed in Farooq *et al.* [12]. For each leaf, two sets of fluorescence decay were recorded in series. One set was recorded using low excitation intensity (250 nW) to assess the fluorescence kinetics in conditions of open reaction centers (F_o measurement). A second set was acquired at higher excitation intensity (100 µW) resulting in the partial closure of the reaction centers (F_s measurement).

3.2.5 Chlorophyll extractions

Four leaf disks (area = $0.9 \cdot 10^{-5}$ m^2) were collected after the streak-camera measurement and put in a tube with 2 mL DMF (N,N-Dimethylformamide, 68-12-2, Sigma-Aldrich). The samples were kept in gentle agitation, in the dark and at room temperature for 24 hours. The spectrum of the extracted chlorophyll's was measured with a spectrophotometer (Cary 4000 UV-Vis, Agilent) from 850 nm to 450 nm, with a wavelength resolution of 0.4 nm. The concentration of chlorophyll *a* and *b* was determined using the method described in Wellburn [13]. A molecular weight of 893.509 g/mol and 907.492 g/mol was used for chlorophyll *a* and *b*, respectively.

3.2.6 Statistical analysis

In R (version 4.2.2, R Core Team, 2022), a two-way analysis of variance (ANOVA) was conducted to examine fluorescence parameters ($t_{½}$, k_{avg}(PSII), F_v/F_m, chlorophyll concentration), considering species and growth light intensity as variable factors. Normality was assessed using the Shapiro-Wilk test, and homogeneity of variance was

examined using Bartlett's or Levene's test. In cases where assumptions of normality or equal variance were violated, a two-factor aligned rank transform ANOVA was employed, otherwise a two-way ANOVA [14]. ANOVA significance was determined at $p < 0.05$, and if differences were observed, the differences between groups were assessed using a Tukey post-hoc test.

3.2.7Analysis of Fluorescence Induction curves

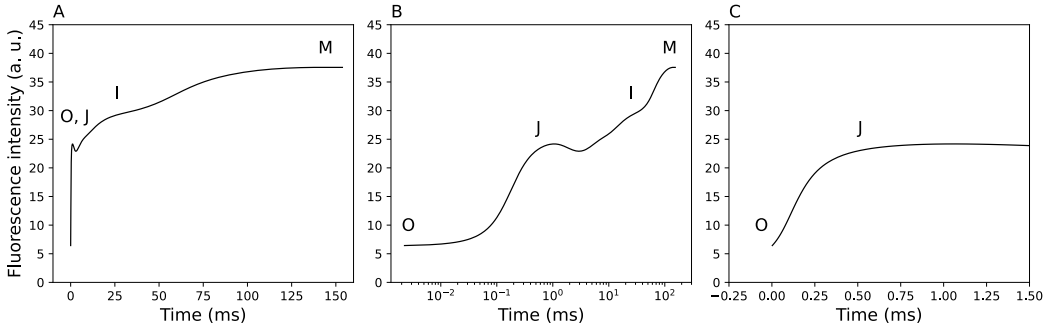

Figure 3.1. *A, Typical fluorescence induction curve (in this case of the leaf adaxial side of B. nigra grown in low light) recorded with a Li-6800 fluorometer plotted on a linear time scale. B, Same fluorescence induction curve plotted on a logarithmic time scale. C, Zoom-in of the first phase of the fluorescence induction curve on a linear time scale. Different stages of the rise are indicated by the characters O (F_o), J (F_j), I (F_i), and M (F_m).*

We used fluorescence induction curves to study differences in PSII functional antennas size, σ_f(PSII). The σ_f(PSII) linearly correlates with the rise kinetics of chlorophyll fluorescence when measured in certain conditions (see below).

In **Figure 3.1**-A a fluorescence induction (FI) curve is shown for the adaxial side of a leaf suddenly exposed to light, measured with millisecond time resolution. The fluorescence evolves from an initial point O (basal fluorescence) to a final point M (maximum fluorescence), with two intermediate "states", J and I. The **Figure 3.1**-A shows the fluorescence induction curve plotted on a linear time scale. The **Figure 3.1**-B shows the same FI plotted on a logarithmic time scale providing a better distinction between the O, J, I and M states. The **Figure 3.1**-C provides an enlarged view of the initial part of the curve. FI curves are usually divided into two parts; the photochemical part (from stage O to stage J) and the photothermal part (from stage J to M) [15].

Two different instruments were used to record the fluorescence induction: a commercial fluorometer (Li-6800, LI-COR, Nebraska, USA) and a custom-built fluorometer (FFP). The commercial fluorometer (Li-6800) was used to record full fluorescence induction curves

(see **Figure 3.1**). The custom-built fluorometer (FFP) was used to record at high speed the photochemical phase of the FI curve on a microsecond time scale (see **Figure 3.2**). **Figure 3.2** shows how the rise kinetics of the photochemical phase depends on the intensity of the flash used to induce the FI; the light intensity was regulated by dimming the power supply driving the light source, which at full power could deliver 1 mol m^{-2} s^{-1}.

The initial fluorescence F_o measured for the dark-adapted plant corresponds to the situation when all PSII reaction centers are still open, i.e. all Q_A molecules are still in the oxidized state. The fluorescence then starts to rise as more and more Q_A molecules become reduced and the emitted fluorescence mirrors somehow the concentration of reduced Q_A (see Lazár [16] and references therein). When blocking the transfer of electrons from Q_A^- to the rest of the electron transport chain (ETC) using DCMU (3-(3,4-dichlorophenyl)-1,1-dimethylurea), the rate of fluorescence induction scales with the intensity of the excitation light and also with the relative functional antenna size of PSII [8, 17]. A larger antenna provides more excitation to the RCs and thus leads to faster reduction of Q_A^-.

The functional PSII antenna size is the product of the PSII optical cross section, σPSII, which include the number of LHCs and the efficiency of the excitation energy transfer, and the PSII maximum quantum yield of charge separation, Φ_{CS}(PSII), both dependent on the excitation wavelength. While DCMU (3-(3,4-dichlorophenyl)-1,1-dimethylurea) is commonly used to block the electron flow from Q_A^- to the rest of the ETC (see application in Malkin & Fork [6], Melis & Homann [17], and Belgio *et al.* [18]), it is a destructive treatment.

We measured σ_f(PSII) non-destructively using an alternative approach. The FI was obtained using a very strong light intensity, achieving a full rise of the photochemical phase that occurs faster than the time required for the electrons to move from Q_A to Q_B (the corresponding time constant is about 100-200 µs, see De Wijn & Van Gorkom [19]). The FFP induces the photochemical part of the FI, from step O to J, within microseconds (see **Figure 3.2**), isolating Q_A kinetically from its acceptor side, Q_B. The excitation is centered in the green wavelength region to maximize the homogeneity of the light intensity throughout the leaf [20, 21]. The fluorescence signal is detected around the PSII peak emission (680 ± 10 nm) and mostly originates from PSII located at the outermost leaf surface. Measurements were carried out on dark-adapted leaves as a precaution to avoid any effect of longed lived non-photochemical quenching mechanism (NPQ). To obtain a measure for the relative functional PSII antenna size, we estimated the half-time ($t_{½}$) of the rise of the photochemical phase, with $t_{½}$ becoming shorter when σ_f(PSII) increases. It should be noted that the fluorescence yield of PSI is relatively small as compared to that

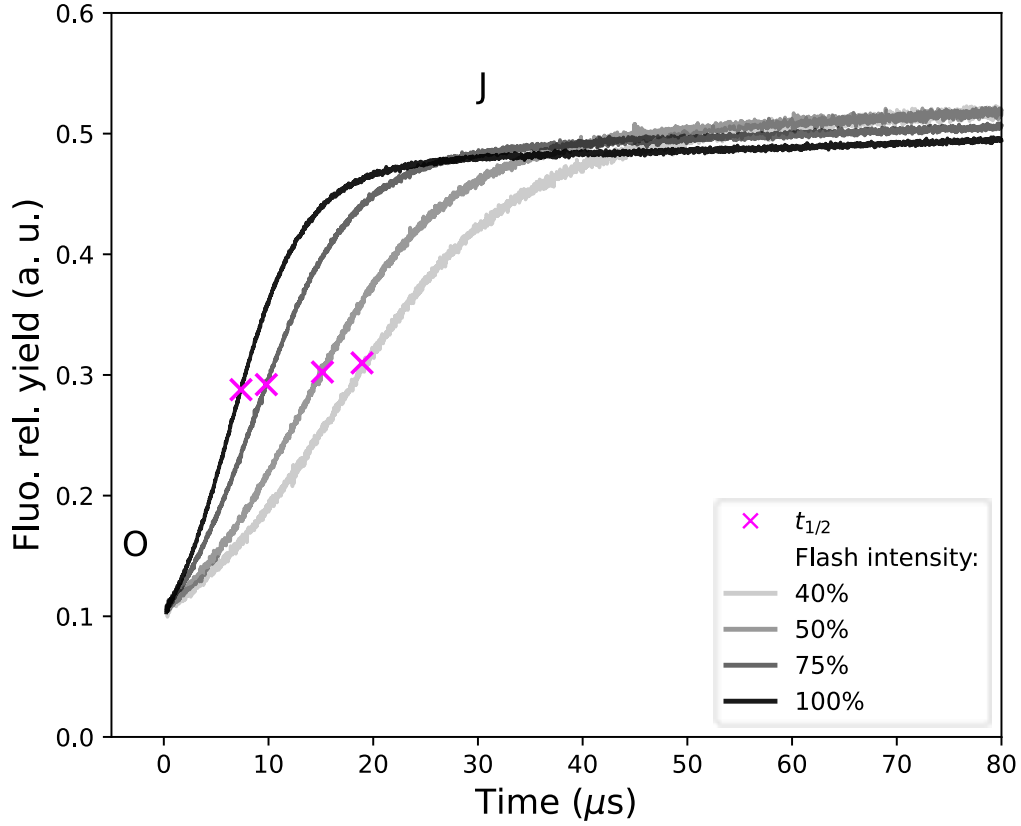

Figure 3.2. *Photochemical phase of a fluorescence induction curve for the adaxial side of a leaf of B. nigra grown in low light measured at different flash intensities adjusted by dimming the power source, the crosses indicate the* $t_{½}$

of PSII and moreover it does not depend on the state of its RC, i.e. whether it is in an open or closed state (see also below).

3.2.8 Deconvolution of PSI and PSII spectra from ultrafast fluorescence measurements

The decay matrices (i.e. streak camera images) were analyzed using the R-based software package TIMP for global and target analysis of time-resolved spectroscopy data [22, 23]. The matrix was fitted with a minimal number of parameters using the following

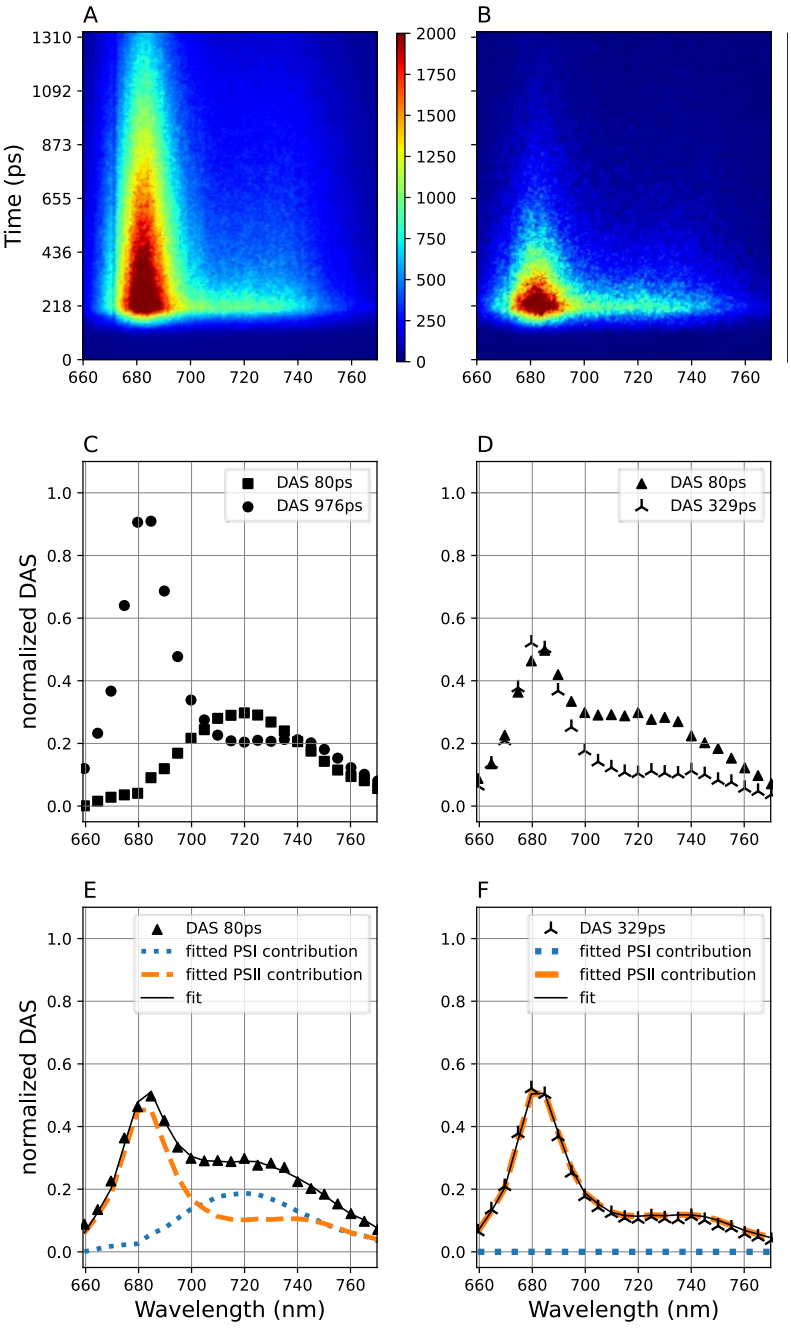

Figure 3.3. (Caption next page.)

Figure 3.3. (Previous page.) *A, Raw image of fluorescence decay measured with 100 µW laser intensity (F_s measurement); B, Fluorescence decay measured with 250 nW laser intensity (F_o measurement); C, Decay Associated Spectra for the F_s measurement, where the sum of the two DAS was normalized to 1 at the maximum; D, Decay Associated Spectra for the F_o measurement, where the sum of the two DAS was normalized to 1 at the maximum; E, 80 ps DAS of the F_o measurement fitted with the PSI and PSII spectra derived from the F_s measurement, with the contribution of PSI and PSII represented by dotted and dashed lines; F, 319 ps DAS of the F_o measurement fitted with the PSI and PSII spectra derived from the F_s measurement, with the contribution of PSI and PSII as dotted and dashed lines.*

equation:

$$f(x,t) = \sum_{i=1}^{n_{comp}} [A_i(\lambda) \cdot e^{-k_i t}] \circledast IRF(t) \tag{3.2}$$

with t being time, λ the wavelength, Ai(λ) the fluorescence amplitude at a given wavelength and k_i the decay rate of component i. The global analysis constrains the fit to a limited number of the same decay lifetimes/rates (τ_i/k_i) at all wavelengths, whereas the amplitude (A_i) is allowed to vary per wavelength. Plotting the amplitudes of each component at all wavelengths results in the so-called Decay-Associated Spectra (DAS). The minimum number of components for the fit was found by factorizing the decay matrix with Singular Value Decomposition (SVD). Two components were usually required to satisfactorily fit the measurements in both F_s and F_o conditions. The F_s and F_o measurements were used to disentangle the contribution of photosystems I and II (PSI, PSII) in every DAS. PSI and PSII are different in their decay kinetics [12, 24]. When measuring in partially closed reaction center conditions (F_s measurements, **Figure 3.3**-A), decay components with a lifetime above 0.7 ns and between 50-100 ps were assigned to PSII and PSI, respectively (see **Figure 3.3**-C). The intensity of the fluorescence spectra at time zero is proportional to the amount of light absorbed by the sample. We normalized the DAS to the light absorbed by the sample by dividing them by the peak-value of the time-0 spectra ($t_0 = \sum_{i=1}^{n_{comp}} A_i$). The normalized DAS were then fitted using the PSI and PSII spectra estimated from the F_s measurement as:

$$DAS_i(\lambda) = a_i \cdot PSI(\lambda) + b_i \cdot PSII(\lambda) \tag{3.3}$$

Figure 3.3-E,F shows the results of the fit and the underlying PSI and PSII composition for the two DAS of the F_o measurement, with a_i and b_i being the contribution of the PSI and PSII spectra, respectively. The contributions of PSI and PSII were then used to calculate the average lifetime for PSII as:

$$\text{Average lifetime PSII} = \frac{\sum_{i=1}^{n_{comp}} \int_{\lambda_{min}}^{\lambda_{max}} b_i \cdot PSII(\lambda) d\lambda \cdot \tau_{avg}}{\sum_{i=1}^{n_{comp}} \int_{\lambda_{min}}^{\lambda_{max}} b_i \cdot PSII(\lambda) d\lambda} \tag{3.4}$$

3.3 Results

3.3.1 Antenna size measurements

3.3.1.1 Chlorophyll extractions

Table 3.1. Total leaf chlorophyll content and chlorophyll a/b ratio. Mean values (± SD) not connected by the same letter are significantly different ($p < 0.05$).

Species	Treatment	Chl. a/b	Tot chl. (µmol m^{-2})
A. thaliana	HL	3.92 ± 0.04 ^{ab}	251 ± 19 ^{ab}
	LL	3.62 ± 0.10 ^{c}	180 ± 4 ^{a}
B. nigra	HL	4.14 ± 0.19 ^{ade}	384 ± 46 ^{cd}
	LL	3.76 ± 0.09 ^{bc}	276 ± 4 ^{be}
B. rapa	HL	4.50 ± 0.02 ^{d}	303 ± 15 ^{fg}
	LL	4.10 ± 0.22 ^{ae}	286 ± 13 ^{ef}
H. incana	HL	4.34 ± 0.25 ^{de}	397 ± 7 ^{c}
	LL	3.57 ± 0.19 ^{c}	343 ± 8 ^{dg}

To get insights into the differences of the photosynthetic apparatus and in particular the light-harvesting part we started by comparing the amount of Chl per leaf area and the Chl *a*/Chl *b* ratio for leaves of the different plant species grown in high light (HL, 1100 µmol m^{-2} s^{-1}) and low light (LL, 250 µmol m^{-2} s^{-1}). The results are given in **Table 3.1**. Leaves are thicker when grown in HL because there is more light to "share" and this results in increased numbers of total Chl per leaf area, for instance 251 vs. 180 µmol m^{-2} for *A. thaliana* in HL and LL, respectively. Because of these higher intensities one might also expect an average decrease of light-harvesting antenna size because each pigment on average absorbs more photons so less pigments are needed per RC.
The outer antenna complexes of PSI and PSII contain both Chl *a* and Chl *b* whereas the PSI and PSII core complexes do not contain Chl *b*. Therefore, a reduction of the outer antenna size should lead to an increase in the Chl *a*/Chl *b* ratio and this is indeed observed (**Table 3.1**). However, these results do not allow us to discriminate between the abaxial and adaxial sides of the leaf and also not between the antenna of PSI and PSII.
To delve further into this topic we applied additional methods to determine differences in the light-harvesting antenna size of PSII for different plants at different light intensities at both sides of the leaves: ms fluorescence induction curves to estimate the rise half-time ($t_{½}$) and ps-ns fluorescence decay measurements to obtain the average fluorescence decay rate constant of PSII, k_{avg}(PSII).

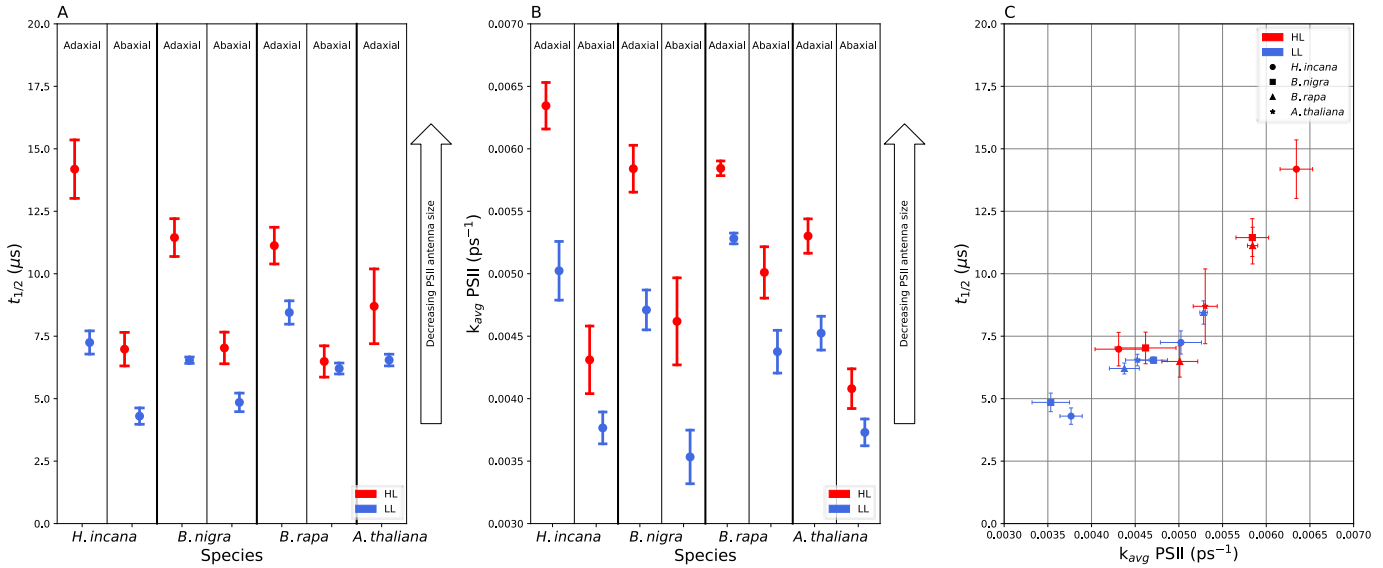

Figure 3.4. *Leaves from different plant species grown in high light (HL, red) and low light (LL, blue) were measured on both sides of the leaf (adaxial, top; abaxial, bottom); A, half-time, $t_{½}$, of the fluorescence rise measurements acquired with the FFP; B, average decay rate, k_{avg}(PSII) (the inverse of the τ_{avg}PSII) of PSII fluorescence decay acquired with the streak-camera setup; C, Correlation between the $t_{½}$ and k_{avg}(PSII) measurements; Points and error bars represent mean and standard deviation, respectively*

3.3.1.2 Fast fluorescence rise measurements

The fast fluorescence rise measurements done with the FFP were performed on plants grown at the BIAM, in France. In Figure **Figure 3.4**-A we observe that plants grown under high light intensities have an increased $t_{½}$ value as compared to plants grown in low light, reflecting a reduction of σ_f(PSII). The $t_{½}$ also varied between opposite sides of leaves grown in the same light environment (Figure **Figure 3.3**-A), indicating that σ_f(PSII) is adjusted according to the local light intensity. We can observe significant differences in the $t_{½}$ value between plant species grown in similar conditions; the leaf adaxial side of *Hirschfeldia incana* shows higher $t_{½}$ values as compared to the leaf adaxial side of *Brassica rapa*, *Brassica nigra* and *Arabidopsis thaliana* for HL growth conditions, indicating a smaller antenna size. Differences in $t_{½}$ for leaf sides exposed to the same light intensity during their growth indicate a species-dependent variation in the σ_f(PSII) adaptation.

3.3.1.3 Fluorescence decay measurement

The measurements of fluorescence lifetimes using the streak-camera system were performed on plants grown at WUR. In this set of data, the model plant species *Arabidopsis thaliana* was also measured on the abaxial side of the leaf. **Figure 3.4**-B shows that k_{avg}(PSII) is also affected by the growth light conditions, with higher k_{avg}(PSII) values for plants grown in HL as compared to LL. Similarly, we observe differences in the k_{avg}(PSII) between the opposite sides of the same leaf grown at a specific light environment. This is fully in line with the observations made with the FFP that the ratio of light-harvesting complexes and PSII reaction centers (i.e. the σ_f(PSII)) is adjusted according the local light intensity. Different plant genotypes showed significant differences in the measured k_{avg}(PSII) when exposed to the same light condition. In HL growth condition, the adaxial side of *Hirschfeldia incana* had the highest k_{avg}(PSII) followed by *Brassica nigra*, *Brassica rapa* and *Arabidopsis thaliana*. The differences of k_{avg}(PSII) between genotypes grown in similar light intensities indicates that different plant species have different adaptation strategies to specific light intensities. We can appreciate that the relative differences between $t_{½}$ correlate rather well with those in k_{avg}(PSII) even if the measurements were performed on different plants grown in two separate locations and times using similar growth conditions (**Figure 3.4**-C)

3.2 Measurement of PSII maximum quantum yield

The observed adaptation of σ_f(PSII) across plants species to the light environment (**Figure 3.4**-A and **Figure 3.4**-B) could have been due to either a reduction of the PSII absorption cross-section σ(PSII), or the PSII maximum efficiency for charge separation

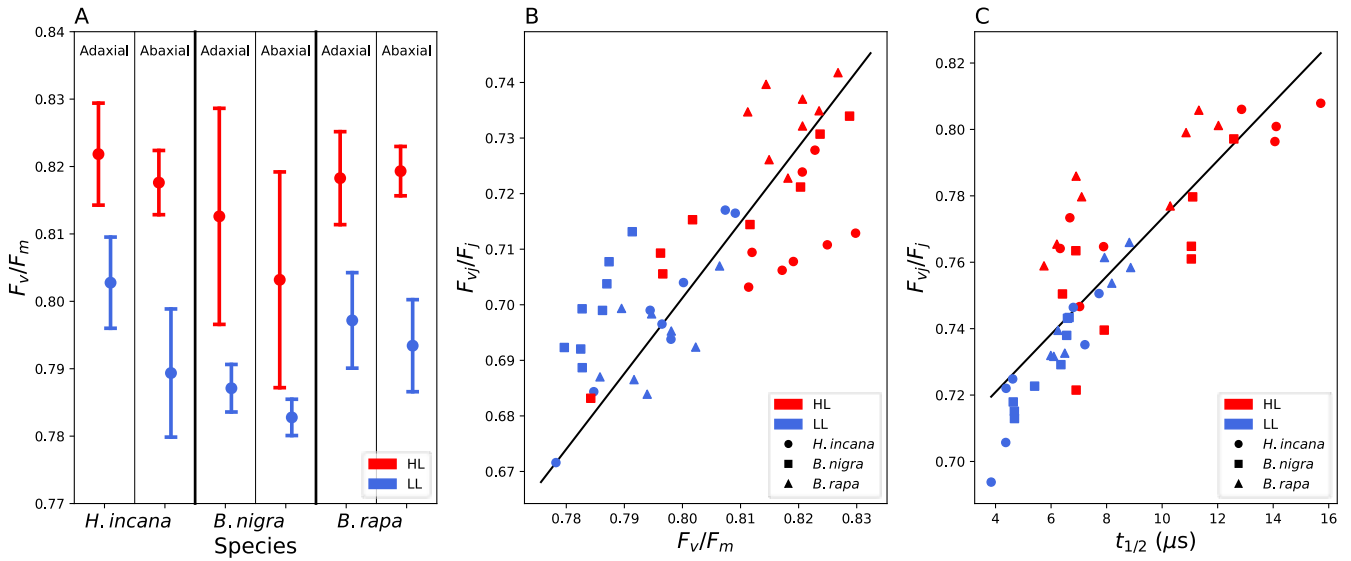

Figure 3.5. *A,* F_v/F_m *measured with Li-6800 fluorometer of leaves from different plant species grown in different light intensities (HL, LL), measured on both sides of the leaf. Points and error bars represent mean and standard deviation, respectively (n=4); B, Correlation between the* F_{vj}/F_j *and* F_v/F_m *measured with the Li-6800 fluorometer; C, Correlation between* F_{vj}/F_j *and the half-time of the photochemical rise (*$t_{½}$*) measured with the FFP*

Φ_{CS}(PSII)). To get more insight into which parameter (i.e. σ(PSII) or Φ_{CS}(PSII)) was regulated to achieve changes in σ_f(PSII), we measured the maximum quantum efficiency of PSII using the F_v/F_m ratio (with $F_v = F_m - F_o$) as a proxy, a parameter routinely used to estimate the maximum quantum efficiency of PSII. **Figure 3.5**-A shows small, but significant differences in F_v/F_m between leaves of the same species grown in different light environments. Leaves grown in HL resulted having higher F_v/F_m compared to plants grown in LL. Similarly, the F_v/F_m tends to be lower on the abaxial side as compared to the adaxial side of the leaf, despite no always being statistically significant. We investigated if the F_v/F_m ratio would correlate with the functional antenna size measured with the FFP through the $t_{½}$ parameter. We initially assessed that the F_{vj}/F_j(with F_{vj}=F_j-F_o) scaled with F_v/F_m (**Figure 3.4**-B). The F_{vj}/F_j parameter was then used as a proxy for the F_v/F_m, and we observed a good correlation with the $t_{½}$ parameters (**Figure 3.4**-C), indicating that a decrease of σ_f(PSII) positively correlates with an increase of the PSII quantum yield.

3.4 Discussion

The functional antenna size of photosystem II defines the amount of light that can be absorbed to perform charge separation [25]. On the short term, regulation involves processes such as non-photochemical quenching that regulate the amount of energy that drives charge separation [4]. Long-term acclimation involves changes in the ratio between light-harvesting complexes (LHC) and PSII reactions centers, resulting in changes in σ_f(PSII) [5, 26]. In this work we assessed the adaptation of σ_f(PSII) of different plants species grown under two different irradiance by applying two different techniques, using µs time-resolved fluorescence rise kinetics measured on plants grown in controlled conditions in France (BIAM, CEA-Cadarache) and ps-ns time-resolved fluorescence decay kinetics measured on plants grown in controlled conditions in the Netherlands (WUR). We observed differences in σ_f(PSII) across different plants species when grown under the same light intensity (**Figure 3.4**-A and B). Both when grown at HL and LL, the Brassicaceae (*H. incana*, *B. nigra*, *B. rapa*) with reported higher rates of light-saturated carbon fixation as compared to *A. thaliana* [3] expressed a smaller σ_f(PSII) than *A. thaliana* (**Figure 3.4**-B). When grown at HL, *H. incana* expressed the smallest σ_f(PSII) on the adaxial side of the leaf (**Figure 3.4**-A and B), followed by *B. nigra* and *B. rapa* and finally *A. thaliana*. The reduction of σ_f(PSII) across the different plant species grown at HL scales relatively well with the higher A_{sat} reported in the work of Garassino and colleagues (smaller σ_f(PSII) for species with reported higher A_{sat}),indicating a possible link between high light-use efficiency and reduced PSII functional antenna size. Our results support the idea that reducing PSII antenna size could be part of a series of mechanisms that

allows to maintain high rates of carbon fixation under light-saturating conditions. For example, *Arabidopsis thaliana* mutants with reduced σ_f(PSII) grown at high light were shown to express a lower yield of non-photochemical quenching and increased biomass accumulation compared to wild type [27]. Similarly, plants of *A. thaliana* with a reduced σ_f(PSII) through targeted mutagenesis were reported to possess higher electron transport rates and lower rates of NPQ, although they did not show any improvement of biomass accumulation [28].

Our results indicate the strong effect of light intensity on the acclimation of PSII functional antenna size. The influence of light intensity on σ_f(PSII) is a well-documented phenomenon [5, 10, 29], with higher light intensities resulting in decreased values for σ_f(PSII). Accordingly, we observed that plants grown in HL compared to LL acclimated to the higher irradiance by decreasing their σ_f(PSII) (**Figure 3.4**-A and B). Similarly, the opposite sides of a leaf showed differences in σ_f(PSII) indicating an acclimation to the local light intensity (**Figure 3.4**-A and B). The increase in σ_f(PSII) between the two leaf faces (from top to bottom) reflects the adaptation of the thylakoid membrane to the decreasing light intensity profile within the leaf that especially occurs in leaves oriented perpendicular to the incident light [30–32]. The differences in σ_f(PSII) between opposite leaf sides are more marked for plants grown in HL than LL (**Figure 3.4**-A and B), likely caused by the increase of leaf thickness that takes place when plants are grown under higher light intensities [33, 34]; thicker leaves absorb more light along a longer profile which results in a larger difference of light intensity between both sides of the leaf.

Because the PSII functional antenna size is the product of PSII absorption cross-section (σPSII) and its maximum quantum yield (Φ_{CS}(PSII)), we investigated whether the reduction of σ_f(PSII) at higher light conditions (**Figure 3.4**-A and B) could be caused by a lowering of Φ_{CS}(PSII). The Φ_{CS}(PSII) is commonly estimated via the F_v/F_m parameter using a saturating pulse analysis [35]. Our results indicate that plants grown in HL had a slightly but significantly higher F_v/F_m compared to plants grown in LL (**Figure 3.5**-A). This indicates that the decrease of σ_f(PSII) at HL is likely caused by a reduction of σPSII (i.e. by adjusting the ratio of PSII LHCs to RCs) rather than a decrease in PSII maximum quantum yield.
Previous work indicated that a decrease of σPSII affects the quantum efficiency of charge separation [29], because of the increased PSII trapping time for a larger antenna size [24]; the F_v/F_m parameter is equal to $(F_m - F_o)/F_m$ or in terms of fluorescence lifetimes ($\langle\tau m\rangle - \langle\tau 0\rangle)/\langle\tau m\rangle$, with $\langle\tau 0\rangle$ the average fluorescence lifetime for open PSII RCs and $\langle\tau m\rangle$ for closed RCs. Because $\langle\tau m\rangle$ is expected to be more or less independent of the antenna

size, a bigger antenna size should result in an increase of $<\tau 0>$ and therefore in a decrease of $F_v/F_m = (<\tau m> - <\tau 0>)/ <\tau m>)$. It should be noted that it was technically not feasible to measure a fluorescence lifetime in conditions of closed reaction center ($<\tau m>$). Using the F_{vj}/F_j parameter as a measure of Φ_{CS}(PSII) and the $t_{½}$ parameter as a measure of σ_f(PSII), we observed a linear correlation between σ_f(PSII) and Φ_{CS}(PSII) (**Figure 3.4**-C). Despite being expected, no previous studies reported a clear correlation between σ_f(PSII) and F_v/F_m. Jin *et al.* [27] showed that plants with reduced σ_f(PSII) due to down-regulated chlorophyll synthesis had significantly higher values of F_v/F_m [27]. An additional hint to the relation between σ_f(PSII) and F_v/F_m can be found in the work of Oberhuber *et al.* [36], who found that the adaxial side of dicots exhibited a higher PSII quantum efficiency than the abaxial side. Similarly, in a study conducted by Kitajima & Hogan [37], leaves of *Tabebuia rosea* grown in the same nitrogen regime showed higher F_v/F_m values when grown in high light conditions as compared to low light, although these differences were statistically non-significant.

An alternative explanation for the correlation between PSII functional antenna size and PSII maximum quantum yield (**Figure 3.5**-C) that we could not fully test within this work is the possible effect of a fluorescence quenching occurring in the PSII antenna. When exciting fluorescence with a strong light intensity (as during a saturating pulse), the energy harvested by the PSII antenna can form chlorophyll *a* triplets that are scavenged by certain carotenoids located in the PSII LHCs [38–40]. In Figure **Figure 3.1**-B we see that higher flash intensities result in a slightly lower fluorescence intensity of the F_j point, likely due to reversible quenching taking place in the antenna (singlet-triplet annihilation and more, see Barzda *et al.* [41]). This reversible quenching has been recently reported to be a potential cause of error when measuring F_v/F_m [42]. It is therefore possible that when measuring the PSII maximum quantum yield using a saturating pulse, plants with a higher LHCs/RCs ratio might have been more affected by this reversible quenching of the F_m, leading to an underestimation of the maximum quantum yield.

In conclusion, plants adapt to higher light intensities by adjusting their σ_f(PSII). The Brassicaceae reported to express high rates of carbon fixation under saturating light conditions reduce their antenna size more compared to the model plant *A. thaliana*, indicating that reduction of σ_f(PSII) may have a role in maintaining high light-use efficiency under saturating light intensities.

The reduction in σ_f(PSII) is not caused by a down-regulation of the maximum quantum efficiency of PSII, measured via the F_v/F_m parameter. This indicates that a decrease of σ_f(PSII) is likely caused by a decrease in PSII optical cross-section rather than its inner maximum quantum efficiency.

A decrease in σ_f(PSII), maybe somewhat counter-intuitively, positively correlates with increases in PSII maximum quantum efficiency. The most likely explanation is that a reduced PSII optical cross-section results in a reduced migration time of excitations from the LHCs to the PSII reaction centers, increasing the quantum efficiency of the PSII supercomplex. Alternatively, an increased PSII optical cross-section could increase the occurrence of reversible quenching in the antenna, leading to an underestimation of the PSII maximum quantum efficiency measured using the F_v/F_m ratio. Additional measurements will be required to fully disentangle the effect of quenching in the PSII antenna and the increased efficiency of charge separation on the maximum quantum yield of PSII.

References

1. Zhu, X.-G., Long, S. P. & Ort, D. R. Improving photosynthetic efficiency for greater yield. *Annual Review of Plant Biology* **61,** 235–261 (2010).
2. Monteith, J. L. Climate and the efficiency of crop production in Britain. *Philosophical Transactions of the Royal Society of London. B, Biological Sciences* **281,** 277–294 (1977).
3. Garassino, F., Wijfjes, R. Y., Boesten, R., Reyes Marquez, F., Becker, F. F. M., Clapero, V., Van Den Hatert, I., Holmer, R., Schranz, M. E., Harbinson, J., De Ridder, D., Smit, S. & Aarts, M. G. M. The genome sequence of *Hirschfeldia incana* , a new Brassicaceae model to improve photosynthetic light-use efficiency. *The Plant Journal* **112,** 1298–1315 (2022).
4. Genty, B. & Harbinson, J. *Regulation of light utilization for photosynthetic electron transport* in *Photosynthesis and the Environment* (ed Baker, N. R.) 67–99 (Kluwer Academic Publishers, Dordrecht, 1996).
5. Anderson, J. M. Photoregulation of the composition, function, and structure of thylakoid membranes. *Annual Review of Plant Physiology* **37,** 93–136 (1986).
6. Malkin, S. & Fork, D. C. Photosynthetic units of sun and shade plants. *Plant Physiology* **67,** 580–583 (1981).
7. Gu, L. Optimizing the electron transport chain to sustainably improve photosynthesis. *Plant Physiology* **193,** 2398–2412 (2023).
8. Malkin, S., Armond, P. A., Mooney, H. A. & Fork, D. C. Photosystem II photosynthetic unit sizes from fluorescence induction in leaves: correlation to photosynthetic capacity. *Plant Physiology* **67,** 570–579 (1981).
9. Ort, D. R., Zhu, X., () & Melis, A. Optimizing antenna size to maximize photosynthetic efficiency. *Plant Physiology* **155,** 79–85 (2011).
10. Bielczynski, L. W., Schansker, G. & Croce, R. Effect of light acclimation on the organization of photosystem II super- and sub-complexes in Arabidopsis thaliana. *Frontiers in Plant Science* **7** (2016).
11. Blankenship, R. E. & Chen, M. Spectral expansion and antenna reduction can enhance photosynthesis for energy production. *Current Opinion in Chemical Biology* **17,** 457–461 (2013).
12. Farooq, S., Chmeliov, J., Wientjes, E., Koehorst, R., Bader, A., Valkunas, L., Trinkunas, G. & Van Amerongen, H. Dynamic feedback of the photosystem II reaction centre on photoprotection in plants. *Nature Plants* **4,** 225–231 (2018).
13. Wellburn, A. R. The spectral determination of chlorophylls a and b, as well as total carotenoids, using various solvents with spectrophotometers of different resolution. *Journal of Plant Physiology* **144,** 307–313 (1994).
14. Leys, C. & Schumann, S. A nonparametric method to analyze interactions: The adjusted rank transform test. *Journal of Experimental Social Psychology* **46,** 684–688 (2010).
15. Samson, G., Prášil, O. & Yaakoubd, B. Photochemical and thermal phases of chlorophyll a fluorescence. *Photosynthetica* **37,** 163–182 (1999).
16. Lazár, D. Chlorophyll a fluorescence induction. *Biochimica et Biophysica Acta (BBA) - Bioenergetics* **1412,** 1–28 (1999).
17. Melis, A. & Homann, P. H. Kinetic analysis of the fluorescence induction in 3-(3,4-Dichlorophenyl)-1,1-dimethylurea poisoned chloroplasts. *Photochemistry and Photobiology* **21,** 431–437 (1975).
18. Belgio, E., Kapitonova, E., Chmeliov, J., Duffy, C. D. P., Ungerer, P., Valkunas, L. & Ruban, A. V. Economic photoprotection in photosystem II that retains a complete light-harvesting system with slow energy traps. *Nature Communications* **5,** 4433 (2014).
19. De Wijn, R. & Van Gorkom, H. J. Kinetics of electron transfer from Q_A to Q_B in photosystem II. *Biochemistry* **40,** 11912–11922 (2001).
20. Ghirardi, M. L. & Melis, A. Photosystem electron-transport capacity and light-harvesting antenna size in maize chloroplasts. *Plant Physiology* **74,** 993–998 (1984).
21. Melis, A. & Anderson, J. M. Structural and functional organization of the photosystems in spinach chloroplasts. Antenna size, relative electron-transport capacity, and chlorophyll composition. *Biochimica et Biophysica Acta (BBA) - Bioenergetics* **724,** 473–484 (1983).
22. Mullen, K. M. & Stokkum, I. H. M. V. **TIMP** : An *R* package for modeling multi-way spectroscopic measurements. *Journal of Statistical Software* **18** (2007).
23. Snellenburg, J. J., Laptenok, S. P., Seger, R., Mullen, K. M. & Stokkum, I. H. M. V. **Glotaran** : A *Java* -Based Graphical User Interface for the *R* Package **TIMP**. *Journal of Statistical Software* **49** (2012).
24. Van Oort, B., Alberts, M., De Bianchi, S., Dall'Osto, L., Bassi, R., Trinkunas, G., Croce, R. & Van Amerongen, H. Effect of antenna-depletion in photosystem II on excitation energy transfer in Arabidopsis thaliana. *Biophysical Journal* **98,** 922–931 (2010).
25. Van Amerongen, H. & Wientjes, E. *Harvesting light* in *Photosynthesis in Action* 3–16 (Elsevier, 2022).
26. Caffarri, S., Broess, K., Croce, R. & van Amerongen, H. Excitation energy transfer and trapping in higher plant photosystem II complexes with different antenna sizes. *Biophysical Journal* **100,** 2094–2103 (2011).

27. Jin, H., Li, M., Duan, S., Fu, M., Dong, X., Liu, B., Feng, D., Wang, J. & Wang, H.-B. Optimization of light-harvesting pigment improves photosynthetic efficiency. *Plant Physiology* **172,** 1720–1731 (2016).
28. Bielczynski, L. W., Schansker, G. & Croce, R. Consequences of the reduction of the photosystem II antenna size on the light acclimation capacity of *Arabidopsis thaliana*. *Plant, Cell & Environment* **43,** 866–879 (2020).
29. Wientjes, E., Van Amerongen, H. & Croce, R. Quantum yield of charge separation in photosystem II: functional effect of changes in the antenna size upon light acclimation. *The Journal of Physical Chemistry B* **117,** 11200–11208 (2013).
30. Iermak, I., Vink, J., Bader, A. N., Wientjes, E. & Van Amerongen, H. Visualizing heterogeneity of photosynthetic properties of plant leaves with two-photon fluorescence lifetime imaging microscopy. *Biochimica et Biophysica Acta (BBA) - Bioenergetics* **1857,** 1473–1478 (2016).
31. Terashima, I. & Inoue, Y. Palisade tissue chloroplasts and spongy tissue chloroplasts in spinach: biochemical and ultrastructural differences. *Plant and Cell Physiology* (1985).
32. Terashima, I. & Inoue, Y. Vertical gradient in photosynthetic properties of spinach chloroplast dependent on intra-leaf light environment. *Plant and Cell Physiology* **26,** 781–785 (1985).
33. Oguchi, R., Hikosaka, K. & Hirose, T. Does the photosynthetic light-acclimation need change in leaf anatomy? *Plant, Cell & Environment* **26,** 505–512 (2003).
34. Terashima, I., Miyazawa, S.-I. & Hanba, Y. T. Why are sun leaves thicker than shade leaves? — consideration based on analyses of CO2 diffusion in the leaf. *Journal of Plant Research* **114,** 93–105 (2001).
35. Kitajima, M. & Butler, W. Quenching of chlorophyll fluorescence and primary photochemistry in chloroplasts by dibromothymoquinone. *Biochimica et Biophysica Acta (BBA) - Bioenergetics* **376,** 105–115 (1975).
36. Oberhuber, W., Dai, Z.-Y. & Edwards, G. E. Light dependence of quantum yields of Photosystem II and CO2 fixation in C3 and C4 plants. *Photosynthesis Research* **35,** 265–274 (1993).
37. Kitajima, K. & Hogan, K. P. Increases of chlorophyll *a* / *b* ratios during acclimation of tropical woody seedlings to nitrogen limitation and high light. *Plant, Cell & Environment* **26,** 857–865 (2003).
38. Barzda, V., Peterman, E. J. G., Van Grondelle, R. & Van Amerongen, H. The Influence of aggregation on triplet formation in light-harvesting chlorophyll *a* / *b* pigment-protein complex II of green plants. *Biochemistry* **37,** 546–551 (1998).
39. Peterman, E., Dukker, F., Van Grondelle, R. & Van Amerongen, H. Chlorophyll a and carotenoid triplet states in light-harvesting complex II of higher plants. *Biophysical Journal* **69,** 2670–2678 (1995).
40. Peterman, E. J. G., Gradinaru, C. C., Calkoen, F., Borst, J. C., Van Grondelle, R. & Van Amerongen, H. Xanthophylls in light-harvesting complex II of higher plants: light harvesting and triplet quenching. *Biochemistry* **36,** 12208–12215 (1997).
41. Barzda, V., Vengris, M., Valkunas, L., Van Grondelle, R. & Van Amerongen, H. Generation of fluorescence quenchers from the triplet states of chlorophylls in the major light-harvesting complex II from green plants. *Biochemistry* **39,** 10468–10477 (2000).
42. Schreiber, U., Klughammer, C. & Schansker, G. Rapidly reversible chlorophyll fluorescence quenching induced by pulses of supersaturating light in vivo. *Photosynthesis Research* **142,** 35–50 (2019).

3.7 Supplementary - The PSI contribution to F_o fluorescence

Table 3.2. Relative contribution of PSII fluorescence to F_o measured at different wavelength ranges derived from the streak camera data. The F_o PSII contribution was calculated for the different plant species grown in different conditions and for different leaf sides. The F_o PSII contribution was calculated for three wavelength ranges, for the full detected wavelength range (660-790 nm), centered at the PSII emission peak (680±10 nm), and for the typical detection range of commercial fluorometers used for measuring F_v/F_m (>700nm).

Species	Treatment	Leaf side	660 - 790 nm	680 ± 10 nm	>700 nm
A. thaliana	HL	adaxial	0.862 ± 0.008	0.954 ± 0.011	0.790 ± 0.009
		abaxial	0.906 ± 0.013	0.98 ± 0.008	0.847 ± 0.019
	LL	adaxial	0.892 ± 0.02	0.976 ± 0.01	0.830 ± 0.027
		abaxial	0.936 ± 0.017	0.998 ± 0.006	0.883 ± 0.026
B. nigra	HL	adaxial	0.842 ± 0.034	0.952 ± 0.017	0.759 ± 0.047
		abaxial	0.902 ± 0.024	0.985 ± 0.009	0.833 ± 0.034
	LL	adaxial	0.874 ± 0.02	0.965 ± 0.008	0.806 ± 0.029
		abaxial	0.930 ± 0.009	0.996 ± 0.003	0.880 ± 0.015
B. rapa	HL	adaxial	0.745 ± 0.083	0.905 ± 0.045	0.633 ± 0.097
		abaxial	0.826 ± 0.087	0.947 ± 0.039	0.732 ± 0.115
	LL	adaxial	0.852 ± 0.013	0.961 ± 0.009	0.776 ± 0.015
		abaxial	0.909 ± 0.009	0.987 ± 0.006	0.849 ± 0.013
H. incana	HL	adaxial	0.812 ± 0.023	0.934 ± 0.012	0.723 ± 0.03
		abaxial	0.901 ± 0.013	0.977 ± 0.003	0.843 ± 0.021
	LL	adaxial	0.874 ± 0.013	0.958 ± 0.021	0.816 ± 0.009
		abaxial	0.926 ± 0.021	0.985 ± 0.026	0.882 ± 0.016

It might be argued that the observed variation in F_v/F_m for leaves grown in different light intensities or and or different sides of the leaves (**Figure 3.5**-A) is (partially) caused by a difference in the amount of Chls associated to PSI and PSII. Because the contribution of PSI to F_o is not negligible [1, 2] a relative increase of the number of Chls attached to PSI as compared to PSII would increase F_o without increasing the maximum fluorescence resulting in an apparently lower value of F_v/F_m. Using the streak-camera data, we deconvoluted the PSI and PSII composition in the F_o measurement. The spectrally resolved PSI and PSII contribution in the F_o measurements (**Figure 3.3**-E) were used to calculate the fraction of PSII fluorescence for three different detection wavelength ranges (660-790nm, 680±10nm and >700nm).

The PSI_{fluo} and $PSII_{fluo}$ were derived by converting the PSI and PSII contribution to F_o

from a time-resolved base to an intensity base as follow: the PSI and PSII amplitude in the two F_o measurement DAS (**Figure 3.3**-E and F, dotted and dashed line) were integrated along the specific wavelength range and multiplied by the lifetime of the respective DAS (e.g. in the Figure **Figure 3.3**-E and F, 80 ps and 329 ps). In Supplementary Table 1 the relative PSII contribution to F_o ($PSI_{contribution}$ = $PSII_{fluo}$/ [$PSII_{fluo}$+ PSI_{fluo}]) is reported for the full spectrum analyzed (from 600 nm to 790 nm), at the PSII peak emission (680 ± 10 nm) and for the wavelength range that is used by the commercial fluorometer (> 700 nm) that was used to determine Fv/Fm. In **Table 3.2** it can be observed that the $PSII_{contribution}$ to F_o varies approximately between 75% to 93% over the whole spectral range (660 to 790 nm), between 91% to 100% for the wavelength range around the PSII emission peak (680 ± 10 nm) and between 63% to 88% above 700 nm. Additionally, it can be observed that the light intensity used during growth affects the $PSII_{contribution}$ to F_o; a higher light intensity (i.e. HL growth condition or adaxial side of the leaf) results in a lower $PSII_{contribution}$ in F_o as compared to a lower light intensity (i.e. LL growth condition or abaxial leaf side). The higher light intensity tends to decrease the antenna size of PSII and the ratio of the amount of chlorophyll associated with PSII and PSI, respectively [3–5], likely causing the changes of $PSII_{contribution}$ in F_o. The F_v/F_m (**Figure 3.5**-A) were corrected for the PSI fluorescence in F_o using the PSII contribution derived from streak camera measurement (**Table 3.2**). We observe that the adaxial and abaxial side of the leaf shows more marked difference when comparing the F_v/F_m values corrected for PSI fluorescence (**Figure 3.6**-B).

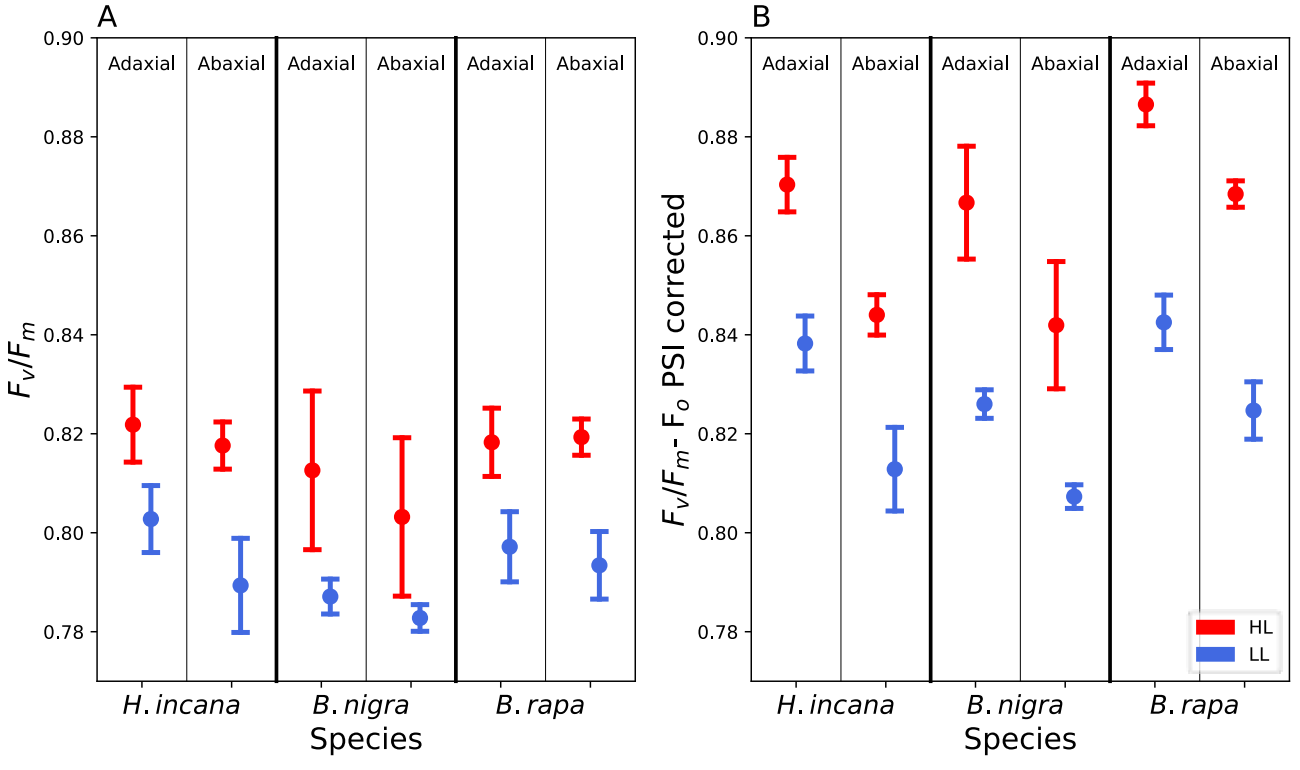

Figure 3.6. *Expected* F_v/F_m *ratio when corrected for PSI fluorescence in the wavelength range >700 nm*

Chapter 4

Natural variability in the response of chloroplast morphology to light intensity, a 3D approach *in folio*.

A version of this chapter is in preparation by: Ludovico Caracciolo, Maximilian Dostmann, Norbert de Ruijter, Arjen Bader, Herbert van Amerongen, Jeremy Harbinson.

4

Abstract

In plants and algae photosynthesis occurs within organelles called chloroplasts, which in higher plants are predominantly located in the cells of leaves. Photosynthesis depends on the coordinated action of several distinct processes: light harvesting and electron and proton transport (the so-called light reactions), the Benson-Basham-Calvin cycle and associated metabolic pathways, and the diffusive transport of carbon dioxide and oxygen. Many of these processes take place partly or even entirely in chloroplasts and their morphology and abundance therefore play a critical role in determining maximum carbon assimilation rates. For example, the chloroplasts size and distribution affect the leaf mesophyll's resistance to gas flows. Thus it is crucial to assess chloroplast characteristics such as the their area exposed to the intercellular air space and their volume. The state-of-the-art for measuring these parameters generally involves the utilization of brightfield and electron microscopy images. However, these techniques necessitate fixation of the samples, which can lead to potential alteration of the chloroplast's shape. Additionally, measuring the parameters in 2D may result in the underestimation of the actual size of the chloroplast. A new method utilizing two-photon fluorescence microscopy has been developed to observe chloroplasts directly within the leaf without the need for a fixation procedure. This method relies on the chlorophyll fluorescence signal emitted by the chloroplast, allowing for 3D imaging and estimation of chloroplast volume, maximum size and organisation in the cell. Additionally, a machine learning algorithm was trained to automatically detect individual chloroplasts.

4.1 Introduction

As in other eukaryotic oxygenic photosynthetic organisms, the light-dependent metabolism of higher plants takes place within specialized cell organelles, the chloroplasts. Chloroplasts originated from an endosymbiotic event with a cyanobacterium, resulting in the core functioning of photosynthetic light harvesting and energy transduction being quite conserved across different eukaryotic phototrophic groups. In the Archaeplastida, the taxonomic group comprising those organisms that have only a primary endosymbiosis (e.g. red algae, green algae, land plant), chloroplasts comprise a double membrane named the chloroplast envelope. The chloroplast envelope contains the stroma, and a continuous, additional folded inner membrane called the thylakoid membrane that envelopes the lumen, which like the stroma, is an aqueous phase. The subsequent description of photosynthesis will reflect the process as it occurs in the vascular plants (the tracheophytes). In the thylakoid membrane are located the different pigment-protein complexes that transduce light energy to highly energetic molecules (e.g. ATP, NADPH, ferredoxin, etc..) [1]. The chemically stored energy is used in the stroma to either assimilate NH_3 into amino acids through the glutamine synthetase, or to assimilate carbon dioxide into triose phosphate and starch [2, 3].

The "domestication" of the free-living photosynthetic prokaryote into an organelle has resulted in genetic and developmental regulation of chloroplast development (e.g. number, size, etc.) becoming tightly controlled by the nucleus of the eukaryotic cell [4, 5]. The coordination exerted by the cell nucleus is reflected by the vast variability in chloroplast morphology and numbers per cell across plant species [6]. The abundance and the size of the chloroplasts in a leaf affect the photosynthetic capacity of a plant [7], defined as the maximum achievable rate of carbon fixation. Therefore, the natural variability in the regulation of chloroplast development reflects the adaptation of the photosynthetic machinery to a particular ecosystems to maximize the fitness of the species.

Chloroplast size and number can affect photosynthetic capacity in different ways. The number of chloroplasts per unit leaf area scales with the number of available rubisco active sites and total thylakoid membrane per unit leaf area [8]. For example, developing leaves usually rely on the positive energy balance of older leaves (i.e. higher photosynthetic capacity) until they develop a sufficient amount of mature chloroplasts to support their energy needs; in the long term, senescent leaves see their chloroplast activity decrease and the photosynthetic machinery dismantled [9]. It should be noted that a chloroplast contains roughly 3000 different proteins, of which only 80-100 are encoded in the plastid [10]; it results that the higher the number of chloroplast per cell,

the higher is the metabolic cost for the cell because of the need to synthesize and import the proteins into the organelle [11].
The organization and size of the chloroplasts within the mesophyll cells can additionally affect photosynthetic capacity by influencing the diffusivity of CO_2 to the site of carboxylation. Before being reduced, CO_2 needs to diffuse through a series of resistances, which are usually evaluated and described as conductance [12]. Terrestrial plants can increase the CO_2 conductance of their mesophyll (i.e. mesophyll conductance, g_m) by increasing the area of chloroplasts exposed to the interleaf air space [13]. Smaller chloroplasts allow more chloroplast per cell [14] and are more easily arranged at the margin of the cell to increase the surface for gas-exchange.
Chloroplast size may also play a role in the intra-leaf irradiance distribution. An even light distribution within a leaf is expected to improve the photosynthetic efficiency, expressed as the net rate of carbon assimilation per unit irradiance, by reducing the activation of protective dissipation mechanisms [15, 16]. An even light distribution through the leaf would reduce the risk of saturating photochemistry of the chloroplasts located on the upper-face of the leaf [17, 18], while providing sufficient energy to the chloroplasts located in the spongy mesophyll to drive carbon fixation [19]. Moreover, smaller chloroplasts might improve the fitness of plants adapted to saturating irradiance because small chloroplast are more easily re-arranged by the cytoskeleton (i.e. photo-relocation) increasing the light adaptation capabilities [20] and may improve light penetration in the leaf [21]. Similarly, the spatial (re)arrangement of the chloroplasts within leaf cells has been shown to affect leaf absorptance up to 20-30%, likely allowing the plant to tune the amount of absorbed light energy [22, 23].

Finding physiological mechanisms that result in improvements in rates of photosynthesis has gained a renewed interest since increase in photosynthetic efficiency has been proposed as a way to enhance crop yield [24, 25]. Work based on genetic modification of chloroplast size has shown that larger chloroplasts decrease photosynthetic rate by limiting mesophyll conductance [26]. However, smaller chloroplasts do not increase g_m, and despite slight improvement in light penetration, do not improve the photosynthetic efficiency [27].
We studied the possible effect of chloroplast morphology on photosynthetic efficiency looking on some plant species (Brassicaceae) with different photosynthetic capacity. We compared chloroplast morphology across three different plants species: *Arabidopsis thaliana*, *Brassica rapa*, and *Hirschfeldia incana*. The three plants species belong to the Brassicaceae family, lack carbon concentration mechanisms, and express contrasting photosynthetic capacity. *A. thaliana* is a model organism that exhibits "typical" C3

plant rates of carbon fixation, ranging up to 30 µmol m^{-2} s^{-1} when grown under high irradiance [28]. *B. rapa* is a crop plants with reported rates of light-saturated carbon fixation ($\sim$ 40 µmol m^{-2} s^{-1}) higher than a usual C3 plants [29]. *H. incana* is a plant species adapted to nutrient-rich disrupted-environment, in which it grows quickly to out-compete potential contenders. The fast growth is paralleled by high rates of carbon fixation (> 50 µmol m^{-2} s^{-1} at an irradiance of 2 000 µmol m^{-2} s^{-1}) [28, 30].
Chloroplast morphology was assessed in three dimensions in fresh sections of leaves by optically sectioning the leaves using multiphoton excitation microscopy. Single chloroplasts were then automatically detected in the three dimensional image using a machine learning approach [31, 32] allowing us to better estimate chloroplast morphology *in folio* compared to approaches based on analysis of two dimensional images [33, 34]. We compare the change in chloroplast morphology across the three plants species grown in two opposite light conditions, high light (HL, 1600 µmol m^{-2} s^{-1}) and low light (LL, 250 µmol m^{-2} s^{-1}). To investigate inter-leaf variability, the morphology of chloroplasts located in the palisade mesophyll were compared to the ones located in the spongy mesophyll.

4.2 Materials and Methods

4.2.1 Plant material and growth conditions

Seeds of *Arabidopsis thaliana*, *Brassica rapa*, and *Hirschfeldia incana* were sown in 2 L pots (radius 140 mm, height 175 mm, Soparco) filled with a peat-based potting mixture enriched with 2.5 g/L slow-release fertilizer (Osmocote® Exact Standard 5-6M, ICL Specialty Fertilizers) and grown in climate controlled compartments. The seeds were germinated under an irradiance of 250 µmol m^{-2} s^{-1} and after germination the plants were grown under two different light intensities, low light (LL; 250 µmol m^{-2} s^{-1}) and high light (HL; 1800 µmol m^{-2} s^{-1}), provided by LED light modules (Fluence VYPR2p, Fluence, Austin, US). The light intensities were controlled as described in Caracciolo *et al.* [35]. The plants were watered with a nitrogen-rich nutrient solution (12.4 mM $NO3^{-}$, 7.2 mM K^{+}, 4 mM Ca^{2+}, 3.32 mM SO_4^{2-}, 1.82 mM Mg^{2+}, 1.2 mM NH_4^{+}, 1 mM $H_2PO_4^{-}$, 35 µM Fe^{3+}, 20 µM B^{3+}, 8 µM Mn^{2+}, 5 µm Zn^{2+}, 0.5 µM Cu^{2+}, 0.5 µM Mo^{4+}). The growth conditions were kept constant throughout the experiment, with 12 h day/12 h night, day/night temperatures of 23 °C and 20 °C and 70 % RH.

4.2.2 Microscopy measurements

4.2.2.1 Sampling and preparation

To ensure that the leaves from the different plants species were imaged at a similar developmental stage, we tracked leaf development of the newly initiated leaf that appeared 14 days after germination. This was measured daily, and considered fully-developed when its extension ceased. These fully-developed leaves were detached within the first two hours after the start of the photo-period. Fresh leaf sections approximately 300 µm thick were prepared with a rotary microtome and placed on a microscopy slide. The leaf sections were always taken in the middle of the leaf, between the central vein and the leaf margin. To reduce chloroplast movement during imaging, an actin-disruptor, latrunculin B (Abcam, ab144291, Lot:GR3419708-3, Cambridge, UK), was added to the aqueous mounting solution with a final concentration of 10 µM. The sample was placed on a slide and covered with a square cover slip 170 ± 5 µm, No. 1.5H (Marienfeld Superior, cat. no. 0107032, Lauda-Königshofen, Germany). A spacer was used between the slide and the cover glass to avoid compressing the sample. After sectioning and mounting the specimen, the microscopy slides were dark-adapted for at least one hour before imaging.

4.2.2.2 Microscopy imaging

Chloroplast morphological parameters, such as volume and surface area, were measured using fluorescence microscopy. The resolution of fluorescence microscopy is diffraction limited. This means that the smallest observable feature (d) depends on the excitation wavelength (λ) and the numerical aperture of the objective lens (NA), as described by the equation $d = \lambda/2NA$. For the imaging setup based on multiphoton excitation the resolution was approximately 0.4 µm.

Chloroplasts have an ellipsoidal shape and the dimensions of the three axes needed to describe an ellipsoid typically falls between one and five micrometers, making them observable via fluorescence microscopy with the wavelength of light we used. The microscope images were acquired with a Leica SP8 two-photon microscope. The laser wavelength was set to 850 nm. The intensity of the scanning beam was set to maximize the signal, the scanning speed was 200 Hz, and the dwell time of the laser in each pixel was 1.91 µs. The fluorescence was detected in the wavelength range 650-750 nm, comprising the fluorescence emission spectrum of chlorophyll a in vivo. The images were acquired with a X25/0.95 water-immersion objective (Leica, Fluotar VISIR, Wetzlar, Germany) without additional magnification. The image had a size of 2048 x 2048 pixels

with a pixel size of 0.23 x 0.23 m^2. For each sample, a z-stack was acquired with z-steps (i.e. a vertical displacement) of 0.57 µm. The imaging depth (i.e. depth z-axis) usually ranged between 80 and 100 µm, beyond which the signal was too weak to have an acceptable S/N ratio. Three replicates for each plant species and growth condition were sectioned and imaged between two to four times at different leaf section locations.

4.2.3 Chloroplast analysis in three dimensions

The chloroplasts in the images acquired were segmented using a convolutional neural network (CNN) named StarDist [31, 32]. We chose StarDist as algorithm because it is optimized to detect round objects and supports 3D segmentation. The output of the CNN is an image of the same size as the original one, with pixel coordinates used as specific labels. All the background pixels (i.e. no chloroplasts) have a pixel value of zero, every pixel containing part of a chloroplast had a specific value, unique for each single chloroplast. This means that each chloroplast detected gets its own label, allowing us to calculate its morphology in three dimensions. To improve the accuracy of the StarDist CNN on our specific dataset, we re-trained it using a subset of our dataset and followed the instructions provided in the Jupyter Notebook available on GitHub page for StarDist (https://github.com/stardist/stardist). Eight representative images were cropped (40 x 65 x 65 pixel) and the chloroplast were manually annotated using 3D Slicer (version 5.6.2, [36]) . The annotated images were used as a training and validation dataset. The images were transformed in silico (i.e. rotated, adding gaussian blur etc..) to increase the diversity of the dataset. The configuration of the model was optimized until subjective satisfactory results were obtained. The palisade or spongy mesophyll regions of the three-dimensional images of the leaf sections were selected and the chloroplasts contained in these subsets were automatically segmented using the trained CNN. The segmentation results were manually inspected using 3D Slicer, and instances with poor detection (i.e. chloroplasts' size under or overestimated) were manually corrected. The segmented chloroplasts were then analyzed to extract the volume of each individual chloroplast by counting the number of voxels (three-dimensional pixels) in the segmentation.

4.2.4 Statistical analysis

We first compared whether the volume of chloroplasts located in the same mesophyll cell was affected by the growth light intensity (i.e. LL, HL) using a Kolmogorov-Smirnov test (SciPy version 1.13.0, [37]) in Python (version 3.11.7, Python Software Foundation). An equal number of chloroplasts (n = 105) was randomly selected from the initial dataset (changing the set of randomly sampled chloroplasts did not change the outcome, data not

shown) and their distribution was compared; the null-hypothesis was rejected when $p < 0.05$.
We then assessed the distribution of the chloroplasts' volume when comparing the three species, grown under different irradiance, in different mesophylls cells. We assumed that the light treatment and the location in the mesophyll would have the same effect (i.e. changed the local light intensity) and we grouped them as a single factor (growth light condition and mesophyll). The statistical analysis was performed in R (version 4.2.2, R Core Team, 2022). After testing for normal distribution and homogeneity of the variance we analyzed possible differences in chloroplasts' volume across genotype and light factor using a two-way ANOVA. In the case in which the null-hypothesis of the two-way ANOVA was rejected (p value threshold <= 0.05) we performed a pairwise comparison using a Tukey test. Significative grouping differences (p <= 0.05) were represented using different letter (i.e. Compact Letter Display (CLD)).

4.3 Results

Chloroplasts in leaf cells can be tightly packed. **Figure 4.1**-A shows the chloroplasts imaged in a leaf section. The images were acquired with a two-photons confocal microscope with the detectors coupled to a fluorescence lifetime imaging microscopy (FLIM) device (example in **Figure 4.1**-A), but the lifetime information was not used in this work. We analyzed single chloroplasts using automatic detection in 3D performed by a convolutional neural network (CNN). **Figure 4.1**-B shows an example of chloroplasts in a cropped cell. The CNN was sufficiently robust to detect densely packed chloroplasts, assigning to each of the chloroplast a unique class (i.e. a different color for each single chloroplasts, **Figure 4.1**-C).

In a cell the shape of a single chloroplasts is usually represented as an ellipsoid rather than a sphere, most probably because the vacuole and the cell wall compress the chloroplast volume. To assess if the chloroplasts in our sections were spherical or ellipsoidal, we analyzed the relationship between volume and surface area for each single chloroplast in the dataset. While a sphere has a fixed ratio of surface area to volume an ellipsoid can have any combination of sizes along three axes (a, b and c). ; in our analysis we chose the same axis ratio of a=2b = 6c reported in Lee *et al.* [38]. Our results show that the volume to surface area ratio for each single chloroplast (**Figure 4.2**) are more like an ellipsoid than a sphere, whereas small chloroplasts are more spherical while larger chloroplasts are more ellipsoidal.

The volume of chloroplasts per unit leaf area can influence both the resistance of CO_2 diffusion from the inter-cellular air space to the carboxylation site in the chloroplast, and

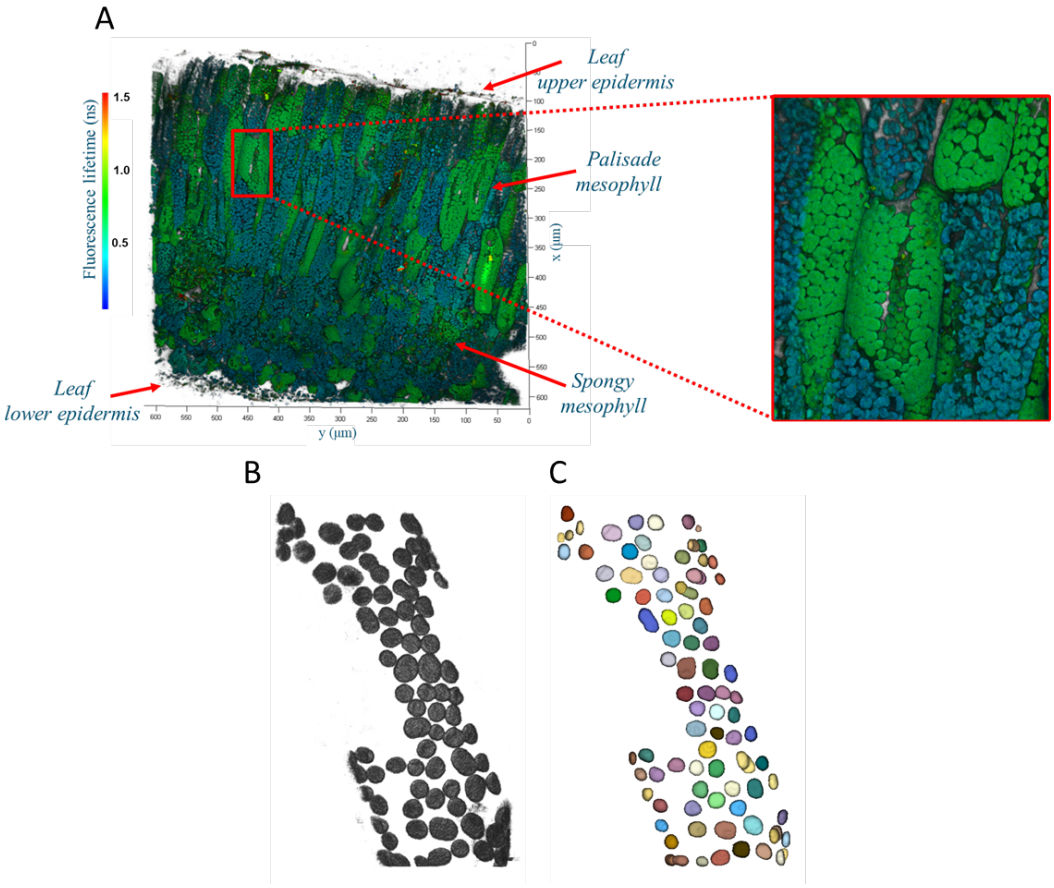

Figure 4.1. *A, Example image acquired with a two-photon confocal microscope with FLIM of a leaf section of Hirschfeldia incana grown at HL. Individual chloroplasts can be easily resolved and the color code indicates the average fluorescence lifetime for each chloroplast. Chloroplasts located in cells damaged in the sectioning cell have shorter lifetimes (blue color) than chloroplast located in non-damaged cells (green color). B, A close-up of chloroplasts located in a palisade mesophyll cell. C, Example of the automatic detection of chloroplasts using the Stardist algorithm in the cell, with different colors indicating different chloroplasts.*

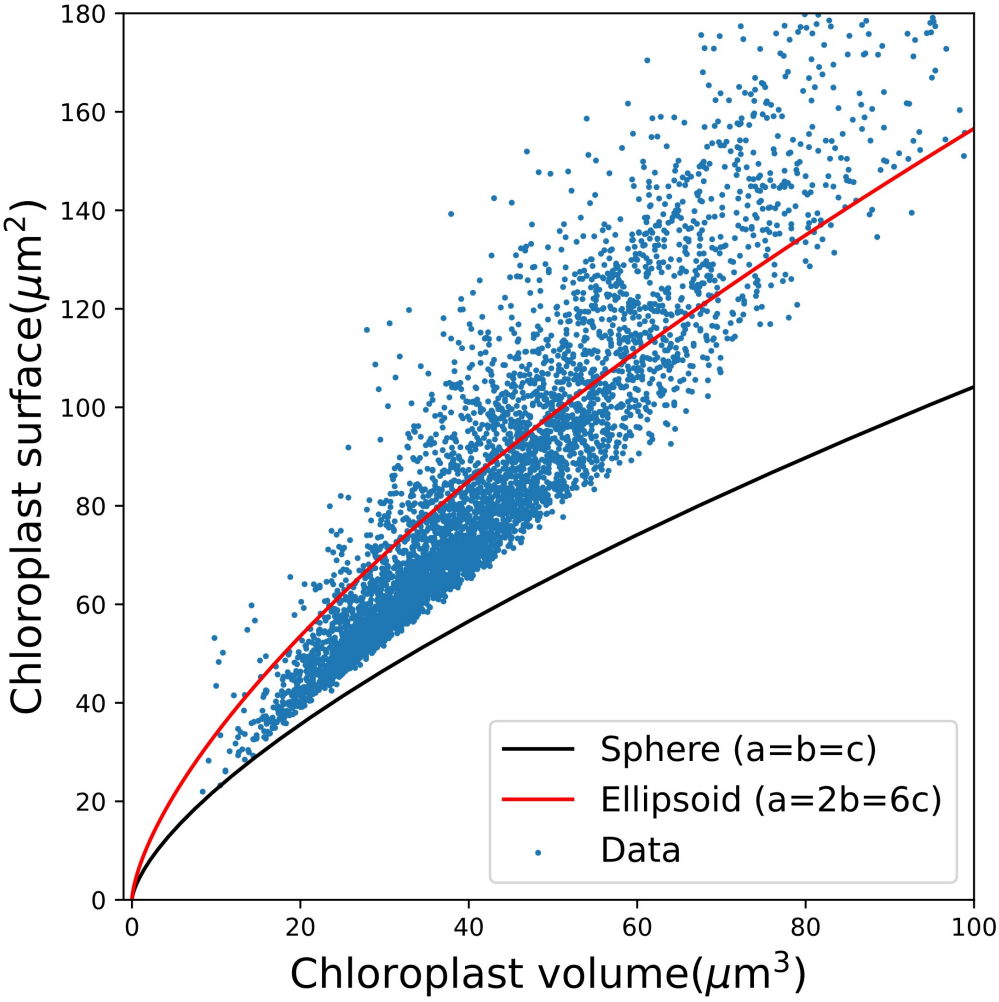

Figure 4.2. *Relationship between chloroplast volume and surface area. The black line shows the relationship between volume and surface for a sphere while the red line shows the relationship between volume and surface for an ellipsoid with axes a=2b=6c.*

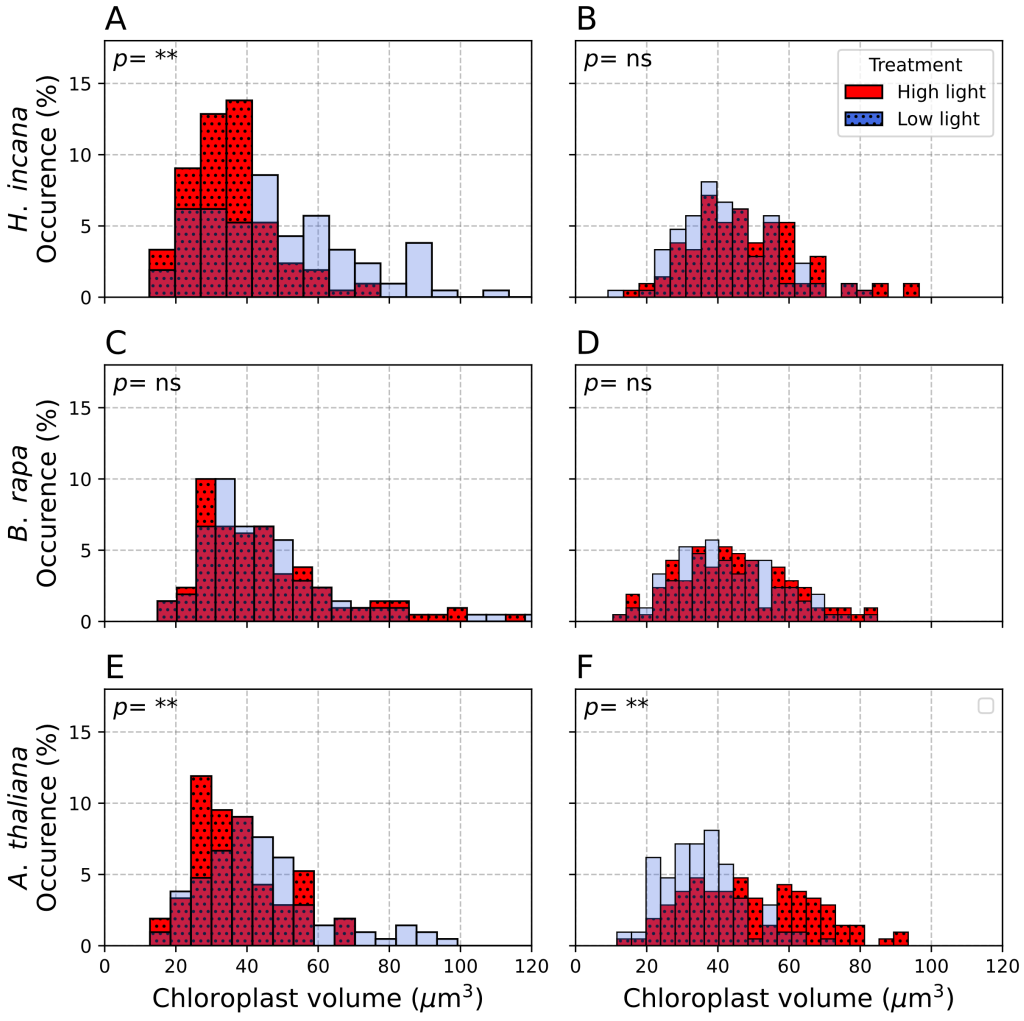

Figure 4.3. *Histograms of chloroplast volumes located in the palisade (A, C and E) and spongy mesophyll (B, D and F) for the three plant species. Colors represent growth light conditions: red for high light (HL) and dotted blue for low light (LL). A Kolmogorov-Smirnov test was used to assess significant difference in chloroplasts' volume between HL and LL treatment, the result is reported in the caption, with "ns" (non-significant) when p-value > 0.05 and "**" when p-value < 0.01 .*

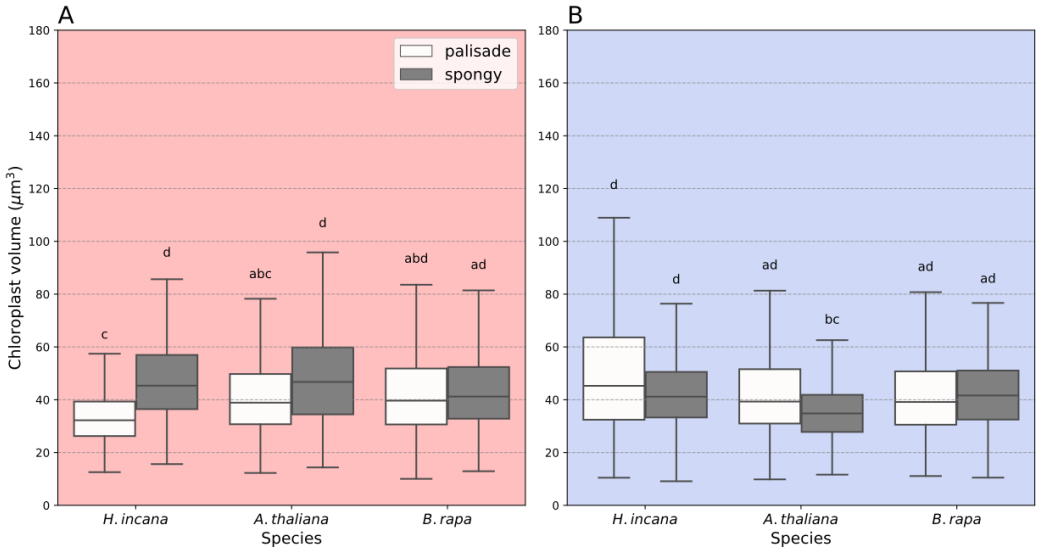

Figure 4.4. *A, boxplot of the volume of chloroplasts located in the palisade and spongy mesophyll for H. incana, A. thaliana and B. rapa grown under HL. B, boxplot of the volume of chloroplasts located in the palisade and spongy mesophyll for H. incana, A. thaliana and B. rapa grown under LL. The volume of chloroplasts located in the palisade mesophyll are in the white boxplot, while chloroplasts located in the spongy mesophyll are in the grey boxplot. Difference in chloroplasts volume across a light treatment (i.e. HL, inset A and LL, inset B) were assessed using a pairwise Tukey test (p threshold < 0.05) with statistically differences reported as different letter groups (n=105 per boxplot).*

the distribution of light within a leaf. Each cell has a pool of chloroplasts with their own genome which could allow each chloroplast some autonomy. These chloroplasts, however, share the same nucleus and nuclear gene expression. Cell level signaling will reduce any autonomy of the chloroplast proteome that arises from the activity of the chloroplast genome. In any case no mechanism is currently known to allow specialization within the cell chloroplast pool. To investigate if there was chloroplast specialization within a C3 leaf we examined if different plant species would differently regulate chloroplast development located in the palisade and spongy mesophylls when grown under different growth irradiance. Chloroplasts located in the palisade mesophyll decreased their size when grown in HL compared to LL for *H. incana* and *A. thaliana* (**Figure 4.3**-A and E), while no changes in volume could be observed for *B. rapa* under HL or LL conditions. The chloroplasts located in the spongy mesophyll showed smaller volume changes when grown at different light intensities, and only for *A. thaliana* we could observe significant changes (**Figure 4.3**-F).

Given that the light intensity under which the different species were grown was shown to affect chloroplast volume in some cases (**Figure 4.3**-A, E, and F), we investigated whether the lower irradiance in the spongy mesophyll compared to the palisade mesophyll would result in any differences in chloroplast volume. When grown under HL *H. incana* and *A. thaliana* showed a significant decrease in the volume of chloroplasts located in the palisade mesophyll compared to the ones located in the spongy mesophyll (**Figure 4.4**-A). In contrast in LL the chloroplasts located in the palisade mesophyll of *H. incana* and *A. thaliana* were larger than the ones located in the spongy mesophyll, though this difference was significant only for *A. thaliana* (**Figure 4.4**-B). In neither HL or LL growth conditions (**Figure 4.4**-A and B) did *B. rapa* show any significant changes in chloroplast volume.

4.4 Discussion

In this work, we estimated chloroplast morphology by analyzing 3D sections of leaves from three different species, imaged with a laser scanning fluorescence microscope with multi-photon excitation (MP). In multiphoton excitation, fluorescence is excited using a wavelength that does not have sufficient energy to form an excited S1 state in the target molecule (chlorophyll *a* (Chl *a*) in our case). By focusing the excitation to the imaging focal point (optical focusing) using femtosecond laser pulse, the non-linear phenomenon of two-photon absorption may occur in chlorophyll *a*, followed by internal conversion, leading to fluorescence from the Chl *a* S1 state [39]. Since the leaf is relatively transparent to the multiphoton excitation wavelength (in our case 850nm; near-infrared) before it

reaches the focal point, it permits confocal imaging of the sample down to a depth of 100 µm. Using MP microscopy has two advantages; chloroplasts can be imaged in 3D, which allows us to measure more accurately parameters such as volume and surface than a 2D approach [33, 34] and because multiphoton excitation induce chloroplast movement to a lesser extent than single photon excitation, we can image leaf section *in vivo* avoiding fixation steps (which might lead to the shrinking of the cells as reported in Winter *et al.* [40]).

Because the chloroplasts are abundant and tightly packed in leaves (**Figure 4.1**-A), the manual measure of each single chloroplast would take an unreasonable amount of time. By using a machine learning algorithm developed to detect round-shaped objects in three dimensions named StarDist [31, 32] we were able to compare thousands of chloroplasts (n=1260) grown under two irradiances and located in the palisade and spongy mesophyll of *H. incana*, *B. rapa* and *A. thaliana*. Despite being diffraction-limited to a resolution of $\sim$ 0.4 µm, MP fluorescence microscopy can resolve chloroplasts, which usually have sizes ranging in the order of micrometers. Recent work reported non-significant differences when measuring chloroplast volume using fluorescence microscopy or EM-based techniques [41]. The average chloroplast volume reported in our work is in line with that reported in other EM or fluorescence studies [33, 38, 42].

Similarly to what was reported in Lee *et al.* [38], we found that the relationship between chloroplast volume and surface area became more like that of an ellipsoid than a sphere as chloroplast size increased (**Figure 4.2**). Chloroplasts are appressed between the vacuole and the cell wall, resulting in a limitation of chloroplast size along one axis. The physical restriction forcing expansion in one direction might be the reason why it is unlikely to find round chloroplast especially when the volume increases (**Figure 4.2**).

The chloroplasts were imaged using the fluorescence emitted from the chlorophylls located in the thylakoid membrane which can lead to a small underestimation of chloroplast volume [41]. In preliminary experiments, we observed that chloroplast volume could be underestimated especially when grains of starch were present in the chloroplasts. The starch creates non-fluorescent areas that result in the underestimation of the chloroplast volume. To minimize the effect of starch accumulation, we sampled the leaf within the first hour of light exposure.

Our results indicate a wide natural variability in chloroplast volume and its response to light intensities. The species *H. incana* and *A. thaliana* had more control of chloroplast volume, reflected by the change in the chloroplasts' volume distribution across growth conditions and chloroplast location in the mesophyll (**Figure 4.3** and **Figure 4.3**). On the other hand, *B. rapa* did not show any significant acclimation of chloroplasts volume to

either the light intensity or mesophyll location (**Figure 4.3** and **Figure 4.4**). Within this study, we can distinguish two groups of plant species, the ones that show regulation in chloroplast morphology (*H. incana* and *A. thaliana*) in response to the light intensity, and the others in which the distribution of chloroplast size is fixed, at least within the parameters of the experiment (*B. rapa*). When grown at HL the chloroplasts of the "responsive" plants tended to be smaller compared to LL grown (**Figure 4.3**-A, E, and F) in alignment with what was reported in previous studies [43–45]. Similarly, when grown at HL, the chloroplasts located in the palisade mesophyll of *H. incana* and *A. thaliana* show a significant decrease in volume compared to the ones located in the spongy mesophyll. The difference in chloroplast volume between palisade and spongy mesophyll could be a response to the local light gradient. Within a leaf, light intensity diminishes from the surface exposed to light to the opposite side [46, 47], it has been shown that chloroplasts adapt to the decreasing light intensity by exhibiting shade-like adaptation by increasing the PSII absorption cross-section [48, 49]. We can speculate that it could be also an adaptation to maximize light penetration since smaller chloroplasts on the adaxial side of the leaf could result in decreased absorbance in the upper part of the leaf [27] and better light distribution to the deeper part of the leaf. When grown under LL, the trend is inverted, and chloroplast volumes were larger for the adaxial side (i.e. top) of the leaf compared to the abaxial (i.e. bottom) size (**Figure 4.4**-B). A possible explanation could be that at relatively low irradiance (250 µmol m^{-2} s^{-1}, 12 hour photo-period) the irradiance might not be strong enough to result in any advantage in optimizing chloroplast size to increase light penetration. It has been reported that different plant species do not adapt in the same way their chloroplast volume in response to light intensity; when grown at low light plants of *Sinapis alba* have smaller chloroplasts than when grown at high light [50], while plants of *Atriplex patula* have smaller chloroplasts when grown at low light than high light [51].

What mechanism are beyond the changes in the chloroplast volume observed? Chloroplast ultrastructure was shown to be quite sensitive to light intensity. At increasing light intensities, the ratio between stroma and grana thylakoid membrane lamellae usually decreases along with the number of thylakoid layers per grana stack [52–55]. Because we derived the 3D structure of chloroplasts by imaging the fluorescence of the chlorophylls located exclusively in the thylakoids, changes in thylakoid architecture will result in changes in the apparent volume of the chloroplasts. We indeed observed a decrease in volume for the chloroplasts adapted to HL as compared to LL (**Figure 4.3**). However, only *H. incana* and *A. thaliana* showed a change of their chloroplast volume in response to the light intensity, while *B. rapa* seems to have a more constant chloroplast volume.

The nuclear control on chloroplast development results in a wide natural variability in chloroplast size even within the same species, as was shown for different ecotypes of *A. thaliana* [56] and can be changed across different cells within the same leaf according to Ahmadabadi & Bock [57]. Our results indicate that some plant species as *A. thaliana* and *H. incana* exert a control on chloroplast volume in response to light intensity, while for other species, as *B. rapa*, we do not observe any change in the distribution of its chloroplast volume in response to light intensity. The natural variability in the regulation of chloroplast volume likely results from different physiological trade-offs to which different species are exposed.

References

1. Cooper, G. M. *The cell: a molecular approach* 2. ed (ASM Press [u.a.], Washington, DC, 2000).
2. Hirel, B. & Lea, P. J. *Ammonia assimilation* in *Plant Nitrogen* (eds Lea, P. J. & Morot-Gaudry, J.-F.) 79–99 (Springer Berlin Heidelberg, Berlin, Heidelberg, 2001).
3. Lewis, C. E., Noctor, G., Causton, D. & Foyer, C. H. Regulation of assimilate partitioning in leaves. *Functional Plant Biology* **27,** 507 (2000).
4. Jarvis, P. & López-Juez, E. Biogenesis and homeostasis of chloroplasts and other plastids. *Nature Reviews Molecular Cell Biology* **14,** 787–802 (2013).
5. Pyke, K. A. Divide and shape: an endosymbiont in action. *Planta* **237,** 381–387 (2013).
6. Honda, S. I., Hongladarom-Honda, T., Kwanyuen, P. & Wildman, S. G. Interpretations on chloroplast reproduction derived from correlations between cells and chloroplasts. *Planta* **97,** 1–15 (1971).
7. Leech, R. M. & Baker, N. R. *The development of photosynthetic capacity in leaves* in *The growth and functioning of leaves* p. 271–307 (Cambridge University Press, Cambridge, U.K., 1983).
8. Henriques, F. Reduction in chloroplast number accounts for the decrease in the photosynthetic capacity of Mn-deficient pecan leaves. *Plant Science* **166,** 1051–1055 (2004).
9. Ford, D. M. & Shibles, R. Photosynthesis and other traits in relation to chloroplast number during soybean leaf senescence. *Plant Physiology* **86,** 108–111 (1988).
10. De Vries, J. & Archibald, J. M. Plastid genomes. *Current Biology* **28,** R336–R337 (2018).
11. Shi, L.-X. & Theg, S. M. Energetic cost of protein import across the envelope membranes of chloroplasts. *Proceedings of the National Academy of Sciences* **110,** 930–935 (2013).
12. Lawson, T., Emmerson, R., Battle, M., Pullin, J., Wall, S. & Hofmann, T. A. *Carbon fixation* in *Photosynthesis in Action* 31–58 (Elsevier, 2022).
13. Evans, J., Caemmerer, S., Setchell, B. & Hudson, G. The relationship between CO2 transfer conductance and leaf anatomy in transgenic tobacco with a reduced content of rubisco. *Functional Plant Biology* **21,** 475 (1994).
14. Pyke, K. A. & Leech, R. M. Chloroplast division and expansion Is radically altered by nuclear mutations in *Arabidopsis thaliana*. *Plant Physiology* **99,** 1005–1008 (1992).
15. Ort, D. R., Zhu, X., () & Melis, A. Optimizing antenna size to maximize photosynthetic efficiency. *Plant Physiology* **155,** 79–85 (2011).
16. Slattery, R. A. & Ort, D. R. Perspectives on improving light distribution and light use efficiency in crop canopies. *Plant Physiology* **185,** 34–48 (2021).
17. Oguchi, R., Douwstra, P., Fujita, T., Chow, W. S. & Terashima, I. Intra-leaf gradients of photoinhibition induced by different color lights: implications for the dual mechanisms of photoinhibition and for the application of conventional chlorophyll fluorometers. *New Phytologist* **191,** 146–159 (2011).
18. Schreiber, U., Khl, M., Klimant, I. & Reising, H. Measurement of chlorophyll fluorescence within leaves using a modified PAM Fluorometer with a fiber-optic microprobe. *Photosynthesis Research* **47,** 103–109 (1996).
19. Evans, J. Carbon fixation profiles do reflect light absorption profiles in leaves. *Functional Plant Biology* **22,** 865 (1995).
20. Dutta, S., Cruz, J. A., Imran, S. M., Chen, J., Kramer, D. M. & Osteryoung, K. W. Variations in chloroplast movement and chlorophyll fluorescence among chloroplast division mutants under light stress. *Journal of Experimental Botany* **68,** 3541–3555 (2017).
21. Jeong, W. J., Park, Y.-I., Suh, K., Raven, J. A., Yoo, O. J. & Liu, J. R. A large population of small chloroplasts in tobacco leaf cells allows more effective chloroplast movement than a few enlarged chloroplasts. *Plant Physiology* **129,** 112–121 (2002).
22. Baránková, B., Lazár, D. & Nauš, J. Analysis of the effect of chloroplast arrangement on optical properties of green tobacco leaves. *Remote Sensing of Environment* **174,** 181–196 (2016).
23. Brugnoli, E. & Björkman, O. Chloroplast movements in leaves: Influence on chlorophyll fluorescence and measurements of light-induced absorbance changes related to ?pH and zeaxanthin formation. *Photosynthesis Research* **32,** 23–35 (1992).
24. Croce, R., Carmo-Silva, E., Cho, Y. B., Ermakova, M., Harbinson, J., Lawson, T., McCormick, A. J., Niyogi, K. K., Ort, D. R., Patel-Tupper, D., Pesaresi, P., Raines, C., Weber, A. P. M. & Zhu, X.-G. Perspectives on improving photosynthesis to increase crop yield. *The Plant Cell,* koae132 (2024).
25. Zhu, X.-G., Long, S. P. & Ort, D. R. Improving photosynthetic efficiency for greater yield. *Annual Review of Plant Biology* **61,** 235–261 (2010).
26. Xiong, D., Huang, J., Peng, S. & Li, Y. A few enlarged chloroplasts are less efficient in photosynthesis than a large population of small chloroplasts in Arabidopsis thaliana. *Scientific Reports* **7,** 5782 (2017).
27. Głowacka, K., Kromdijk, J., Salesse-Smith, C. E., Smith, C., Driever, S. M. & Long, S. P. Is chloroplast size optimal for photosynthetic efficiency? *New Phytologist* **239,** 2197–2211 (2023).

28. Garassino, F., Wijfjes, R. Y., Boesten, R., Reyes Marquez, F., Becker, F. F. M., Clapero, V., Van Den Hatert, I., Holmer, R., Schranz, M. E., Harbinson, J., De Ridder, D., Smit, S. & Aarts, M. G. M. The genome sequence of *Hirschfeldia incana* , a new Brassicaceae model to improve photosynthetic light-use efficiency. *The Plant Journal* **112,** 1298–1315 (2022).
29. Taylor, S. H., Orr, D. J., Carmo-Silva, E. & Long, S. P. During photosynthetic induction, biochemical and stomatal limitations differ between *Brassica* crops. *Plant, Cell & Environment* **43,** 2623–2636 (2020).
30. Canvin, D. T., Berry, J. A., Badger, M. R., Fock, H. & Osmond, C. B. Oxygen exchange in leaves in the light. *Plant Physiology* **66,** 302–307 (1980).
31. Schmidt, U., Weigert, M., Broaddus, C. & Myers, G. *Cell Detection with star-convex polygons* in *Medical Image Computing and Computer Assisted Intervention – MICCAI 2018* (eds Frangi, A. F., Schnabel, J. A., Davatzikos, C., Alberola-López, C. & Fichtinger, G.) 265–273 (Springer International Publishing, Cham, 2018).
32. Weigert, M., Schmidt, U., Haase, R., Sugawara, K. & Myers, G. *Star-convex polyhedra for 3D object detection and segmentation in microscopy* in *2020 IEEE Winter Conference on Applications of Computer Vision (WACV)* (IEEE, Snowmass Village, CO, USA, 2020), 3655–3662.
33. Harwood, R., Goodman, E., Gudmundsdottir, M., Huynh, M., Musulin, Q., Song, M. & Barbour, M. M. Cell and chloroplast anatomical features are poorly estimated from 2D cross-sections. *New Phytologist* **225,** 2567–2578 (2020).
34. Kubínová, Z., Janáček, J., Lhotáková, Z., Kubínová, L. & Albrechtová, J. Unbiased estimation of chloroplast number in mesophyll cells: advantage of a genuine three-dimensional approach. *Journal of Experimental Botany* **65,** 609–620 (2014).
35. Caracciolo, L., Philippi, J., Theeuwen, T. P. J. M., Van Amerongen, H. & Harbinson, J. An open-source controller to build a dynamic light intensity setup. *Plant Methods* **20,** 35 (2024).
36. Fedorov, A., Beichel, R., Kalpathy-Cramer, J., Finet, J., Fillion-Robin, J.-C., Pujol, S., Bauer, C., Jennings, D., Fennessy, F., Sonka, M., Buatti, J., Aylward, S., Miller, J. V., Pieper, S. & Kikinis, R. 3D Slicer as an image computing platform for the Quantitative Imaging Network. *Magnetic Resonance Imaging* **30,** 1323–1341 (2012).
37. Virtanen, P. *et al.* SciPy 1.0: fundamental algorithms for scientific computing in Python. *Nature Methods* **17,** 261–272 (2020).
38. Lee, M.-S., Boyd, R. A., Boateng, K. A. & Ort, D. R. Exploring 3D leaf anatomical traits for C $_4$ photosynthesis: chloroplast and plasmodesmata pit field size in maize and sugarcane. *New Phytologist* **239,** 506–517 (2023).
39. Denk, W., Strickler, J. H. & Webb, W. W. Two-photon laser scanning fluorescence microscopy. *Science* **248,** 73–76 (1990).
40. Winter, H., Robinson, D. G. & Heldt, H. W. Subcellular volumes and metabolite concentrations in spinach leaves. *Planta* **193,** 530–535 (1994).
41. Knoblauch, J., Waadt, R., Cousins, A. B. & Kunz, H.-H. Probing the *in situ* volumes of Arabidopsis leaf plastids using three-dimensional confocal and scanning electron microscopy. *The Plant Journal* **117,** 332–341 (2024).
42. Pipitone, R., Eicke, S., Pfister, B., Glauser, G., Falconet, D., Uwizeye, C., Pralon, T., Zeeman, S. C., Kessler, F. & Demarsy, E. A multifaceted analysis reveals two distinct phases of chloroplast biogenesis during de-etiolation in Arabidopsis. *eLife* **10,** e62709 (2021).
43. Chow, W., Qian, L., Goodchild, D. & Anderson, J. Photosynthetic acclimation of Alocasia macrorrhiza (L.) G. Don. *Functional Plant Biology* **15,** 107 (1988).
44. McCain, D. C., Croxdale, J. & Markley, J. L. Water is allocated differently to chloroplasts in sun and shade leaves. *Plant Physiology* **86,** 16–18 (1988).
45. Terashima, I. & Takenaka, A. *Organization of photosynthetic system of dorsiventral leaves as adapted to the irradiation from the adaxial side* in *Biological Control of Photosynthesis* (eds Marcelle, R., Clijsters, H. & Van Poucke, M.) 219–230 (Springer Netherlands, Dordrecht, 1986).
46. Terashima, I. & Saeki, T. Light environment within a leaf. Optical properties of paradermal sections of camellia leaves with special reference to differences in the optical properties of palisade and spongy tissues. *Plant and Cell Physiology* **24,** 1493–1501 (1983).
47. Vogelmann, T. C. & Evans, J. R. Profiles of light absorption and chlorophyll within spinach leaves from chlorophyll fluorescence. *Plant, Cell & Environment* **25,** 1313–1323 (2002).
48. Terashima, I. & Inoue, Y. Palisade tissue chloroplasts and spongy tissue chloroplasts in spinach: biochemical and ultrastructural differences. *Plant and Cell Physiology* (1985).
49. Terashima, I. & Inoue, Y. Vertical gradient in photosynthetic properties of spinach chloroplast dependent on intra-leaf light environment. *Plant and Cell Physiology* **26,** 781–785 (1985).
50. Wild, A. & Wolf, G. The effect of different light intensities on the frequency and size of stomata, the size of cells, the number, size and chlorophyll content of chloroplasts in the mesophyll and the guard cells during the ontogeny of primary leaves of Sinapis alba. *Zeitschrift für Pflanzenphysiologie* **97,** 325–342 (1980).
51. Björkman, O., Troughton, J. & Malcolm, N. *Photosynthesis in relation to leaf stucture* in *Basic Mechanisms in Plant Morphogenesis* (Brookhaven Natial Laboratory, 1974).

52. Kirchhoff, H. Chloroplast ultrastructure in plants. *New Phytologist* **223,** 565–574 (2019).
53. Lichtenthaler, H. K., Buschmann, C., Döll, M., Fietz, H.-J., Bach, T., Kozel, U., Meier, D. & Rahmsdorf, U. Photosynthetic activity, chloroplast ultrastructure, and leaf characteristics of high-light and low-light plants and of sun and shade leaves. *Photosynthesis Research* **2,** 115–141 (1981).
54. Lichtenthaler, H. K., Kuhn, G., Prenzel, U., Buschmann, C. & Meier, D. Adaptation of chloroplast-ultrastructure and of chlorophyll- protein levels to high-light and low-light growth conditions. *Zeitschrift für Naturforschung C* **37,** 464–475 (1982).
55. Wood, W. H. J., MacGregor-Chatwin, C., Barnett, S. F. H., Mayneord, G. E., Huang, X., Hobbs, J. K., Hunter, C. N. & Johnson, M. P. Dynamic thylakoid stacking regulates the balance between linear and cyclic photosynthetic electron transfer. *Nature Plants* **4,** 116–127 (2018).
56. Kadirjan-Kalbach, D. K., Turmo, A., Wang, J., Smith, B. C., Chen, C., Porter, K. J., Childs, K. L., DellaPenna, D. & Osteryoung, K. W. Allelic variation in the chloroplast division gene *FtsZ2-2* leads to natural variation in chloroplast size. *Plant Physiology* **181,** 1059–1074 (2019).
57. Ahmadabadi, M. & Bock, R. Plastid division and morphology in the genus Peperomia. *Biologia plantarum* **56,** 301–306 (2012).

Chapter 5

How to develop an open-source opto-electronic instrument to measure the molecular complexes involved in photochemistry “at work”.

A version of this chapter is in preparation by: Ludovico Caracciolo, John Philippi, Herbert van Amerongen, Maarten Wassenaar, Jeremy Harbinson.

5

Abstract

In photosynthesis, light reactions encompass a series of processes that capture light energy and convert it into chemical energy in the form of ATP and NADPH. These energy-rich molecules are subsequently utilized in the dark reactions, also known as the Calvin cycle, to produce carbohydrates and other organic compounds. The speed at which these reactions occur is a factor that influences the rate of carbon fixation and, therefore, biomass production in plants.

While numerous techniques exist to study the kinetics of light reactions, their use is sometimes hindered by the unavailability of suitable instrumentation. To address this issue, we have developed a flexible instrument capable of measuring fluorescence or absorbance changes in a leaf exposed to a background light. The signal is modulated using Pulse Amplitude Modulation (PAM), enabling high signal-to-noise ratios with a good background rejection at a relatively high sampling frequency of 10 kHz. Additionally, this instrument is modular and programmable, allowing to adjust the number of recording channel and, or sampling based on the specific requirements of each experiment.

5.1 Introduction

Photosynthesis converts light energy to chemically fixed energy via photochemical reactions and this chemical energy is then converted into metabolically useful forms, such as ATP and NADPH, which are then used to drive the metabolic processes of photosynthesis. Photosynthesis provides virtually all the energy needs of life in the biosphere and has played a pivotal role in shaping the chemistry of the Earth's atmosphere, hydrosphere and surface. Despite being such an essential process, measuring the amount of photosynthesis or primary production and how its light-use efficiency is constrained remains challenging. One problem that attends the measurement of primary production is that of scaling; the most elemental processes of photosynthesis occur at the molecular level, but these are up-scaled to progressively larger structures - protein complexes, organelles, cells, tissues, organisms, communities, and the biosphere itself. This is an inevitable consequence of how organisms are built and occupy the biosphere. Thus the question of how to measure primary production and how it is constrained needs to be asked alongside the question of the scale at which this measurement should be made.

The most direct way to "measure photosynthesis" is by measuring how much carbon dioxide is absorbed by a photosynthetic cell, tissue, organ, organism, community, or the biosphere. The leaf is commonly seen as a useful scale at which to measure and understand photosynthesis. There is no clear biological justification why the leaf is naturally the best level at which to evaluate and understand photosynthesis; in agriculture, for example, the crop canopy is probably the most appropriate level at which to evaluate assimilation. Leaves are, nonetheless, seen to be the photosynthetic organs, making them obvious targets for studies into how photosynthesis operates in an integrated way at the organ level. The size and shape of leaves were also convenient for the measurement of carbon dioxide fixation in early investigations into plant photosynthesis (e.g. in Björkman & Holmgren [1]). While leaf-level carbon assimilation is a conspicuously essential consequence of photosynthesis it does not mirror perfectly how much energy is needed by photosynthetic processes nor ultimately transformed to biomass. Other metabolic pathways such as photorespiration (especially in C3 plants) or leaf nitrogen assimilation, place significant demands on the energy budget of photosynthesis [2, 3] and the link between photosynthesis and biomass accumulation at the whole plant level depends on how much of the chemically reduced, energy-rich molecules produced by photosynthesis are respired or lost during the building of the long-lived biomass of the plant, canopy etc.

5.1.1 The photosynthetic process

To understand which photosynthetic related processes should be measured it is useful to begin with an overview of these processes. While photosynthesis is strongly identified with carbon assimilation, it is a complex process that depends on the effective coordination of numerous sub-processes, any of which might act to limit the process or be adjusted to optimize the process acting as a whole.
In eukaryotic photosynthetic organisms, the bulk of the processes associated with photosynthesis take place in chloroplasts, specialized organelles derived from endosymbiotic cyanobacteria. Chloroplasts are composed of a dynamically folded inner membrane, the thylakoid, which separates the aqueous phase of the stroma from that of the lumen. The stroma is where many metabolic activities take place of which the most iconic is carbon assimilation. Many of the subprocesses that absorb light and use this absorbed light energy to generate the metabolic driving forces for carbon assimilation occur at the level of the thylakoid. The supply of carbon dioxide, the substrate for the carbon assimilation process, depends on diffusion and in those organisms with leaves is typically evaluated at leaf level, while the chemical reduction of carbon dioxide to carbohydrates occurs in the chloroplast stromal.
The fixation of carbon dioxide, which is a reductive process, begins with the carboxylation of ribulose-1,5-bisphosphate (RuBP), a reaction catalyzed by the enzyme ribulose-1,5-bisphosphate carboxylase oxygenate (Rubisco). This is commonly seen to be the starting point of the Benson-Bassham-Calvin cycle, a cycle because it leads to the regeneration of RuBP, a process that needs 3 ATP and 2 NADPH per carboxylation [3]. The carboxylation of RuBP occurs alongside the oxygenation of RuBP, which is the starting point of a complex metabolic pathway that is commonly referred to as the photosynthetic carbon oxidation pathway (PCO) or, somewhat inaccurately, as photorespiration. This pathway requires 3.5 ATP and 2 NADPH per oxygenation. NADPH and ATP are supplied by the combined actions of light-harvesting, photochemistry, and photosynthetic electron and proton transport.

To answer, therefore, the question, “How much is the leaf photosynthesizing?” or “How is photosynthesis working?” it is necessary to measure several processes concurrently.
The measurement of water vapor and carbon dioxide fluxes out of or into the leaf via gas analysis, provides information about carbon assimilation, the diffusive limitation of transport of carbon dioxide to the site of carboxylation in the stroma, and how the limitation of assimilation under light- saturating conditions can be understood in terms of the regeneration of RuBP, the carboxylation of RuBP, and the demand for triose

phosphates [4].
Light harvesting, photochemistry, and electron and proton transport, which results in the sources of ATP and NADPH, require a different suite of measuring technologies which can usefully be applied alongside gas analysis in order to understand the integrated operation of photosynthesis . These techniques are based on chlorophyll fluorescence and light-induced absorbance changes. This chapter will focus on the design of a new instrument that can measure 5 channels; as presented this is comprised of 2 chlorophyll fluorescence channels and 3 light-induced absorbance change channels, though this is flexible. This system allows to broadly measure the operation of light-harvesting, photochemistry, and electron and proton transport, thus complementing the measurement of diffusive limitation of carbon dioxide, carbon dioxide fixation, and the PCO using gas analysis.

The choice of measurement methods for the thylakoid level processes of light - harvesting, photochemistry, and proton and electron transport emerges from the nature of these processes. Photochemistry uses light energy in the form of absorbed photons to create a flux of reducing equivalents (i.e. electrons) through the electron transport chain (ETC) and a proton flux within the thylakoid lumen. The flux of electrons is used to form metabolically useful reductants such as reduced ferredoxin, and NADPH and is connected to a release of protons into the lumen. This release builds up a proton potential gradient across the thylakoid membrane forming the proton motive force (pmf) which the ATP-synthase uses to re-phosphorylate adenosine diphosphate (ADP) into adenosine triphosphate (ATP). The fluxes of reducing equivalents and protons are generated by the catalytic activity of the reaction centers of photosystems I and II (PSI, PSII).
Photochemistry is initiated once a photon's energy is absorbed by a chlorophyll of the light harvesting complexes (LHCs) coupled to the photosystems reaction centers (RC). The absorbed energy results in the formation of a singlet excited state chlorophyll (Chl*) which swiftly transfers the excitation to the photosystems reaction where it is used to generate charge separation. Charge separation results in the formation of a strong oxidant on PSII's donor side and a strong reductant on PSI's acceptor side. The strong oxidizer formed on the donor side of the PSII reaction center is commonly referred to as $P680^{+}$. On a side note, P680 was formerly believed to be a single pigment with an absorption peak at 680 nm (by analogy with P700 of the PSI RC and P865 from the purple bacterial RC) but now the absorption peak at P680 is understood to be caused by the excitonic coupling of the chlorophylls *a* that form the whole PSII RC [5, 6]. $P680^{+}$ oxidizes, step-by-step, four manganese ions in the oxygen-evolving complex (OEC) that then oxidize two bound water molecules, releasing in total four protons on the

lumenal side of the thylakoid membrane, one dioxygen molecule, and four electrons. The electrons released from P680 reduce Q_A via pheophytin. These electrons then flow via the electron transport chain (ETC), composed by Q_B/plastoquinol, the cytochrome b_6f, and plastocyanin, to PSI where light-induced charge separation generates a strong and chemically stable reductant: ferredoxin. Ferredoxin is a mobile hydrophilic protein that distributes the electron received from PSI to various electron acceptors in the chloroplast stroma.

According to the electron acceptor of ferredoxin, electron flow can be separated into three types; linear electron flow (LEF), cyclic electron flow (CEF), and pseudo-cyclic electron flow (pseudo-CET). In LEF, ferredoxin transfers the electrons to reduce NADP+, or be used directly as a source of reducing power, through the catalytic activity of the ferredoxin:NADP(H) oxidoreductase. The LEF generates both reducing power in the form of ferredoxin or NADPH, and participates in the buildup of the *pmf* used to re-phosphorylate ADP via the proton released on the lumen side by water splitting and the oxidation of PQH_2 by the cyt. b_6f (a process that is associated with the Q-cycle [7]). CEF creates a flow of electrons in a loop around PSI; reduced ferredoxin transfers its electron back to the plastoquinone pool via mechanisms that are not fully understood yet [8]; these electrons flow back to the PSI through the cytochrome b_6f and the plastocyanin. While the CEF does not result in the formation of reducing power, it participates in the formation of the *pmf* across the thylakoid membrane. In the pseudo-CET, the reducing power of ferredoxin is used to reduce O_2 to water via the catalytic activity of flavodiiron proteins (Flv) or reduce O_2 superoxide via the Mehler reaction. Flv form a large class of enzymes that catalyze the reduction of O_2 or NO to respectively H_2O and N_2O. In the Mehler reactions [9], which is the starting point of the water-water cycle, O_2 is directly reduced by ferredoxin, forming superoxide, an oxygen radical that is then scavenged by superoxide dismutase (SOD) and ascorbate peroxidase (APX) to form H_2O. Quantitatively, these different types of electron flow are non-mutually exclusive [10], and depending on the energy needs of the metabolism, the ATP/NADPH ratio can be adjusted by balancing the electron flow through the LEF or the CEF [11]. Other electron transport activities, such as the one associated with nitrite activity or the export of reducing power from the chloroplast via the malate shuttle, which are associated with high overall ATP/NADPH can usefully be included in the class of pseudo-CET [2].

The translocation of protons from the stroma to the lumen by the electron flow, combined with the impermeability of the thylakoid membrane to protons, results in the formation of an electrochemical gradient, referred to as trans- thylakoid proton potential (Δ_{H^+}) or *pmf*. The *pmf* is comprised of two components: the difference in $[H^+]$ acidifies the lumen compared to the stroma forming a proton concentration difference (ΔpH), and the

increase of protons positive changes translocated from the stroma, results in the formation of a difference in electric potential ($\Delta\Psi$) (i.e. a voltage). When the proton potential across the membrane is measured expressed in J mol^{-1} the ΔpH and $\Delta\Psi$ contribute to the potential as follows:

$$\Delta_{H^+} = \Delta\Psi + \frac{2.3 \cdot R \cdot T \cdot \Delta pH}{F} \tag{5.1}$$

With F as the Faraday constant, R as the gas constant, and T as the temperature in Kelvin [12]. The proton potential is used by the ATP-synthase to drive the re-phosphorylation of nucleoside phosphate molecules.

5.1.2 Measurement of photosynthetic operation and regulation

The thylakoid electron transport and the proton motive force are energetically coupled, resulting in a regulation referred to as photosynthetic control [13]. Increases of the proton concentration difference component of the *pmf* (specifically the lumen pH) can exert a feedback mechanism on the electron flow by downregulating the rate of plastoquinol oxidation of the cytochrome b_6f [14–16]. The decrease in lumen pH also activates non-photochemical quenching (i.e. qE) which decreases the intrinsic quantum yield of PSII (i.e. that with all PSII traps open) [17–19] and thus limits the degree of reduction on the PSII acceptor side. The measure of the efficiency and operation of the photosystem I, II, and the *pmf* along with the measure of carbon assimilation are necessary to characterize the limitation of photosynthesis in its whole. The operating efficiency of the photosystems, the rates of electron transport, and the amplitude of the pH component across the thylakoid membrane can be monitored non-destructively in folio using various spectroscopic measurements [20]. The spectroscopic feature of specific processes associated with photosynthetic electron and proton transport machinery depends either on the trans-thylakoid electric field related to the trans-thylakoid proton motive force (*pmf*) or the redox state changes associated with electron transport.
Usually, and depending on the research question, the measure of only one of those spectroscopic features is employed. For example, a comparison of PSII efficiency across different ecotypes can be done exclusively using chlorophyll fluorescence. However, the simultaneous measure of different spectroscopic features associated with a photosynthetic process is necessary to understand the response of photosynthesis in a more holistic way. We provide hereafter a summary of some of the spectroscopic features that can be measured to derive information on the operation and regulation of the photochemical reaction *in vivo*.

Of the methods used to probe thylakoid level processes *in folio* chlorophyll *a* fluorescence is certainly the most commonly used due to its well-established theoretical framework that allows a robust interpretation of the signal [21, 22]. Once a photon, with energy within the absorption range of the pigment composing the pigment bed (i.e. carotenoid, chlorophyll *a*, and *b*) of either photosystem, is absorbed, it can promote a chlorophyll *a* to its first singlet excited state (Chl*). The excited state of Chl* is dissipated by either photochemistry, fluorescence, or non-radiative quenching. The general assumption is that the three quenching mechanisms compete with each other and that fluorescence is a constant proportion of all nonphotochemical losses [23]. When the photosystem reaction centers are dissipating photochemically Chl* excited-states energy, their trap is considered to be "closed" and any additional excited-states energy will reside in the pigment bed, increasing the chances of being dissipated as fluorescence or by non-radiative quenching. At the PSI level, a closed trap generally occurs via the formation of $P700^+$. Since no marked variable fluorescence is observed with PSI closed trap, $P700^+$ is considered to be a quencher comparable to the non-oxidized and open trap state, P700 [24]. On the other hand, at the PSII level, closed traps lead to a strong increase in the fluorescence yield, which scales (though non-linearly) with the $[Q_A^-]$ [25]. As previously mentioned, assuming that chlorophyll fluorescence always represent a constant portion of the non-radiative quenching and that the variable fluorescence is mainly emitted by PSII closed traps, the measurement of chlorophyll fluorescence can be used to provide deep insight into the functioning of PSII, as its efficiency or activation of protective mechanisms (i.e. NPQ). The basic functioning of PSII photochemistry is derived from measures of the basal fluorescence (F_o), which is, however, emitted by both PSII and PSI [26, 27], and maximum fluorescence (F_m), measured during a saturating light flash and which comes largely from PSII. In dark-adapted samples, the measure of F_o and F_m are used to derive the maximum quantum efficiency of PSII using the F_v/F_m parameter ($F_v/F_m = (F_m-F_o)/F_m$).

In light-adapted samples, Genty *et al.* [28] showed empirical evidence that the measure of PSII operating efficiency via saturating pulse analysis is linearly correlated to CO_2 quantum yield, allowing to estimate the quantum efficiency of linear electron transport through PSII, and opening the door to fast in-field phenotyping. It is noteworthy that different sources of inaccuracies need to be kept into account during the analysis of a chlorophyll measurement [29]. For example, PSI fluorescence can affect the amplitude of F_o up to 30 % and 50 % in C3 and C4 plant species respectively [27], which can lead to underestimation of the efficiency of PSII. Moreover, the light-saturating pulse used to temporally saturate photochemistry and reach F_m can either be not sufficiently

strong in light-adapted plants to saturate photochemistry [30] or conversely, be too strong and induce a transient fluorescence quenching [31], both mechanisms leading to an underestimation of F_m, and those parameters derived from F_m. Chlorophyll fluorescence can therefore provide powerful insight into the regulation and efficiency of photochemistry *in vivo*, however, its information is limited to PSII. To characterize other components of the photosynthetic machinery, such as PSI regulation and efficiency, and the *pmf* that drives the ATP-synthase, additional spectroscopic measurements based on absorption change are required.

Photosystem I efficiency and regulation can be probed by absorption changes in the near-infrared (NIR). Once a photon is absorbed by the pigment bed associated with PSI, the excited-state energy is used by PSI to catalyze a transmembrane electron transfer from a chlorophyll a that acts as the primary electron donor (P700) to a terminal electron acceptor composed of two closely arranged [4Fe-4S] clusters (F_A and F_B) [32]. Ferredoxin can also be seen as the terminal acceptor of PSI. The formed $P700^+$ is reduced either by plastocyanin using the electron provided by the ETC, and the terminal electron acceptor ($F_{A/B}$) transfer its electron to one of several possible electron carriers (e.g. ferredoxin, flavodoxin, etc.) [33]. The formation of $P700^+$ results in an absorbance increase with a peak around 820 nm ($\Delta A(820)$), which can be conveniently monitored to assess the redox state of PSI [34]. Absorbance changes are usually reported as $\Delta I/I_0$, with ΔI the fraction of change in intensity and I_0 the intensity of the incident light before it passes through the sample.

The quantum yield of PSI can be assessed by applying far-red light to oxidize most of the P700 (typically about 90 %) and the intersystem electron transport system and then superimposing a 1 - 2 ms flash of light on top of the far-red light [20, 35]. This approach assumes oxidation of P700 is not limited on the PSI acceptor side, something which is clearly not always the case (e.g. during photosynthetic induction or at steady-state under conditions of low carbon dioxide mole fraction c. 50 ppm, 2% O_2). A method to measure limitation on the PSI acceptor side has been proposed [36] but uses a long flash that would turn PSI over more than once and which could produce a post-PSI acceptor side limitation that it is intended to measure . It should be noted that the measure of $\Delta A(820)$ does not exclusively reflect changes in $P700^+$ but also the redox state of ferredoxin and plastocyanin; dual-wavelength difference signals can be used to deconvolute the absorbance change in each of its components [37].

Measurement of $\Delta A(820)$ is not limited to the assessment of the quantum yield of PSI and can provide insight into the kinetics of the electron transport. Under conditions of steady-state irradiance the rate-limiting step in the electron flow is believed to lie in the

oxidation of the plastoquinol pool by the cytochrome b_6f [16, 38]. Millisecond-resolved kinetics of $P700^+$ reduction after a light-to-dark transition can be used to estimate the rate constant of plastoquinol oxidation by the cytochrome b_6f [39].

As previously mentioned, the rate of electron flow along the ETC is coupled to the rate of formation of the proton potential, a decrease of pH in the thylakoid lumen will downregulate the rate of electron transport. Assessing the proton concentration and the associated electric potential forming the *pmf* can be measured using absorbance changes in the visible (green) region of the spectra. The electric environment in which a molecule is located affects its absorbance spectra due to the electro-chromic shift effect (ECS). The ECS is the shift in the absorption peak of a molecule caused by the surrounding electric field and the change in the dipole moment between the ground and excited states. Usually, the electric field is assumed to linearly scale to the ΔA [40], however, in a more complete analysis, the polarizability of the molecule, which leads to a quadratic, non-linear relationship between ΔA and the electric field, also needs to be taken into account. The total ECS spectrum measured on plants and green algae is due to the sum of the ECS spectra of carotenoids and chlorophyll *b* [41]. This combined spectrum has several absorbance change maxima and minima in the range 400 - 750 nm, of which the ΔA maximum at 518 nm (or 520 nm) is most widely used to assess the *pmf*.
Measurement of the $\Delta A(520)$ is routinely used to assess nondestructively and in folio the proton potential generated across the thylakoid membrane [42–44]. The measure of *pmf* relaxation with millisecond time resolution following a light-to-dark transition can allow to probe the kinetics of the proton efflux (gH^+) and the recovery of the signal taking place on a longer time scale (i.e. tens of second, to minutes) the partitioning of the *pmf* in ΔpH and $\Delta\Psi$ [7, 45].

From a technical point of view, the measure of absorbance or fluorescence changes in a leaf "at work" (i.e. exposed to an actinic irradiance) requires to separate the signal (i.e. fluorescence, ΔA) from the background (i.e. ambient light). The use of optical filtering can reduce the effect of the background on the signal (unless they spectrally overlap). However, a more robust approach to reject ambient light is to modulate (e.g. pulses, sine, etc.) the excitation light (in the case of fluorescence) or measuring beam (in the case of absorbance changes) and subsequently demodulate the signal from the detector (typically a photodiode) to recover the signal corresponding to the modulated fluorescence or absorbance light. Horton [46] and colleagues were the first to implement a system to measure chlorophyll fluorescence in the presence of background light by modulating the measuring light and extracting the changes in its amplitude using a

lock-in amplifier. Another measuring technology was that of Joliot and coworkers which made use of intense, short, and discrete measurement pulses each of which provided a measurement of absorbance or chlorophyll fluorescence, often applied with increasing time intervals [47, 48]. The use of a continuous series of high-frequency weak pulses at fixed time intervals is the foundation of the so-called PAM (pulse amplitude modulation) technology [49], which has been extensively used to measure fluorescence, even spatially (for a review see Oxborough [50]).
By simply changing the wavelengths of the excitation or measuring beams, and the filtration or type of detector (and depending on the S/N ratio of the system), it is possible to measure any type of fluorescence (e.g. chlorophyll a, NAD(P)H, etc.) or absorbance change (e.g. related to $P700^+$, ECS, etc.) of photosynthetic samples exposed to a background light. By combining within a single instrument multiple excitation and measuring beams with either different modulation frequencies or, in the case of a short-pulse system, with different pulse timings, and with one or more detectors, the same instrument can be used to measure all the above-mentioned fluorescence and absorbance changes more or less simultaneously [34, 37, 51, 52].

In this work, we aimed to develop an instrument that could measure up to five different fluorescence or absorbance changes sequentially within a time window of 500 microseconds. Five different measuring channels would allow us to measure chlorophyll fluorescence with two excitation wavelengths while allowing for three absorbance wavelengths, in our case 810 nm 940 nm, and 520 nm. The time window of 500 microseconds was chosen to enable the resolution of fast components (down to 1 kHz), such as the effect of proton efflux of ECS relaxation and the kinetics of $P700^+$ reduction by electrons coming from the PQH_2 pool. In contrast to earlier designs of similar instruments (e.g. Hogewoning *et al.* [51]) this new design is flexible and modular, with much functionality implemented at the level of firmware. This allows to the instrument to be easily re-configured by changing the firmware - instead of 2 fluorescence excitation wavelengths and 3 absorbance change wavelengths (810 nm, 940, nm, and 520 nm), the system could be easily reprogrammed to allow 5 fluorescence excitation wavelengths to be used. Additionally, the instrument was aimed to be assembled within a temperature-controlled leaf chamber coupled to a differential gas analyzer to measure the water released by transpiration and carbon assimilation of a leaf while exposed to a controlled mixture of gas (e.g. Hogewoning *et al.* [51]). The instrument is named Fast Light Unit Device for Observation, also referred to as the Fludometer . The instrument is meant to be an open-source platform with the flexibility to be modified according to the needs of the experimentalist to assess the photosynthetic machinery.

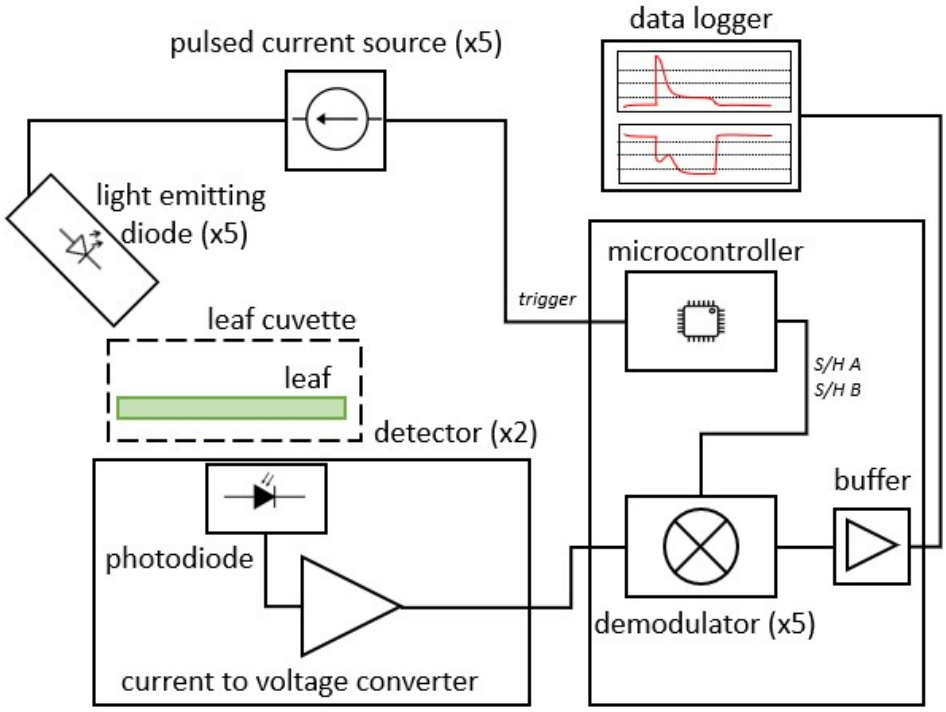

Figure 5.1. *Block diagram of one channel of the Fludometer; The detector is composed of a photodiode and a current to voltage converter; The leaf cuvette was designed to hold two optically filtered photodiodes; The microcontroller controls up to five independent pulsed current source and demodulator; The microcontroller is located on the same electronic boards as the demodulators; The number of components composing the Fludometer are referred to as (xN); The controlling signals produced by the microcontroller are reported in italic.*

5.2 Materials and Methods

The Fludometer was designed around the idea of being a flexible platform that could be coupled to a gas-exchange system to correlate the measure of carbon assimilation with the photochemical activity taking place at the thylakoid level with controlled conditions of temperature, humidity, and gas mixtures. The Fludometer modulate and demodulate up to five independent channels of which the modulation characteristic could be programmatically defined and easily modified. This flexibility was meant to allow experimentalists to adjust the measurement characteristic according to their specific research question.

5.2.1 Overview of the setup

To measure fluorescence and absorbance, the instrument produces short (10 µs) flashes of measuring or excitation light, which are guided through optical fibers to a leaf. The amount of transmitted or fluorescent light is measured using a detector and a demodulator. **Figure 5.1** illustrates the components needed to modulate and demodulate one "channel," which includes a pulsed current source, a light-emitting diode, and a demodulator. The final design of the Fludometer contains five independent channels that share two detectors: one optically filtered to measure fluorescence and near-infrared absorbance changes, and one to measure absorbance changes in the range 400-600 nm.
At the core of the instrument is the microcontroller unit (MCU) which sends a pulse sequence to the pulsed current source (**Figure 5.1**, "trigger") and the demodulator (**Figure 5.1**, "S/H A", "S/H B"). Once triggered by the MCU, the pulsed current source generates a short light flash. The detector current-to-voltage convertor (a transimpedance amplifier) converts the photocurrent generated by the light flash on the photodiode to a voltage which is subsequently supplied to a demodulator (**Figure 5.1**). The demodulator is composed of two (A, B) sample and hold (S/H) and amplifiers (an integrated circuit that can sample a changing analog signal and hold it on its output) and an instrumentation amplifier (in our circuit this works as an analog subtractor). The demodulator is triggered by the MCU and samples the signal provided by the detector before (S/H A) and during (S/H B) the light flash (**Figure 5.2**-A). The two sampled signals are then subtracted by the instrumentation amplifier, returning the amplitude of the light flash, and representing the demodulated signal (i.e. signal containing exclusively the light flash's amplitude, without the background light). The demodulated signal is recorded by a datalogger (ADC-24 Pico Technology Ltd, UK) after being buffered to provide a low impedance, protected output (**Figure 5.1**). The MCU is interfaced with the five demodulators using multiplexers, which allows the MCU to send the same pulse sequence (i.e. sample and hold A, trigger light flash, sample and hold B) to each of the five channels **Figure 5.2**-B). The following sections are described the different building blocks (pulsed current source, detector, microcontroller, and demodulator) required to assemble the Fludometer.

5.2.2 The microcontroller unit and the demodulators

The microcontroller unit and the demodulator are located on the same circuit board (see Supplementary **Figure 5.12**). The MCU is at the core of the functioning of the instrument and sends the pulse sequence that triggers the sample and holds in the demodulator (**Figure 5.1**, "S/H A", "S/H B") and the pulsed current source that generates a flash of light (**Figure 5.1**, "trigger"). Additionally to the pulse sequence, the microcontroller

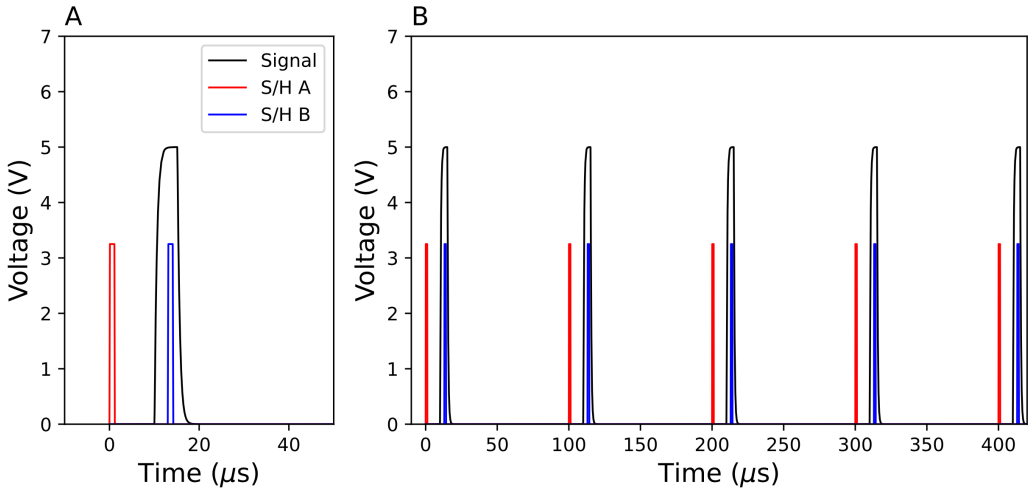

Figure 5.2. *Example of the pulse sequence. A, inset of the pulse sequence required to a single measurement. B, repetitive pulse sequence for five independent channels.*

controls the multiplexers through which the pulse sequence is sequentially "distributed" to each of the five independent demodulators (**Figure 5.3**, U104, U105 and, U106). The triggering needs to be jitter-free to optimally recover the amplitude of the light flash. For example, if the "S/H B" trigger is randomly anticipated or delayed by a few microseconds it might acquire the signal during its rising or descending phase, underestimating its real amplitude and resulting in a poor signal-to-noise ratio (S/N ratio); the same would happen for the other signals.

We used as MCU the RP2040 (Raspberry Pi Foundation, UK) for several reasons: it is low-cost, can be programmed in human-friendly languages (i.e. MicroPython), and, most importantly, its particular hardware architecture consisting of two central processing units (CPU) and eight so-called "state-machine"; tiny sub-processors capable of executing repetitive and time-critical instructions. The state machines allow to use of the RP2040 for operations that in the past might have required the use of field programmable gate arrays (FPGA). The state machines are easily reprogrammable, allowing us to change (if needed) "on the fly" the length of the light flashes, or the number of channels measured. Additionally, using the state machines to take care of the time-critical operations allows the two "idling" CPUs of the MCU to be used to process the request of the user (e.g. switching actinic light sources, FR light, applying saturating light flash, etc.). In our application, we used two of the available state machines. One state machine was used to generate

the pulse sequence, while the other was used to control the multiplexers. The MCU was programmed in MicroPython (see Supplementary code) and the state machines were programmed using the Programmable Input Output (PIO) nomenclature, a derivative of the machines assembly language and which allows direct translation of the code into machine language by the state machine. This machine-level code allows jitter-free toggling of the input/output of the MCU because it directly controls the hardware. On a side note, any other microcontroller could have been used (e.g. Arduino), however, this would have required the use of specific libraries (e.g. DigitalWriteFast) and likely two MCUs working in tandem (one for generating the pulse sequence and the multiplexer and the other to interact with the user and running protocols).

The pulse sequence (**Figure 5.2**-A) generated by the MCU (**Figure 5.3**, U102) is fed sequentially (**Figure 5.2**-B) to the five independent demodulators (**Figure 5.3**, "Demodulator *n*", see the circuit in **Figure 5.4**) via three multiplexers (**Figure 5.3**, U104, U105, U106). On the demodulator board, the signal coming from the photodetector is buffered by a voltage-follower operational amplifier (**Figure 5.3**, U101, and U103). The voltage follower could also have been used to increase the gain of the signal, however, it was mostly used as a unity-gain amplifier. The sample and holds used in the demodulator (**Figure 5.4**, U201, U202, AD781, Analog Devices Inc., Wilmington, MA, US) are characterized by high-speed acquisition time (<1 µs). The demodulator outputs the difference of the two sampled and hold signals (output = S/H B – S/H A, see **Figure 5.2**-A), which are subtracted using a FET-input precision, high-speed instrumentation amplifier (**Figure 5.4**, U203, INA110, Texas Instrument former Burr-Brown, US). The output of the instrumentation amplifier was filtered with a low-pass filter set with a 48 kHz cutoff frequency to reduce possible pick-up noise and digitized using a 24-bit datalogger (Analog to Digital Converter, ADC-24 Pico Technology Ltd, UK) and recorded on a computer. A technical difficulty encountered when building the electronic circuitry containing the MCU and the demodulators on the same electronic board (see Supplementary **Figure 5.12**) was to avoid degrading the low-noise analog signal by the interference originated by the continuous high-frequency switching of the MCU's transistors, which would lead to a poorer S/N ratio. This was achieved by separating the digital and analog ground planes, providing good decoupling of the power supplies, and using low-noise components.

5.2.3 The pulsed current source

The light flashes used to probe the photosynthetic machinery in the leaf sample were generated using a pulsed current source (**Figure 5.5**). The pulsed current source controls

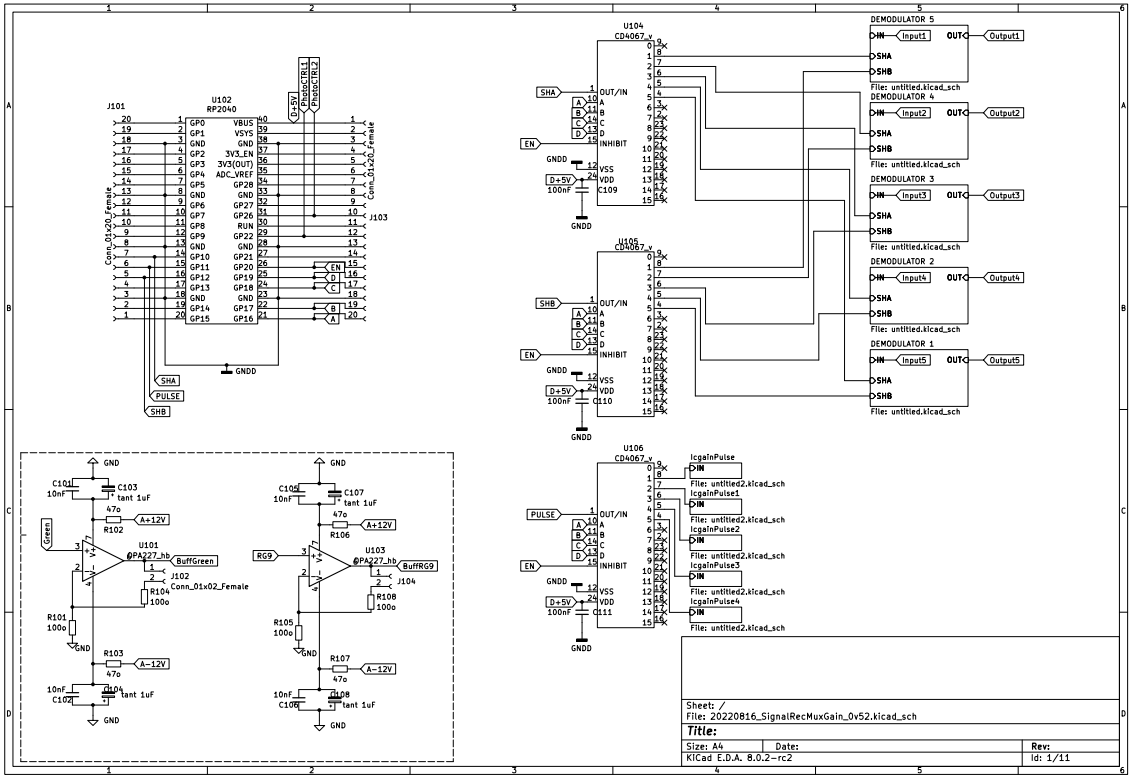

Figure 5.3. *Schematics of the microcontroller and the multiplexing circuit.* U_x *microcontroller, multiplexer and input-buffering operational amplifier;* R_x*, resistances;* C_x*, capacitors;* J_x *connector. The type or value of each component are reported in the caption.*

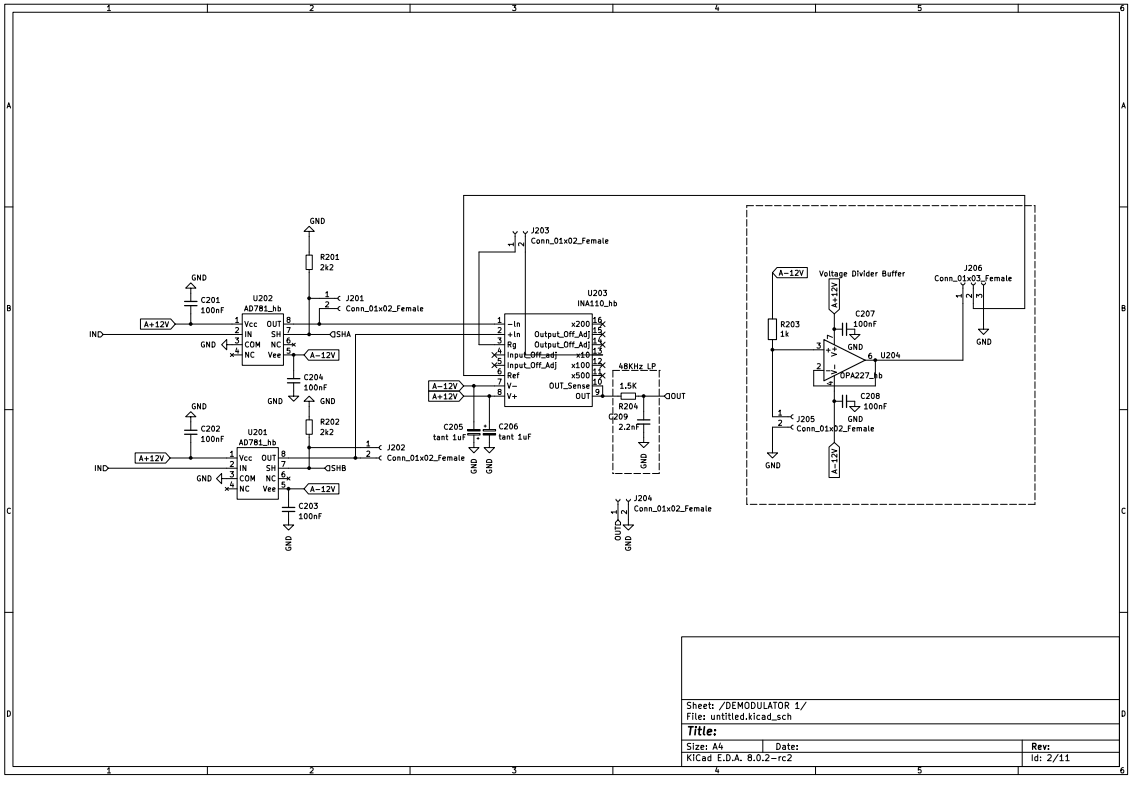

Figure 5.4. *Schematics of the signal recovery circuit.* U_x *sample and hold, instrumentation amplifier and operational amplifier;* R_x*, resistances;* C_x*, capacitors;* J_x *connector. The type or value of each component is reported in the caption.*

the current flowing through a light emitting diode (LED) spectrally filtered according the measuring needs (e.g. 520 nm for an ECS measurement); the radiation output of an LED is almost linearly correlated to the current flowing through it. The pulsed current source was designed to produce low noise, short (10 µs), and intense (up to 5 A) pulses of current. The current source could also have been made using current limiting diodes or resistor. However, we wished to be able to flexibly control the generated current (i.e. brightness of the LED) to enable the user to use different flash intensities according its needs, and therefore we used two high speed low noise operational amplifier (**Figure 5.5**, U1 and U2, ISL55001, Renesas Electronics Corporation, Japan) with very high slew rates (300 V/µs). The pulsed current source is a two stage system. The first stage is composed of an opamp (**Figure 5.5**, U1) configured as a unity gain subtractor (or differential amplifier). This subtractors receive the trigger pulse from the MCU of 3.3 V on the input of its non-inverting pin (**Figure 5.5**, "trigger"). On the input of the inverting pin there is a low noise variable voltage that is adjusted to set the current (**Figure 5.5**, "variable voltage"). If the variable voltage is zero the output of the subtractor is 3.3 V. The output of the first stage (output = "trigger"– "variable voltage") is fed into the second stage in which a second low noise high speed amplifier (**Figure 5.5**, U2) is used to control the current flowing through a light emitting diode is connected (**Figure 5.5**, D1). The opamp in raw second stage is configured as a voltage-controlled current source works by adjusting the current flow through the MOSFET (**Figure 5.5**, Q1, IRLZ14, Vishay Intertechnology, US) until the voltage across the resistor R11 is equal to the voltage input to the non-inverting pin of the second opamp. If the input voltage is 3.3V the current flow will be 5A;

$$I_{D1} = V_{non-invertingU2} \cdot R_{11} \tag{5.2}$$

The two capacitors added in parallel to the power supply (**Figure 5.5**, C10, C12) decouple (i.e. provide an extra source of charge close to the load) the power-supply and provide the charge needed for the fast-rising current pulses the current source must supply.

5.2.4 The detector

The Fludometer uses two independent detectors to measure absorbance changes in the visible (e.g. 520 nm) and fluorescence and absorbance changes in the NIR (e.g. >720 nm). A single detector is composed of large-area photodiodes (S6775, Hamamatsu, Japan) to maximize the photocurrent generated by the light flash to enhance the S/N ratio. One photodiode has a long-pass filter with a cut-off wavelength of 720 nm (RG9, UQG optics, England) while the second has an IR filter (Hot mirror HMC-5051, UQG Optics, England) combined with a cyan dichroic filter with a transmission of over 85 % in the wavelength

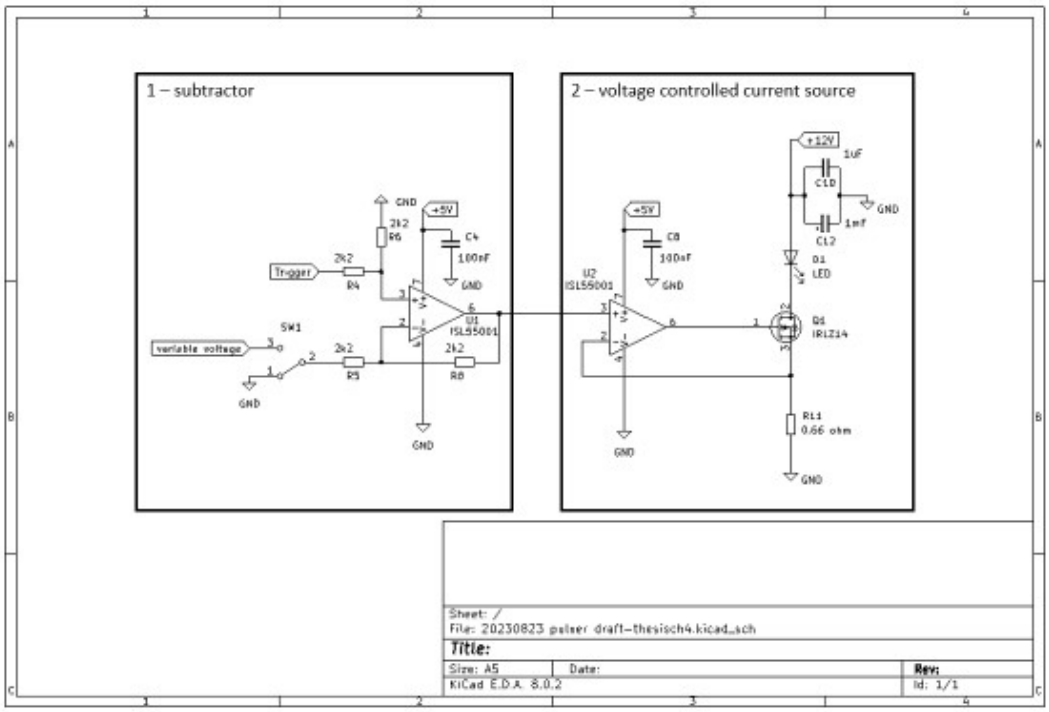

Figure 5.5. *Schematics of the LED pulser. Resistor (R_x), Capacitor (C_x), opamp (U_x), MOSFET (Q1), LED (D1), manual switch (SW1). The type and value of each components are annotated in the figure.*

range 400-600 nm (cyan dichroic filter, UQG Optics, England). The hot mirror is used because the cyan dichroic filter begins to transmit again at wavelengths greater than 750 nm (this tendency to transmit at longer wavelength is a typical property of dichroic mirrors). The detector converts the light flash to a voltage using a current to voltage converter (i.e. transimpedance amplifier, TIA). Because the light flashes are relatively short (10 µs, see **Figure 5.2**-A, to convert the photocurrent generated on the photodiodes in its full amplitude, the current to voltage converter needs to have a fast response (i.e. high bandwidth); the TIA was designed with 100 kHz bandwidth. The photocurrent is converted voltage and feeds the demodulator (**Figure 5.1**). We have successfully used two current to voltage converter in this role: initially we used a commercially produced variable gain low noise amplifier (DLPCA-200, FEMTO Messtechnik GmbH, Berlin, Germany), and subsequently a custom-made 2 channel current to voltage converter was built. The custom-made transimpedance amplifier (see circuit in **Figure 5.6**) was designed to enhance the responsivity of the large area photodiode by decreasing its capacitance using a JFET to "bootstrap" the photodiode (Design note DN399, Linear Technology, Milpitas, CA, USA, now part of Analog Devices). The operational amplifier used in a transimpedance configuration is an LT1028 (Analog Devices, Wilmington, MA, U.S.A.); the output of both TIAs are AC-coupled (∼720 Hz cutoff frequency) with a combination of capacitors (**Figure 5.6**, C4, C11) and resistors (**Figure 5.6**, R4, R8).

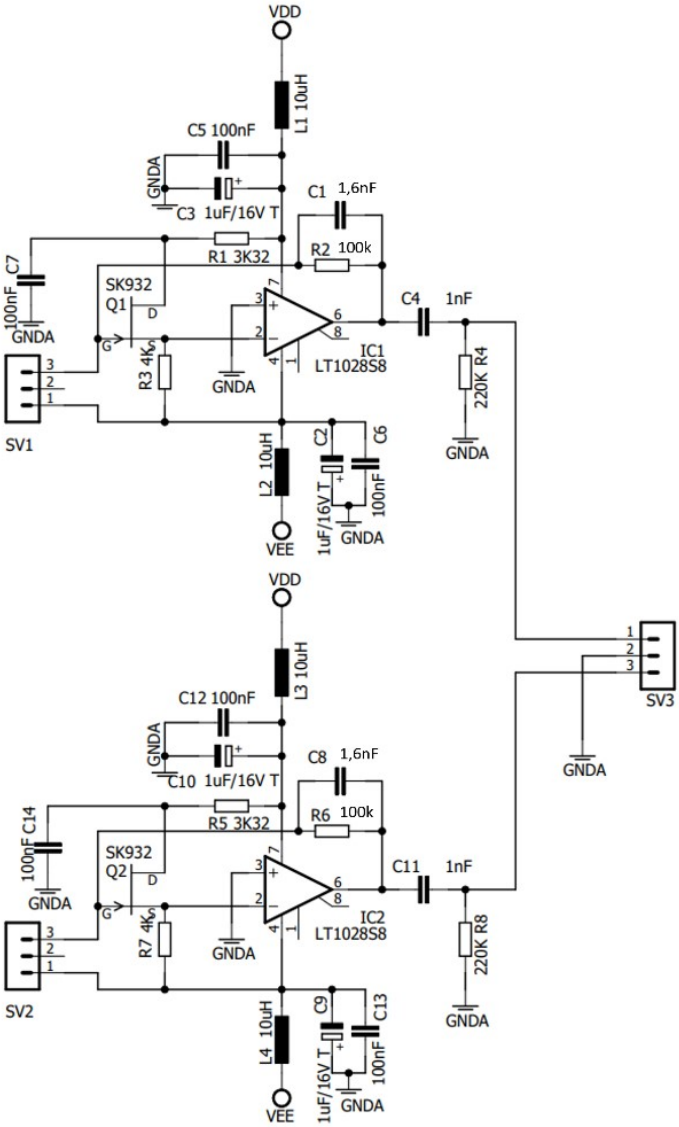

Figure 5.6. *Circuit diagram of the detector.* IC_x*, operational amplifiers;* Q_x*, JFET;* R_x*, resistances;* C_x*, capacitors;* L_x*, inductors;* SV_x *connector. The type and value of each component is reported in the caption.*

5.3 Results

5.3.1 Generation of light pulses

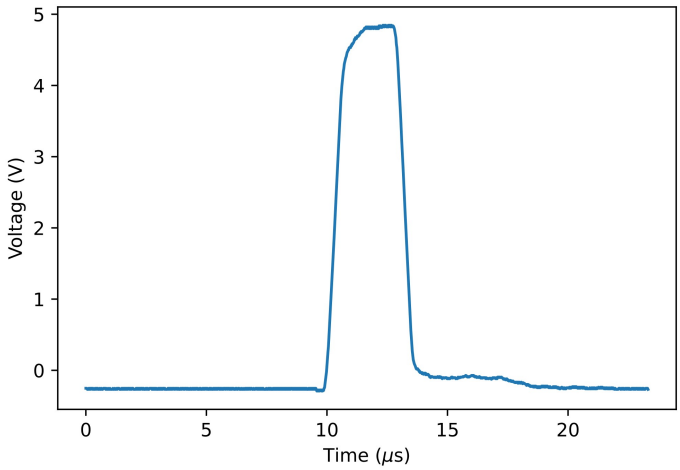

Figure 5.7. *Example of signal generated by a light flash recorded at the output of the photo-detector.*

To generate and to measure a bright light flash of ∼10 µs, the pulsed current source needs to be able to rapidly generate a fast-rising and falling current pulse through the LED while the detector needs to have sufficient bandwidth to quickly respond to this pulse of current. The use of a high speed low noise operational amplifier in the pulsed current source, a "bootstrapped" photodiode to decrease its capacitance and ultralow noise precision high speed opamp as transimpedance amplifier allowed the light flash to be generated in a reproducible form and appropriately detected (**Figure 5.7**).

5.3.2 Measuring absorbance changes along fluorescence

We assessed the capacity of the Fludometer to measure sequentially more than one fluorescence/absorption channel by recording a ΔA(820 nm) along to chlorophyll fluorescence (**Figure 5.8**-A, B). The measure was carried on a leaf of *Brassica rapa* grown under controlled conditions at 500 µmol m^{-2} s^{-1} and dark adapted for 20 minutes. The signals were recorded with a datalogger at 16 Hz and the intensity of the combined measuring light was below ∼1 µmol m^{-2} s^{-1}.
Around five seconds after the start of the measurement an actinic pulse with an intensity

of 800 µmol m^{-2} s^{-1} and an excitation centered around 660 nm was applied. We can appreciate the immediate rise of the fluorescence reflecting the increase of [$Q_A{}^-$] which starts to decrease after around 18 seconds likely due to the induction of photochemistry (**Figure 5.8**-A). Simultaneously to the change in chlorophyll fluorescence signal, we observe a decrease in the ΔA(820 nm) signal (**Figure 5.8**-B), indicating the formation of $P700^+$ which decreases the light transmitted through the leaf due to its absorbance increase in the near-infrared [34]. Interestingly, we observe a temporary decrease in the pool of oxidized P700 (i.e. increase of the ΔA(820 nm) signal) which is mirrored by an increased reduction of PSII primary electron acceptor QA (i.e. increase of chlorophyll fluorescence signal).

5.3.2 Measure of 820 nm and 520 nm absorbance changes and chlorophyll fluorescence during a photosynthetic induction

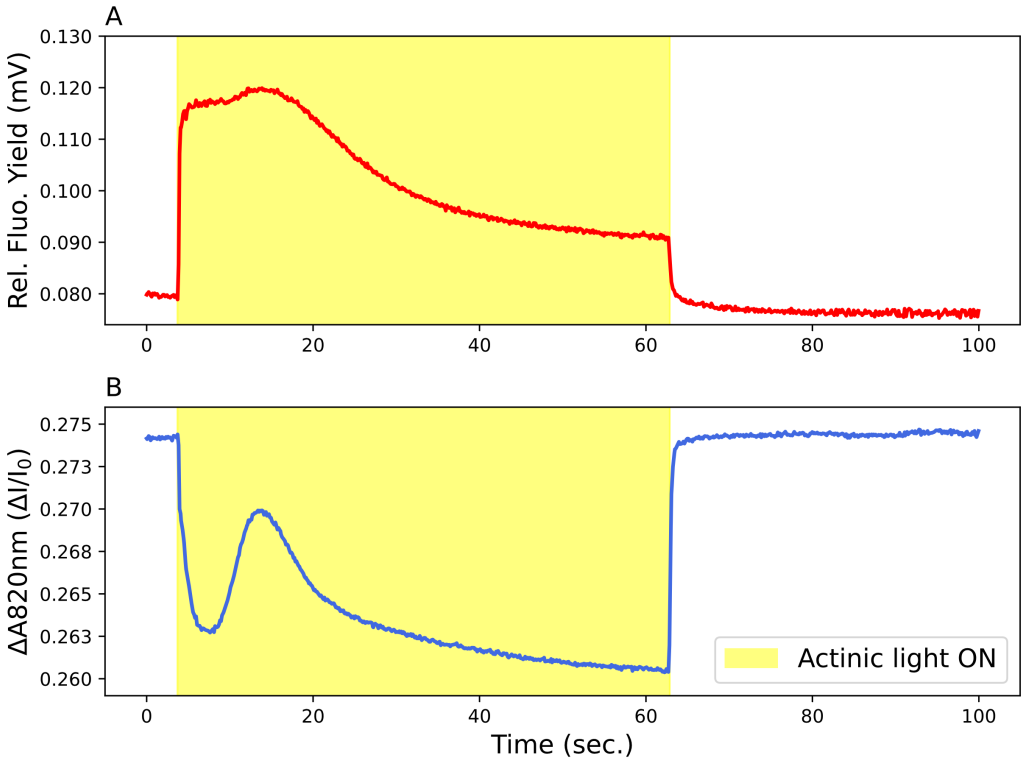

Figure 5.8. *Simultaneous measure of changes in [$Q_A{}^-$] and [$P700^+$] during a photosynthetic induction of a leaf of B. rapa; A, measurement of chlorophyll fluorescence; B, measurement of 820 nm absorbance changes, ΔA(820nm).*

The Fludometer was used to measure ΔA(820nm), ΔA(520nm) and chlorophyll fluorescence signals, respectively **Figure 5.9**-A, **Figure 5.10**-A and **Figure 5.11**-A of different dark-adapted leaves of *Hedera helix* (ivy) that had grown naturally outdoors. A bright red actinic light ($\sim$ 630 nm, $\sim$ 1500 µmol m^{-2} s^{-1}) was manually switched off for approximately 1s every 10 seconds to induce transient light-dark transition. Four light-to-dark transitions in the case of the absorbance changes, and three in the case of the chlorophyll fluorescence measurement, were selected, normalized and the decay fitted with a sum of exponential function, as:

$$f(t) = \sum_{i=1}^{n_{comp}} [A_i(\lambda) \cdot e^{-k_i t}] \tag{5.3}$$

With t being time, A_i the amplitude and k_i the decay rate of component i. We selected the minimum number of components that yielded a good fit, with two components for the ΔA(820nm) signal (**Figure 5.9**-B), three components for the ΔA(520nm) signal (**Figure 5.10**-B), and one component for the chlorophyll fluorescence relaxation from F_s to F_o' (**Figure 5.11**-B). The fits were used to calculate the average lifetime (τ_{avg}) for the four light-to-dark transition of the ΔA(820nm) signal (**Figure 5.9**-C) and the ΔA(520nm) signal (**Figure 5.10**-C), and the three light-dark transients of chlorophyll fluorescence.
We observe that during photosynthetic induction the kinetics of the rate of reduction of $P700^+$ (light-to-dark transition ΔA(820nm)) increases (**Figure 5.9**-C). Similarly we also observe an increase in the decay kinetics of the ECS signal following a light-to-dark transition that correlates with the rate of proton efflux (i.e. gH^+), and an increase in the relaxation kinetics of chlorophyll fluorescence from F_s to F_o', which corresponds to Q_A^- oxidation.

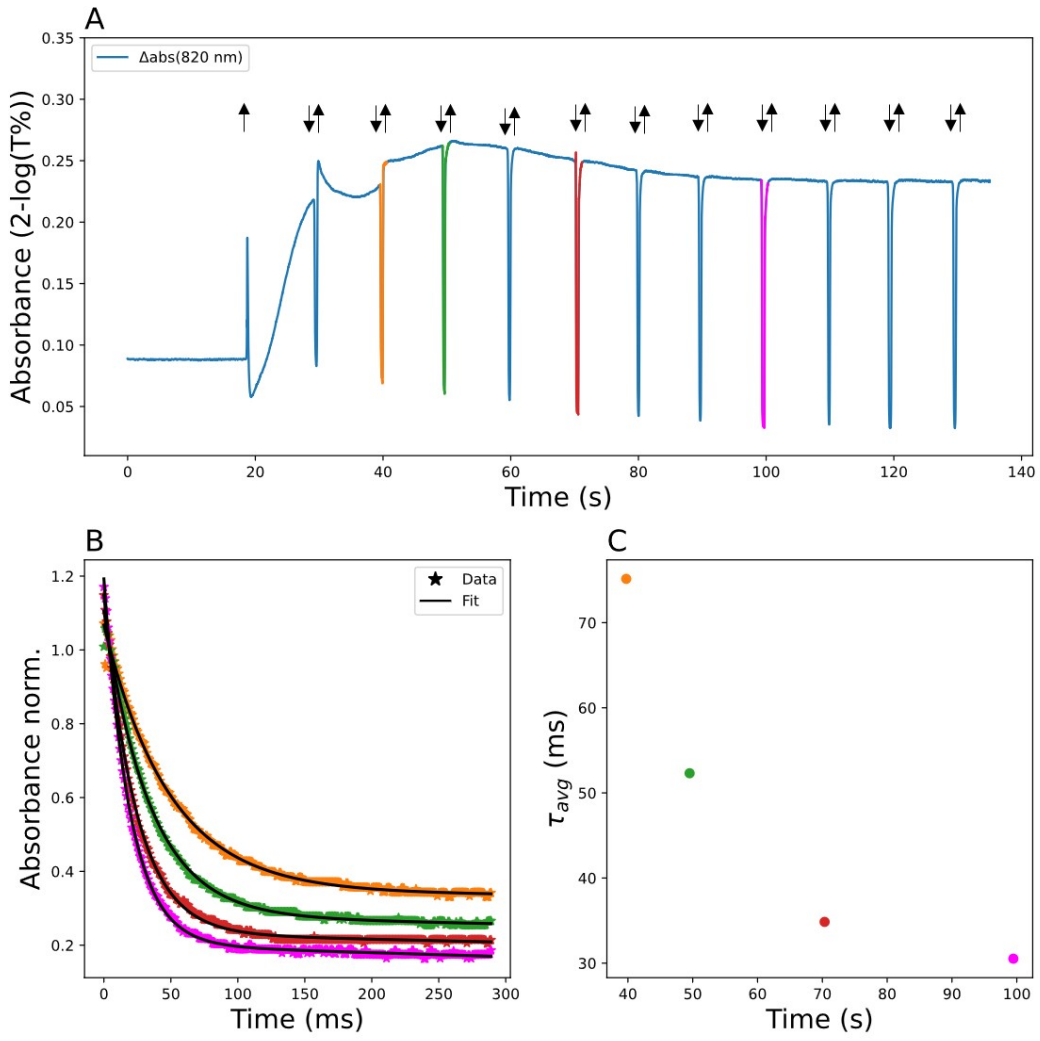

Figure 5.9. *A, Measure of ΔA(820nm) during a photosynthetic induction of a leaf of H. helix , arrows indicate switching on (upward) and off (downward) the actinic light; B, normalized decay of the ΔA(820nm) during a light-to-dark transition, points represent the data, the black line indicates the fit; C, average lifetime of the decay of the ΔA(820nm) signal caused from a light-to-dark transition (fit line reported in panel B). Similar color indicates a specific light-to-dark transition.*

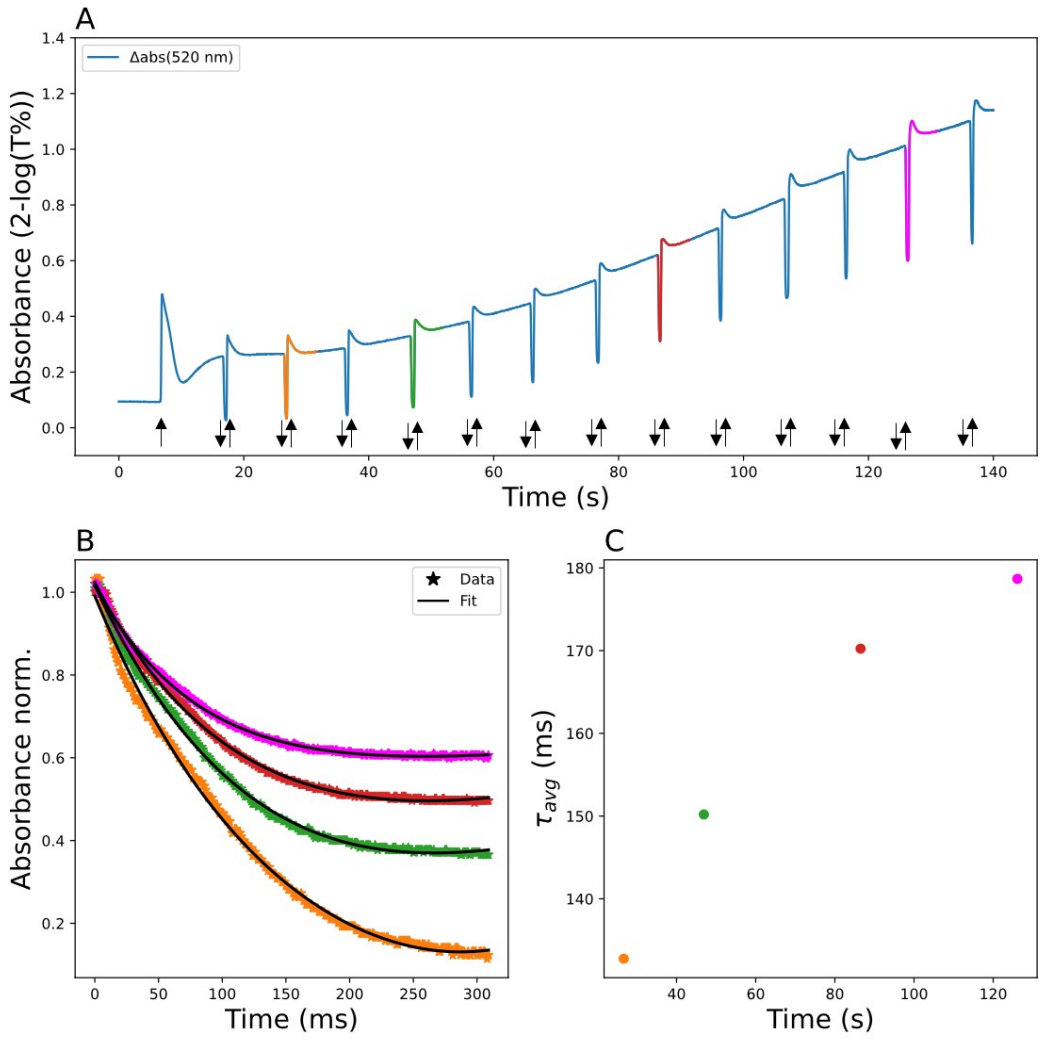

Figure 5.10. *A, Measure of ΔA(520nm) during a photosynthetic induction of a leaf of H. helix, arrows indicate switching on (upward) and off (downward) the actinic light; B, normalized decay of the ΔA(520nm) during a light-to-dark transition, points represent the data, the black line indicates the fit; C, average lifetime of the decay of the ΔA(520nm) signal caused from a light-to-dark transition (fit line reported in panel B). Similar color indicates a specific light-to-dark transition.*

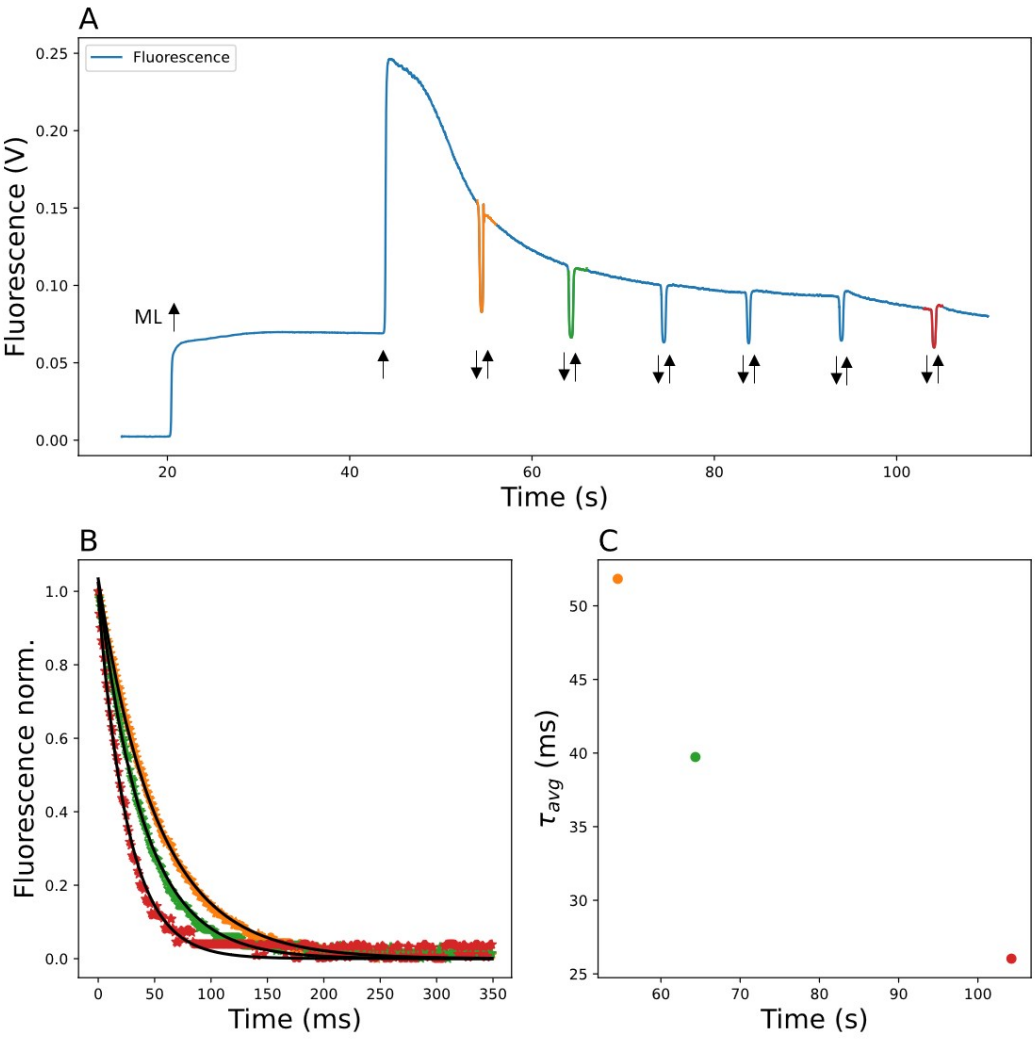

Figure 5.11. *A, The course of chlorophyll fluorescence during photosynthetic induction in a leaf of H. helix; the arrows indicate switching on (upward) and off (downward) the measuring light (noted ML) or the actinic light (not noted); B, the normalized decays of the chlorophyll fluorescence from* F_s *to* F_o' *during a light-to-dark transition, data points represent the data and the black line indicates the fit; C, average lifetime of the decay of the* F_s *to* F_o' *fluorescence yield during the light-to-dark transition (fit line reported in panel B). Different colors represent specific light-to-dark transition.*

5.4 Discussion

The Fludometer was developed with the intent to assess the operation and regulation of PSII by means of chlorophyll fluorescence, the operation and regulation of PSI (including electron transport to PSI via the rate-limiting PQH_2 cytochrome b_6f step) via near-infrared (NIR) absorbance changes, and using the ECS trans-thylakoid voltage and the rate constant for proton efflux from the lumen (normally this will be via the ATPase). As with previous designs (e.g. Kingston-Smith *et al.* [35]) the Fludometer was designed to be integrated with a leaf chamber that allowed carbon assimilation and transpiration to be measured from the leaf area to be subject to biophysical measurements, thus allowing carbon dioxide fixation to be correlated with thylakoid level processes. By implication, this leaf chamber also allowed the leaf environment, as the concentration of CO_2, O_2, H_2O, temperature, and irradiance (intensity and spectrum) to be controlled, and allowed the same leaf to be measured over the course of several days if needed. The Fludometer is based on the same discrete measuring pulse method developed by Joliot [48] and used in many other commercial and laboratory-built instruments (e.g. Joliot *et al.* [47]; Kuhlgert *et al.* [52]).

In building the Fludometer we sought to produce a design with a high degree of flexibility; while the design described here could use two chlorophyll fluorescence excitation channels, one 520 nm absorbance change channel (for ECS) and two NIR (810 nm and 940 nm) absorbance change channels this configuration can be easily altered by changing, as required, the LEDs and thus the measuring light wavelength, the photodiode detectors, and the firmware. The control of the system from a programmable microcontroller creates a great deal of potential flexibility in the functionality of the equipment. The design is also open source and can be easily modified to change the operation of the system (for example replacing the analog signal recovery circuitry with digital signal recovery). The novelty of the Fludometer lies in its programmability and its ability to generate single 10-microsecond light flashes (which can be made shorter) within a 100 microsecond measuring windows and to measure the amplitude of the transmitted or fluorescence produced by these pulses. In the current configuration with five channels, we can cycle through all five channels within 500 microseconds, which is sufficient to measure kinetics (such as the reduction kinetics of $P700^+$) with a half-time in the millisecond time range. These five channels allow processes associated with photosystem II , photosystem I, and *pmf* to be measured near-concurrently and in parallel with carbon dioxide fixation and transpiration under controlled conditions.

We tested the Fludometer's ability to measure sequentially the fluorescence and

absorbance changes associated with the concentration of Q_A^- and $P700^+$ during the photosynthetic induction of a dark-adapted leaf (**Figure 5.8**). The fluorescence signal (**Figure 5.8**-A) reflects the redox state of the first electron acceptor of PSII, Q_A, with increased fluorescence indicating more reduced Q_A. The ΔA(820 nm) signal (**Figure 5.8**-B) is assumed to reflects exclusively the oxidation state of the PSI reaction center, P700, with increased absorbance at 820 nm indicating an increase of the [$P700^+$]. In the early stage of the photosynthetic induction both curves mirror each other, with increased accumulation of $P700^+$ corresponding to an increased accumulation of Q_A^-. Interestingly we observe an increase of the ΔA(820 nm) at around 18 seconds from the start of the illumination (**Figure 5.8**-B), indicating an temporary reduction of $P700^+$ pool. The temporary reduction of $P700^+$ is mirrored by an increase in reduced Q_A (i.e. increase of the fluorescence signal). The temporary (re)accumulation of reduced P700 could be due to a transient decrease in the need for NADPH or ATP. In a transition between darkness to light, a lack of substrates for the carbon-fixating enzyme (RUBISCO) can occurs [53]. The limitation on the acceptor side of PSI can leads to an overall accumulation of reducing power along the electron transport chain (ETC) resulting in a temporary reduction of the first electron acceptor of PSII, Q_A (**Figure 5.8**).

We tested and verified the ability of the Fludometer to record with a high bandwidth (1 kHz) and good signal to noise light-induced absorbance changes at 820 nm (related to P700 redox state) and at 520 nm (related to the ECS), and chlorophyll fluorescence (related to Q_A redox state and non-photochemical quenching) during photosynthetic induction of ivy leaves (*Hedera helix*) collected in the field (**Figure 5.9**, **Figure 5.10** and **Figure 5.11**). The high signal to noise ratio (S/N) of the instrument when measuring with a 1 kHz response time allows us to clearly resolve and analyze light-to-dark decay kinetics taking place within the millisecond time range (**Figure 5.9**-B, **Figure 5.10**-B and **Figure 5.11**-B). These changes are due to:

1: the reduction of the $P700^+$ pool by electrons from the PQH_2 pool, so measuring what is believed to be the rate-limiting step of the electron transport chain (the ΔA(820nm)),
2: the equilibration of the trans-thylakoid proton motive force with the stromal phosphorylation potential following the cessation of electron transport (the ΔA(520nm)), and
3: the re-oxidation of the first stable electron acceptor of photosystem II (QA) due to the ending of the actinic illumination.

The high S/N allowed us to analyze rapid changes in state of the photosynthesis

without the need for signal averaging. The current design of the signal recovery system allows five different fluorescence or absorbance change phenomena to be measured near-concurrently (at most 100 µs between measurement pulses with an overall 500 µs measurement cycle). This allow the near simultaneous measurement of changes in several photosynthetic processes (e.g. electron and proton transport, operation and regulation of PSII, the ΔA(535nm) etc.). As the measurement system was designed around an existing gas analysis chamber these measurements can be made under highly controlled conditions (temperature, irradiance intensity and spectrum, gaseous phase composition), allowing us to measure the integrated operation of photosynthesis and how it responds to the environment. We have shown the instrument working with an analogue output that presents a continuous record of absorbance changes. At its core, however, the instrument depends on short measuring pulses (currently 10 µs long). This pulse-based operation would allow the system, with little modification, to be used purely in a pulse-based mode, analogous to a Joliot-type instrument [47].

In conclusion, simultaneously measuring the different components involved in photochemistry provides a powerful tool for gaining a more cohesive understanding of photosynthetic processes. The development of the Fludometer demonstrates that it is possible to design and build an instrument to probe photochemical processes using off-the-shelf electronic components. Although the design of the Fludometer can be considered relatively simple from an electrical engineer perspective, its development required a significant amount of time due to its didactic purpose. This limited the time available to use the Fludometer to characterize the regulation and limitation of the high rates of light-saturated carbon assimilation in the Brassicaceae species studied in this thesis; we postpone its application to future research.

References

1. Björkman, O. & Holmgren, P. Adaptability of the photosynthetic apparatus to light Intensity in ecotypes from exposed and shaded habitats. *Physiologia Plantarum* **16,** 889–914 (1963).
2. Harbinson, J., Kaiser, E. & Morales, A. S. *Integrating the stages of photosynthesis* in *Photosynthesis in Action* 195–242 (Elsevier, 2022).
3. Noctor, G. & Foyer, C. H. A re-evaluation of the ATP :NADPH budget during C3 photosynthesis: a contribution from nitrate assimilation and its associated respiratory activity? *Journal of Experimental Botany* **49,** 1895–1908 (1998).
4. Farquhar, G. D., Von Caemmerer, S. & Berry, J. A. A biochemical model of photosynthetic CO2 assimilation in leaves of C3 species. *Planta* **149,** 78–90 (1980).
5. Barber, J. & Archer, M. P680, the primary electron donor of photosystem II. *Journal of Photochemistry and Photobiology A: Chemistry* **142,** 97–106 (2001).
6. Müh, F. & Zouni, A. Structural basis of light-harvesting in the photosystem II core complex. *Protein Science* **29,** 1090–1119 (2020).
7. Sacksteder, C. A., Kanazawa, A., Jacoby, M. E. & Kramer, D. M. The proton to electron stoichiometry of steady-state photosynthesis in living plants: A proton-pumping Q cycle is continuously engaged. *Proceedings of the National Academy of Sciences* **97,** 14283–14288 (2000).
8. Nawrocki, W., Bailleul, B., Picot, D., Cardol, P., Rappaport, F., Wollman, F.-A. & Joliot, P. The mechanism of cyclic electron flow. *Biochimica et Biophysica Acta (BBA) - Bioenergetics* **1860,** 433–438 (2019).
9. Mehler, A. H. Studies on reactions of illuminated chloroplasts. *Archives of Biochemistry and Biophysics* **33,** 65–77 (1951).
10. Joliot, P. & Joliot, A. Cyclic electron transfer in plant leaf. *Proceedings of the National Academy of Sciences* **99,** 10209–10214 (2002).
11. Kramer, D. M. & Evans, J. R. The importance of energy balance in improving photosynthetic productivity. *Plant Physiology* **155,** 70–78 (2011).
12. Davis, G. A., Rutherford, A. W. & Kramer, D. M. Hacking the thylakoid proton motive force for improved photosynthesis: modulating ion flux rates that control proton motive force partitioning into $\Delta\ \psi$ and ΔpH. *Philosophical Transactions of the Royal Society B: Biological Sciences* **372,** 20160381 (2017).
13. Foyer, C., Furbank, R., Harbinson, J. & Horton, P. The mechanisms contributing to photosynthetic control of electron transport by carbon assimilation in leaves. *Photosynthesis Research* **25,** 83–100 (1990).
14. Genty, B. & Harbinson, J. *Regulation of light utilization for photosynthetic electron transport* in *Photosynthesis and the Environment* (ed Baker, N. R.) 67–99 (Kluwer Academic Publishers, Dordrecht, 1996).
15. Stiehl, H. H. & Witt, H. T. Quantitative treatment of the function of plastoquinone in photosynthesis. *Zeitschrift für Naturforschung B* **24,** 1588–1598 (1969).
16. Tikhonov, A. N. The cytochrome b6f complex at the crossroad of photosynthetic electron transport pathways. *Plant Physiology and Biochemistry* **81,** 163–183 (2014).
17. Briantais, J.-M., Vernotte, C., Picaud, M. & Krause, G. A quantitative study of the slow decline of chlorophyll a fluorescence in isolated chloroplasts. *Biochimica et Biophysica Acta (BBA) - Bioenergetics* **548,** 128–138 (1979).
18. Murata, N. & Sugahara, K. Control of excitation transfer in photosynthesis. III. Light-induced decrease of chlorophyll a fluorescence related to photophosphorylation system in spinach chloroplasts. *Biochimica et Biophysica Acta (BBA) - Bioenergetics* **189,** 182–192 (1969).
19. Oxborough, K. & Horton, P. A study of the regulation and function of energy-dependent quenching in pea chloroplasts. *Biochimica et Biophysica Acta (BBA) - Bioenergetics* **934,** 135–143 (1988).
20. Baker, N. R., Harbinson, J. & Kramer, D. M. Determining the limitations and regulation of photosynthetic energy transduction in leaves. *Plant, Cell & Environment* **30,** 1107–1125 (2007).
21. Butler, W. & Kitajima, M. Fluorescence quenching in Photosystem II of chloroplasts. *Biochimica et Biophysica Acta (BBA) - Bioenergetics* **376,** 116–125 (1975).
22. Lavergne, J. & Trissl, H. Theory of fluorescence induction in photosystem II: derivation of analytical expressions in a model including exciton-radical-pair equilibrium and restricted energy transfer between photosynthetic units. *Biophysical Journal* **68,** 2474–2492 (1995).
23. Lavorel, J. & Joliot, P. A connected model of the photosynthetic unit. *Biophysical Journal* **12,** 815–831 (1972).
24. Trissl, H.-W. Determination of the quenching efficiency of the oxidized primary donor of Photosystem I, P700+: Implications for the trapping mechanism. *Photosynthesis Research* **54,** 237–240 (1997).
25. Lazár, D. Chlorophyll a fluorescence induction. *Biochimica et Biophysica Acta (BBA) - Bioenergetics* **1412,** 1–28 (1999).
26. Genty, B., Wonders, J. & Baker, N. R. Non-photochemical quenching of Fo in leaves is emission wavelength dependent: consequences for quenching analysis and its interpretation. *Photosynthesis Research* **26,** 133–139 (1990).

27. Pfündel, E. Estimating the contribution of photosystem I to total leaf chlorophyll fluorescence. *Photosynthesis Research* **56,** 185–195 (1998).
28. Genty, B., Briantais, J.-M. & Baker, N. R. The relationship between the quantum yield of photosynthetic electron transport and quenching of chlorophyll fluorescence. *Biochimica et Biophysica Acta (BBA) - General Subjects* **990,** 87–92 (1989).
29. Baker, N. R. & Oxborough, K. *Chlorophyll fluorescence as a probe of photosynthetic productivity* in *Chlorophyll a Fluorescence* (eds Papageorgiou, G. C. & Govindjee) 65–82 (Springer Netherlands, Dordrecht, 2004).
30. Loriaux, S. D., Avenson, T. J., Welles, J. M., Mcdermitt, D. K., Eckles, R. D., Riensche, B. & Genty, B. Closing in on maximum yield of chlorophyll fluorescence using a single multiphase flash of sub-saturating intensity. *Plant, Cell & Environment* **36,** 1755–1770 (2013).
31. Schreiber, U., Klughammer, C. & Schansker, G. Rapidly reversible chlorophyll fluorescence quenching induced by pulses of supersaturating light in vivo. *Photosynthesis Research* **142,** 35–50 (2019).
32. Brettel, K. Electron transfer and arrangement of the redox cofactors in photosystem I. *Biochimica et Biophysica Acta (BBA) - Bioenergetics* **1318,** 322–373 (1997).
33. Sétif, P. Ferredoxin and flavodoxin reduction by photosystem I. *Biochimica et Biophysica Acta (BBA) - Bioenergetics* **1507,** 161–179 (2001).
34. Harbinson, J. & Woodward, F. I. The use of light-induced absorbance changes at 820 nm to monitor the oxidation state of P-700 in leaves. *Plant, Cell & Environment* **10,** 131–140 (1987).
35. Kingston-Smith, A. H., Harbinson, J., Williams, J. & Foyer, C. H. Effect of chilling on carbon assimilation, enzyme activation, and photosynthetic electron transport in the absence of photoinhibition in maize leaves. *Plant Physiology* **114,** 1039–1046 (1997).
36. Klughammer, C. & Schreiber, U. An improved method, using saturating light pulses, for the determination of photosystem I quantum yield via P700+-absorbance changes at 830 nm. *Planta* **192,** 261–268 (1994).
37. Schreiber, U. & Klughammer, C. Analysis of photosystem I donor and acceptor sides with a new type of online-deconvoluting kinetic LED-array spectrophotometer. *Plant and Cell Physiology,* pcw044 (2016).
38. Haehnel, W. Photosynthetic electron transport in higher plants. *Annual Review of Plant Physiology* **35,** 659–693 (1984).
39. Harbinson, J. & Hedley, C. L. The kinetics of P-700 $^{+}$ reduction in leaves: a novel *in situ* probe of thylakoid functioning. *Plant, Cell & Environment* **12,** 357–369 (1989).
40. Witt, H. Energy conversion in the functional membrane of photosynthesis. Analysis by light pulse and electric pulse methods. *Biochimica et Biophysica Acta (BBA) - Reviews on Bioenergetics* **505,** 355–427 (1979).
41. Schmidt, S., Reich, R. & Witt, H. T. *Electrochromic measurements in vitro as a test for the interpretation of field indicating absorption changes in photosynthesis* in *Photosynthesis, two centuries after its discovery by Joseph Priestley* (eds Forti, G., Avron, M. & Melandri, A.) 1087–1095 (Springer Netherlands, Dordrecht, 1972).
42. Bailleul, B., Cardol, P., Breyton, C. & Finazzi, G. Electrochromism: a useful probe to study algal photosynthesis. *Photosynthesis Research* **106,** 179–189 (2010).
43. Junge, W. & Witt, H. T. On the ion transport system of photosynthesis — Investigations on a molecular level —. *Zeitschrift für Naturforschung B* **23,** 244–254 (1968).
44. Mathiot, C., Gontero-Meunier, B., Alric, J., Delrue, F., Hienerwadel, R., Bailleul, B., Finazzi, G., Santé (Marseille), E. D. S. d. l. V. e. d. l. & d'Aix-Marseille, I. d. b. e. b. *Measurement of photosynthetic linear and cyclic electron flows, CO2 capture in green microalgae* (2020).
45. Kanazawa, A. & Kramer, D. M. *In vivo* modulation of nonphotochemical exciton quenching (NPQ) by regulation of the chloroplast ATP synthase. *Proceedings of the National Academy of Sciences* **99,** 12789–12794 (2002).
46. Horton, P. Relations between electron transport and carbon assimilation; simultaneous measurement of chlorophyll fluorescence, transthylakoid pH gradient and O_2 evolution in isolated chloroplasts. *Proceedings of the Royal Society of London. Series B. Biological Sciences* **217,** 405–416 (1983).
47. Joliot, P., Beal, D. & Frilley, B. Une nouvelle méthode spectrophotométrique destinée à l'étude des réactions photosynthétiques. *Journal de Chimie Physique* **77,** 209–216 (1980).
48. Joliot, P. & Delosme, R. Flash-induced 519 nm absorption change in green algae. *Biochimica et Biophysica Acta (BBA) - Bioenergetics* **357,** 267–284 (1974).
49. Schreiber, U., Groberman, L. & Vidaver, W. Portable, solid-state fluorometer for the measurement of chlorophyll fluorescence induction in plants. *Review of Scientific Instruments* **46,** 538–542 (1975).
50. Oxborough, K. *Using chlorophyll a fluorescence imaging to monitor photosynthetic performance* in *Chlorophyll a Fluorescence* (eds Papageorgiou, G. C. & Govindjee) 409–428 (Springer Netherlands, Dordrecht, 2004).
51. Hogewoning, S. W., Wientjes, E., Douwstra, P., Trouwborst, G., Van Ieperen, W., Croce, R. & Harbinson, J. Photosynthetic quantum yield dynamics: from photosystems to leaves. *The Plant Cell* **24,** 1921–1935 (2012).

52. Kuhlgert, S., Austic, G., Zegarac, R., Osei-Bonsu, I., Hoh, D., Chilvers, M. I., Roth, M. G., Bi, K., TerAvest, D., Weebadde, P. & Kramer, D. M. MultispeQ Beta: a tool for large-scale plant phenotyping connected to the open PhotosynQ network. *Royal Society Open Science* **3,** 160592 (2016).
53. Foyer, C. H., Lelandais, M. & Harbinson, J. Control of the quantum efficiencies of photosystems I and II, electron Flow, and enzyme activation following dark-to-light transitions in pea eaves: relationship between NADP/NADPH ratios and NADP-malate dehydrogenase activation state. *Plant Physiology* **99,** 979–986 (1992).

5.5 Supplementary

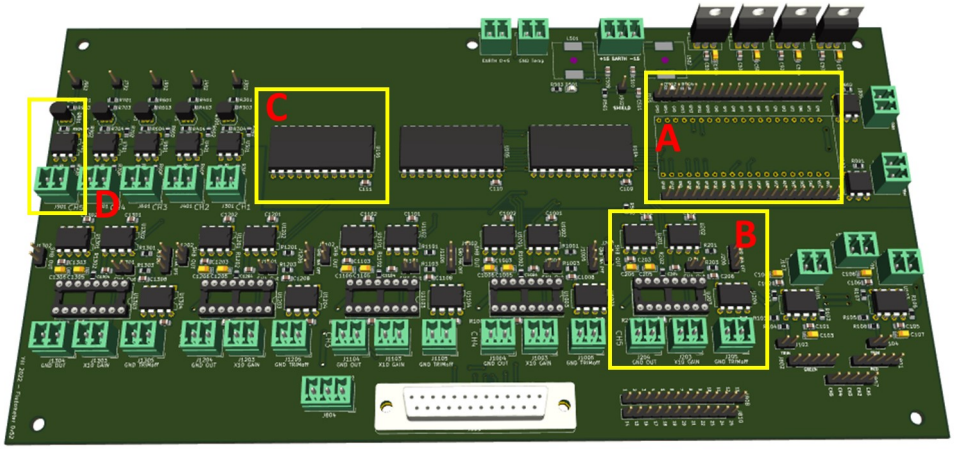

Figure 5.12. *Fludometer electronic board. A, microcontroller; B, one of the five demodulator; C, one of the three multiplexers used to send sequentially the pulse sequence to the pulsed current source (not on this board); D, optocoupled interface to transmit the "trigger" signal to the pulsed current source.*

The MicroPython code initialize two state machines, one used to generate the pulse sequence (Figure 5.1, "trigger", "S/H" A, "S/H B"), and the other to control the multiplexers (Figure 5.3, U104, U105, U106). The two functions are synchronized (wait the end of a pulse sequence before switching multiplexer) by toggling specific input/output or by waiting a certain polarity on them. The length of the pulse and the number of channel sampled can be easily controlled in silico.

```
from rp2 import PIO, StateMachine, asm_pio # Import library
from machine import Pin # Import library
@rp2.asm_pio(set_init=(rp2.PIO.OUT_LOW,)*4) # Set up PIO
    function, pulse function
def pulse_function():  # Define function for the pulse
    sequence
     pull(block) # Load 32bit from TX-FIFO to OSR
     out( y, 32) # Write the OSR value to Y register
     wrap_target() # repeat the function from here
     mov(x, y) # write on X value the value of Y (the delay)
```

```
    set(pins, 0b00000) [20] # Set all the pins LOW for 20
        clock cycles
    set(pins, 0b00001)   # Trigger the sample-and-hold A
    set(pins, 0b00000) [23] # Delay of 23 clock cycles
    set(pins, 0b00010)  # Trigger the light flash
    nop() [10]              # Delay for 10 clock cycles
    set(pins, 0b00110)   # Trigger the sample-and-hold B
    set(pins, 0b00000) [1]  # Switch off the sample-and-
        hold B and the light flash
    label("lp1")        # Loop in the delay
    jmp(x_dec, "lp1")       # Do nothing, decrease X, until
         X is equal to 0.
    set(pins, 0b01000) # End of cycle, set fourth pin high
        to acknowledge
    wait(0,pin,0) # Wait low on first input pin (signal
        from multiplexer that the new channel is configured)
    set(pins, 0b00000) # Set all pins low (send signal to
        multiplexer)
    wrap()    # Repeat
@asm_pio(out_init=(PIO.OUT_LOW,)*4,out_shiftdir=rp2.PIO.
    SHIFT_RIGHT,
         sideset_init=(PIO.OUT_HIGH),set_init=(rp2.PIO.
            OUT_LOW,)) # # Set up PIO function,
            multiplexing function
def mux_function():
    wrap_target()
    set(y,5) # Set register Y to 5 (number of channels)
    set(pins,1) # Set first pin high (communicate to the
        pulse_function that the mux_function is ready)
    label("loop") # Loop
    mov(osr,y)  .side(1) # Load on the OSR the value of Y,
        sideset pin high
    out(pins,4) .side(0) # Output on the pins the value
        loaded on the OSR, sideset pin low
    wait(1,pin,0) # Wait high on first input pin (wait that
         the pulse_function is finished)
```

```
    jmp(y_dec,"loop") # Jump to the loop label and decrease
        the value of Y
    set(pins,0) #End of cycle, repeat
    wrap()

# Setup of multiplexing state machine
mux_sm = rp2.StateMachine(0, mux_function,
                          freq=1_000_000,
                          out_base=Pin(16),
                          in_base=Pin(13),
                          sideset_base=Pin(22),
                          set_base=Pin(21))
mux_sm.active(1) # Activate multiplexing state machine
# Setup of pulse state machine
pulse_sm = rp2.StateMachine(1, pulse_function,
                            freq=1_000_000,
                            set_base=Pin(10),
                            in_base=Pin(22))
pulse_sm.put(100) # Add the delay of 100 clock cycle
pulse_sm.active(1) # Activate the pulse state machine
```

Chapter 6

General Discussion

6.1 Motivation of the research

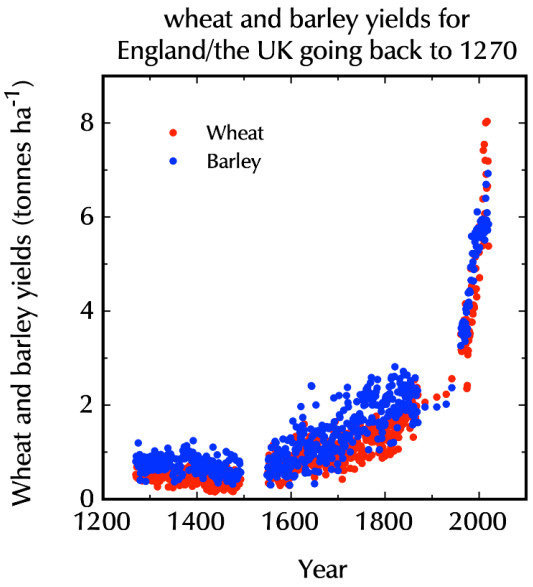

Figure 6.1. *Historical evolution of wheat and barley yield in England/UK from 1270 to present time. Credits: Our World in Data, ourworldindata.org*

In the more agriculturally developed parts of Europe, improved agricultural practices such as crop rotation and fertilizer use resulted in gradually increasing crop yields beginning in the late middle ages or renaissance period (**Figure 6.1**). Further technological improvements (e.g. mechanization, use of pesticide), combined with the breeding of higher-yielding crops suited to environments with reduced (a)biotic stresses produced the much greater year-on-year increases in crops yield that we associate with the Green Revolution [1, 2].

While remarkable, however, these current increases in crop yield are expected to be insufficient to meet the future growing demand driven by the increased meat and dairy consumption of a growing and more wealthy population. To the increased demand for agricultural production due to economic growth and population needs to be added needs of transitioning to a more sustainable bioeconomy in which agriculture will provide the biomass to be used as an industrial feedstock [3–5]. Significative improvements of current crop's yield are necessary to avoid bringing more land into cultivation which is a major factor in the decline of biodiversity [6].

It is currently expected that the yield of crops grown in optimal conditions (i.e. yield potential) can be further increased by enhancing the light absorption and conversion efficiency [7]. This is strongly influenced by the light-use efficiency of canopy photosynthesis, the amount of carbon fixed per unit of absorbed light energy per unit area [8]. Photosynthesis is a complex metabolic process involving numerous physiological processes taking place at different physical and temporal scales, ranging from inter-molecular energy transfer occurring in less than a picosecond to stomatal opening happening within minutes. The complexity of photosynthesis means that numerous genes contribute to any photosynthetic phenotype (e.g. higher rates of carbon assimilation), which makes it difficult to find genetic markers (required for targeted breeding) associated with a specific trait [9, 10]. A better understanding of the physiological mechanisms behind a complex trait, combined with functional genomics and modelling, has the potential to improve breeding for that trait [11, 12], for example improved photosynthesis.

During this thesis project, we investigated the potential physiological mechanisms that could explain the "higher than usual" photosynthetic capacity (i.e. maximum carbon fixation rate per unit leaf area) observed in certain C3 plant species. Within a pool of C3 species, a high maximum carbon fixation rate implies an improved photosynthetic light-use efficiency at high irradiances. This research on the physiological mechanisms leading to increased photosynthetic capacity was motivated by the assumption that the yield potential of a plant is equal to the integration of its photosynthetic rate (i.e. rate of carbon fixation per unit leaf area) throughout the growing season. Leaves with high photosynthetic capacity are not light-saturated by the highest irradiances normally encountered in the field (typically about 2000 µmol m^{-2} s^{-1}). In the case of crop plant with such high photosynthetic rates, even their canopy uppermost leaves would not be light saturated and the lower leaves would be even further from saturation, therefore higher rates of assimilation could be achieved across the range of irradiances encountered in the canopy. Understanding the physiological mechanisms behind high rates of photosynthetic capacity would enable a more targeted search for the underlying genes and, in the longer term, pave the way to develop a new generation of crops with enhanced yield potential.

The plant species studied in this research included the species *Arabidopsis thaliana*, *Brassica rapa*, *Brassica nigra* and *Hirschfeldia incana*. The different plant species belong to the same family (Brassicaceae) and differ in their photosynthetic capacity when grown in the same controlled conditions. For example, when grown under high irradiance (1800 µmol m^{-2}

s^{-1}), the model plant species *Arabidopsis thaliana*, showed a gross photosynthetic capacity up to 30 µmol m^{-2} s^{-1}, while for *Brassica rapa* and *Brassica nigra* it was 40 µmol m^{-2} s^{-1} and for *Hirschfeldia incana* above 50 µmol m^{-2} s^{-1}, most of the time [13, 14].
In Chapter 3 and 4 we investigated whether the higher light-use efficiency observed in some of the Brassicaceae could be explained by a reduction in the photosystem II functional antenna size, σ_f(PSII) and/or via a change of the distribution and size of the chloroplasts within the leaf.

6.2 Physiological adaptations found in this thesis

In this thesis are reported and discussed possible physiological adaptations that might play a role in permitting the high photosynthetic rates observed in some of the Brassicaceae studied. A high assimilation rate implies that these plants can maintain a higher photosynthetic light-use efficiency at high irradiances and that leaves of these plants might have a higher diffusive transport of CO_2 from the free air around the leaves to the site of carboxylation and that the generation of reducing power (i.e. NADPH, ferredoxin) and nucleoside phosphate (i.e. ATP, ADP) is sufficient to meet the demands of the carbon dioxide fixation.

The generation of reducing power is initiated by the photochemical activity of PSII. Photosystem II (PSII) uses light energy to induce charge separation in the PSII reaction center, a process that is the first chemical step in the splitting of water by the oxygen-evolving complex (OEC). Water splitting results in the formation of oxygen, protons, and electrons. The electrons flow through the electron transport chain (ETC) until they reach photosystem I (PSI), where a light-driven charge separation process occurs that is very similar to that found in PSII. On the PSI acceptor side, an electron liberated from the special reaction chlorophyll pair, P700, is used to reduce a final electron acceptor (i.e. ferredoxin). The P700+ formed in the PSI reaction center by this charge separation is reduced by an electron from plastocyanin, which in turn is reduced by cytochrome f, the plastoquinol pool and, ultimately, PSII. A typical leaf has about 1 µmol m^2 of PSI and PSII and leaves are good absorbers of light - in the PAR region the average absorption is about 80 - 90%. This implies that at full sunlight, with an irradiance (PAR) of 2 000 µmol m^{-2} s^{-1} each reaction center type is being excited at a rate (i.e. frequency) of about 1000 s-1. The rate of electron transport between the photosystems is limited by the PQH_2/cytochrome b_6f step - this results in the time constant of 4 ms or more [15] for the reduction of $P700^+$ by electrons from PQH_2. This means that the rate of reaction center excitation can be much greater than the rate of electron transport between the photosystems. If the rate of electrons formed by PSII exceeds the rate of electron transport of the ETC, protective

mechanisms are activated which downregulate the rate of charge separation (i.e. quantum efficiency) of both photosystems [16].
H. incana, *B. nigra* and *B. rapa* were reported to have higher operating PSII quantum efficiency (i.e. light adapted PSII quantum yield, ΦPSII, as calculated as in Genty *et al.* [17]) compared to *A. thaliana* [18]. The higher ΦPSII observed in *H. incana*, *B. nigra* and *B. rapa* indicates that the rate of electron supply into the ETC by PSII, or electron removal from the ETC by PSI, does not outpace the rate of electron transport of the ETC to the same extent as it does in *A. thaliana*. We therefore tested two possible physiological adaptations that can bring the rate (or frequency) of charge separation more into alignment with electron transport capacity.
The PSII functional antenna size, σ_f(PSII), is the product of PSII maximum quantum yield and the PSII optical cross-section. A decrease in σ_f(PSII) lowers the frequency of charge separation and consequently reduces the rate of electron supply into the ETC. In Chapter 3 we compared the σ_f(PSII) across the different plant species grown under two different irradiances (PPFD of 250, and 1100 µmol m^{-2} s^{-1}). We noticed that the Brassicaceae with higher photosynthetic capacity had a more marked reduction of σ_f(PSII) compared to the species with lower photosynthetic capacity. **Figure 6.2** shows the observed σ_f(PSII) for the adaxial side of the leaf (i.e. average lifetime of PSII measured in condition of open reaction centers, Fo PSII $\tau_a$vg) described in Chapter 3 against the rate of photosynthesis measured at 1100 µmol m^{-2} s^{-1} (from Garassino *et al.* [13]). It is clear that a higher photosynthetic rate at high irradiance scales relatively well with smaller σ_f(PSII). Despite the linear correlation between PSII functional antenna size and maximum rates of CO_2 assimilation reveals something of the scale of coordination of adaptation in photosynthesis, the correlation should not be interpreted as revealing a simple, causal relationship between the antenna size of PSII and photosynthetic metabolism.

The reduction of PSII functional antenna size is likely not the simple, single cause for the enhanced photosynthetic capacity observed in some of the Brassicaceae tested. At the leaf level, the photosynthetic capacity reflects the sum of the photosynthetic rates of each single chloroplast exposed to a different intra-leaf light environment [19, 20]. Just as a decrease in irradiance within a canopy leads to a decrease in the rates of photosynthesis [21], the attenuation of irradiance through the depth of a leaf results in a decrease in the rates of photosynthesis of the chloroplasts located on the bottom side (i.e. abaxial) [22–24]. The attenuation of irradiance within a leaf is caused by the combined effect of light absorption by the chlorophylls tightly packaged within the chloroplasts (i.e. sieve effect), and the scattering of light (i.e. path lengthening) caused by the air-liquid interface in the intercellular airspace (see Slattery & Ort [25] and reference therein). The chloroplasts

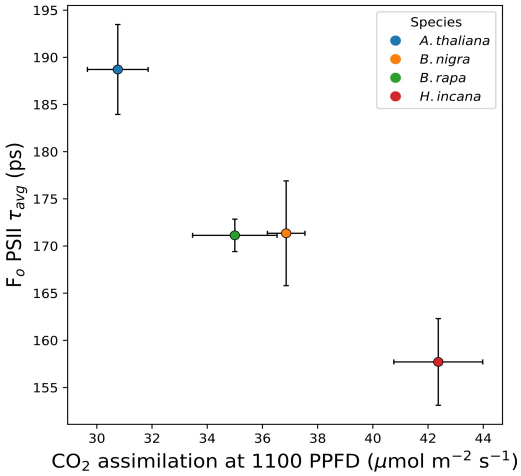

Figure 6.2. *The correlation between PSII fluorescence lifetime with open reaction centers* (F_o) *and rate of* CO_2 *assimilation at an irradiance of 1100 (*μ*mol* m^{-2} s^{-1}*; data of Garassino* et al. *[13]). When measured with PSII in the* F_o *state the PSII average lifetime scales linearly with the PSII functional antenna size (see* ***Chapter 3****).*

that are farthest from the incident irradiance have a lower photosynthetic rate compared to those closer to the incident irradiance. This is due to a decrease in the rate of electron transport rather than a reduction in Rubisco content [26]. Therefore, a flatter inter-leaf irradiance profile could enhance the photosynthetic rates of the chloroplasts located on the lower epidermis, resulting in an increased photosynthetic capacity at the leaf level [27].

We investigated whether the high photosynthetic capacity observed in some of the Brassicaceae tested could be explained by physiological changes that can improve the light distribution within the leaf. In **Chapter 3**, we observed that all plant species reduced the σ_f(PSII) in the pool of chloroplasts located on the adaxial side of the leaf compared to the abaxial side. The decrease in σ_f(PSII) on the one hand reduces the risk of saturating the photosynthetic machinery, and on the other hand facilitates the light penetration to the lower part of the leaf [28, 29]. In addition to the effect of σ_f(PSII), the volume of the chloroplasts within the leaf tissue could in principle modify the penetration of the irradiance in the leaf. In **Chapter 4** we observed that at a high growth irradiance *A. thaliana* and *H. incana* decreased the volume of chloroplasts located in the palisade mesophyll compared to those located in the spongy mesophyll. A decrease in chloroplast volume would increase the transmittance of the leaf improving light penetration to the lower mesophyll [30]. However, the chloroplast regulation observed in **Chapter 4** by itself cannot

explain the higher photosynthetic capacity of *H. incana* or *B. rapa*. Species with a relatively low photosynthetic capacity (i.e. *A. thaliana*) and species with high photosynthetic capacity (i.e. *H. incana*) similarly actively regulate the chloroplast size. On the other hand, species that do not regulate the chloroplast size (*B. rapa*) still achieve relatively high photosynthetic capacity [13, 31].

6.3 What is missing and future outlook

The physiological mechanisms underlying the high photosynthetic capacity of some C3 plants are yet to be fully elucidated. We considered the possible effects on the photosynthetic capacity of adaptation of PSII functional antenna size (**Chapter 3**) and chloroplast morphology (**Chapter 4**), which could affect intra-leaf light distribution and the aqueous phase component of mesophyll conductance. The combined effect of chloroplast size reduction and decreased PSII functional antenna size could result in an improved light distribution in H. incana compared to the other species. Nonetheless, to get better insight into the photosynthetic capacity of the Brassicaceae studied, it is necessary to measure the number of chloroplasts per cell and the surface area of the chloroplasts facing the intercellular air space (i.e. the S_c parameter). The method detailed in **Chapter 4** is suited for measuring the number of chloroplasts per cell and deriving the S_c parameter in 3D. Within the time frame of the thesis, it was not possible to perform this analysis. However, because of the tight link between the photosynthetic capacity of a leaf and the number of chloroplasts per cell (affecting S_c) [32, 33], I hope to pursue the analysis in the future.

The possible effects of decreased PSII functional antenna size on the balancing of the supply of electrons and holes to the ETC with electron flow through the ETC was discussed in **Chapter 3**. Reducing σ_f(PSII) certainly reduces the risk of exceeding the electron transport capacity leading to a decrease in PSII quantum efficiency. However, high rates of carbon fixation generate a high demand for reducing power (i.e. ferredoxin, NADPH) [34]. Leaves with high photosynthetic capacity have more photosystems (i.e. PSI and PSII reaction centers), and especially a higher content of electron transport components [35, 36]. The limiting step of electron transport is the rate of oxidation of the plastoquinol pool (PQH_2) by the cytochrome b_6f [37]. Therefore, in analogy to an electronic circuit, if the resistance to the flow of electrons is fixed (i.e. the rate of PQH_2 oxidation by the cytochrome b_6f), the only way to increase the flow of electrons is to increase the number of resistances in (i.e. more cytochrome b_6f content) which results in an increase in conductivity. To understand whether higher photosynthetic capacity is achieved by "piling up" more photosynthetic machinery or by an increase in the

efficiency of the ETC, we need to quantify the subparts composing the photosynthetic machinery (photosystems reaction center, cytochrome b_6f, etc..) on a leaf area based unit along the measure of the rate constant of the electron transport chain. Measuring the ETC rate constant can be done by following the rate of reduction of $P700^+$ following a light-to-dark transition using near-infrared absorbance changes [38]. The concentration of photosystems I and II could be derived by light-induced absorbance changes measured at specific wavelengths (e.g. ultraviolet, green) in combination with the photosynthetic inhibitors that block forward electron transport from Q_A in PSII or electron transport from plastocyanin to P700 [39, 40], combined with additional biochemical analysis. The instrument detailed in **Chapter 5**, was designed to be broadly applicable and is capable of measuring the above-mentioned spectroscopic changes and was designed to further characterize the limitations and regulation of photosynthesis *in vivo*. Its use will provide additional insight into the physiological mechanisms behind higher photosynthetic capacity in the coming future.

The possible physiological mechanisms behind the high photosynthetic capacity observed in some Brassicaceae were investigated with the hope to enable the breeding of crops with enhanced yield. Nonetheless, it is worth researching the physiological causes (and the underlying genes) of other photosynthetic-related traits. Especially in a world where the frequency of extreme weather events (e.g. heat waves, severe frost) is increasing due to climate change. For example, improving crop's balance between the amount of CO_2 fixed and the connected loss of H_2O via transpiration (i.e. water use efficiency) can result in an advantage (and an increase in yield) in water-limiting environments [41]. The natural variability of photosynthetic traits observed in this thesis (i.e. PSII functional antenna size, chloroplast morphology) can be used as a source of inspiration to find novel physiological mechanisms to improve photosynthesis.

The variability in photosynthetic traits means that there is likely not a "best photosynthesis", but rather an "optimal photosynthesis" depending on the plant eco-physiology. Crop yield can be improved by understanding the physiology and the underlying genes of a photosynthetic phenotype that suits a certain growth environment.

References

1. Evans, L. T. *Crop evolution, adaptation and yield* (Cambridge University Press, Cambridge, 1993).
2. Slafer, G. A., Satorre, E. H. & Andrade, F. H. *Genetic improvement of field crops* 1st (CRC Press, 1993).
3. *The state of the world's land and water resources for food and agriculture: managing systems at risk* (ed FAO) (Earthscan [u.a.], Abingdon, 2011).
4. Hall, A. J. & Richards, R. A. Prognosis for genetic improvement of yield potential and water-limited yield of major grain crops. *Field Crops Research* **143,** 18–33 (2013).
5. Ray, D. K., Mueller, N. D., West, P. C. & Foley, J. A. Yield trends are insufficient to double global crop production by 2050. *PLoS ONE* **8** (ed Hart, J. P.) e66428 (2013).
6. Kleijn, D., Kohler, F., Báldi, A., Batáry, P., Concepción, E., Clough, Y., Díaz, M., Gabriel, D., Holzschuh, A., Knop, E., Kovács, A., Marshall, E., Tscharntke, T. & Verhulst, J. On the relationship between farmland biodiversity and land-use intensity in Europe. *Proceedings of the Royal Society B: Biological Sciences* **276,** 903–909 (2009).
7. Monteith, J. L. Climate and the efficiency of crop production in Britain. *Philosophical Transactions of the Royal Society of London. B, Biological Sciences* **281,** 277–294 (1977).
8. Zhu, X.-G., Long, S. P. & Ort, D. R. Improving photosynthetic efficiency for greater yield. *Annual Review of Plant Biology* **61,** 235–261 (2010).
9. Hammer, G. L., Chapman, S., Van Oosterom, E. & Podlich, D. W. Trait physiology and crop modelling as a framework to link phenotypic complexity to underlying genetic systems. *Australian Journal of Agricultural Research* **56,** 947 (2005).
10. Theeuwen, T. P. J. M., Logie, L. L., Harbinson, J. & Aarts, M. G. M. Genetics as a key to improving crop photosynthesis. *Journal of Experimental Botany* **73** (ed Kromdijk, J.) 3122–3137 (2022).
11. Cooper, M., Van Eeuwijk, F. A., Hammer, G. L., Podlich, D. W. & Messina, C. Modeling QTL for complex traits: detection and context for plant breeding. *Current Opinion in Plant Biology* **12,** 231–240 (2009).
12. Yin, X., Struik, P. C. & Kropff, M. J. Role of crop physiology in predicting gene-to-phenotype relationships. *Trends in Plant Science* **9,** 426–432 (2004).
13. Garassino, F., Wijfjes, R. Y., Boesten, R., Reyes Marquez, F., Becker, F. F. M., Clapero, V., Van Den Hatert, I., Holmer, R., Schranz, M. E., Harbinson, J., De Ridder, D., Smit, S. & Aarts, M. G. M. The genome sequence of *Hirschfeldia incana* , a new Brassicaceae model to improve photosynthetic light-use efficiency. *The Plant Journal* **112,** 1298–1315 (2022).
14. Retta, M. A., Van Doorselaer, L., Driever, S. M., Yin, X., De Ruijter, N. C. A., Verboven, P., Nicolaï, B. M. & Struik, P. C. High photosynthesis rates in *Brassiceae* species are mediated by leaf anatomy enabling high biochemical capacity, rapid CO_2 diffusion and efficient light use. *New Phytologist*, nph.20136 (2024).
15. Harbinson, J., Kaiser, E. & Morales, A. S. *Integrating the stages of photosynthesis* in *Photosynthesis in Action* 195–242 (Elsevier, 2022).
16. *Photosynthesis and the environment* (eds Baker, N. R. & Jee, G.) (Springer Netherlands, Dordrecht, 1996).
17. Genty, B., Briantais, J.-M. & Baker, N. R. The relationship between the quantum yield of photosynthetic electron transport and quenching of chlorophyll fluorescence. *Biochimica et Biophysica Acta (BBA) - General Subjects* **990,** 87–92 (1989).
18. Garassino, F., Caracciolo, L., Van De Belt, J., Albiero, M., Pool, R., Schreurs, F., De Ridder, D., Harbinson, J. & Aarts, M. G. M. Analysis of natural variation in photosynthesis in a panel of Brassicaceae species (2023).
19. Terashima, I. & Saeki, T. Light environment within a leaf. Optical properties of paradermal sections of camellia leaves with special reference to differences in the optical properties of palisade and spongy tissues. *Plant and Cell Physiology* **24,** 1493–1501 (1983).
20. Terashima, I. & Saeki, T. A new model for leaf photosynthesis incorporating the gradients of light environment and of photosynthetic properties of chloroplasts within a leaf. *Annals of Botany* **56,** 489–499 (1985).
21. Saeki, T. Interrelationships between Leaf Amount, Light Distribution and Total Photosynthesis in a Plant Community. *Shokubutsugaku Zasshi* **73,** 55–63 (1960).
22. Nishio, J. N., Sun, J. & Vogelmann, T. C. Carbon fixation gradients across spinach leaves do not follow internal light gradients. *The Plant Cell*, 953–961 (1993).
23. Terashima, I. & Inoue, Y. Palisade tissue chloroplasts and spongy tissue chloroplasts in spinach: biochemical and ultrastructural differences. *Plant and Cell Physiology* (1985).
24. Terashima, I. & Inoue, Y. Vertical gradient in photosynthetic properties of spinach chloroplast dependent on intra-leaf light environment. *Plant and Cell Physiology* **26,** 781–785 (1985).
25. Slattery, R. A. & Ort, D. R. Perspectives on improving light distribution and light use efficiency in crop canopies. *Plant Physiology* **185,** 34–48 (2021).

26. Terashima, I., Fujita, T., Inoue, T., Chow, W. S. & Oguchi, R. Green light drives leaf photosynthesis more efficiently than red light in strong white light: revisiting the enigmatic question of why leaves are green. *Plant and Cell Physiology* **50,** 684–697 (2009).
27. Tholen, D., Boom, C. & Zhu, X.-G. Opinion: Prospects for improving photosynthesis by altering leaf anatomy. *Plant Science* **197,** 92–101 (2012).
28. Ort, D. R., Zhu, X., () & Melis, A. Optimizing antenna size to maximize photosynthetic efficiency. *Plant Physiology* **155,** 79–85 (2011).
29. Pettigrew, W. T., Hesketh, J. D., Peters, D. B. & Woolley, J. T. Characterization of canopy photosynthesis of chlorophyll-deficient soybean isolines. *Crop Science* **29,** 1025–1029 (1989).
30. Jeong, W. J., Park, Y.-I., Suh, K., Raven, J. A., Yoo, O. J. & Liu, J. R. A large population of small chloroplasts in tobacco leaf cells allows more effective chloroplast movement than a few enlarged chloroplasts. *Plant Physiology* **129,** 112–121 (2002).
31. Taylor, S. H., Orr, D. J., Carmo-Silva, E. & Long, S. P. During photosynthetic induction, biochemical and stomatal limitations differ between *Brassica* crops. *Plant, Cell & Environment* **43,** 2623–2636 (2020).
32. Miyazawa, S.-I. & Terashima, I. Slow development of leaf photosynthesis in an evergreen broad-leaved tree, *Castanopsis sieboldii* : relationships between leaf anatomical characteristics and photosynthetic rate. *Plant, Cell & Environment* **24,** 279–291 (2001).
33. Ren, T., Weraduwage, S. M. & Sharkey, T. D. Prospects for enhancing leaf photosynthetic capacity by manipulating mesophyll cell morphology. *Journal of Experimental Botany* **70,** 1153–1165 (2018).
34. Yamori, W., Kondo, E., Sugiura, D., Terashima, I., Suzuki, Y. & Makino, A. Enhanced leaf photosynthesis as a target to increase grain yield: insights from transgenic rice lines with variable Rieske FeS protein content in the cytochrome b_6 / f complex. *Plant, Cell & Environment* **39,** 80–87 (2016).
35. Evans, J. R. The relationship between electron transport components and photosynthetic capacity in pea leaves grown at different irradiances. *Functional Plant Biology* **14,** 157 (1987).
36. Gu, L. Optimizing the electron transport chain to sustainably improve photosynthesis. *Plant Physiology* **193,** 2398–2412 (2023).
37. Tikhonov, A. N. The cytochrome b6f complex at the crossroad of photosynthetic electron transport pathways. *Plant Physiology and Biochemistry* **81,** 163–183 (2014).
38. Harbinson, J. & Hedley, C. L. The kinetics of P-700 $^+$ reduction in leaves: a novel *in situ* probe of thylakoid functioning. *Plant, Cell & Environment* **12,** 357–369 (1989).
39. Fan, D.-Y., Hope, A. B., Smith, P. J., Jia, H., Pace, R. J., Anderson, J. M. & Chow, W. S. The stoichiometry of the two photosystems in higher plants revisited. *Biochimica et Biophysica Acta (BBA) - Bioenergetics* **1767,** 1064–1072 (2007).
40. Melis, A. & Brown, J. S. Stoichiometry of system I and system II reaction centers and of plastoquinone in different photosynthetic membranes. *Proceedings of the National Academy of Sciences* **77,** 4712–4716 (1980).
41. Condon, A. G. Breeding for high water-use efficiency. *Journal of Experimental Botany* **55,** 2447–2460 (2004).

Samenvatting - Summary

Samenvatting

Ik heb mijn PhD uitgevoerd binnen een multidisciplinair project dat de fysiologische oorzaken van de hoge koolstof assimilatie in het bladoppervlak van verschillende Brassicaceae-soorten onderzocht en mogelijke verantwoordelijk genen. Specifiek richtte het onderzoek zich op het vergelijken van *Hirschfeldia incana*, een plantensoort met een uitzonderlijk hoge koolstofopname voor een C3-plant ($\sim$ 50 µmol m^{-2} s^{-1}), met andere Brassicaceae-soorten met een meer typische koolstofopname. Mijn onderzoek richtte zich voornamelijk op fysiologische aspecten. Hiervoor gebruikte ik verschillende spectroscopische technieken om de fotosynthetische lichtgebruiksefficiëntie en morfologische veranderingen op bladniveau te analyseren. Daarnaast ontwikkelde ik specifieke instrumenten om bepaalde aspecten van het onderzoek mogelijk te maken.

In het tweede hoofdstuk ontwikkelde ik een apparaat om de intensiteit van de lichtinstallatie in de groeikamers te regelen. Met deze "intelligente dimmer", bestaande uit een microcontroller en een interface, kon de lichtintensiteit programmatisch worden geregeld. Het apparaat werd gebruikt in alle opvolgende experimenten en maakte het mogelijk om planten onder verschillende lichtomstandigheden te kweken.

In hoofdstuk drie onderzocht ik of de verhoogde lichtgebruiksefficiëntie die in bepaalde Brassicaceae-soorten zoals *H. incana* word waargenomen, het gevolg zou kunnen zijn van een vermindering in de functionele antennegrootte van fotosysteem II (σ_f(PSII)). Om de grootte van σ_f(PSII) te meten gebruikte ik twee spectroscopische technieken gebaseerd op fluorescentiestijging en ultrasnel fluorescentieverval. De resultaten geven aan dat σ_f(PSII) wordt gereguleerd in reactie op lichtintensiteiten, zelfs binnen één blad. Bovendien werd er een lineaire correlatie waargenomen tussen σ_f(PSII) en de maximale PSII-kwantumopbrengst (F_v/F_m). Ik bediscussieer of de correlatie te wijten is aan hoge

intensiteit quenching in de PSII-antenne of aan de verbeterde overdrachtsefficiëntie veroorzaakt door de verminderde optische doorsnede van PSII (d.w.z. een hogere RC/LHCs-verhouding).

In het vierde hoofdstuk onderzocht ik of hoge fotosynthesesnelheden het gevolg zouden kunnen zijn van een verschillende chloroplastgroottes bij verschillende plantensoorten. Ik gebruikte een multiphoton microscoop om 3D-beelden te maken van chloroplasten in een bladdoorsnede. Voor de visualisatie maakte ik gebruik van de autofluorescentie van chlorofyl *a*. Met behulp van beeldanalyse op basis van machine learning richtte ik mijn analyse op mogelijke veranderingen in volume en oppervlak van afzonderlijke chloroplasten. Ik zag dat sommige plantensoorten het chloroplastvolume aanpasten in reactie op lichtintensiteit, terwijl andere plantensoorten hetzelfde chloroplastvolume behouden. De soorten die een reactie op lichtintensiteit vertonen, hebben ook verschillende reacties binnen een blad, afhankelijk van of de chloroplasten zich aan de adaxiale zijde of de abaxiale zijde van het blad bevinden.

In hoofdstuk vijf beschrijf ik de ontwikkeling van een open-source instrument om de fysiologie achter de hoge fotosynthetische capaciteit verder te onderzoeken. Het instrument kan achtereenvolgens tot vijf verschillende fluorescentie- of absorptieveranderingssignalen meten binnen een tijdsvenster van een halve milliseconde. Het instrument is ontworpen om fluorescentie en verschillende absorptieveranderingen te meten. De fluorescentiesignalen zijn gerelateerd aan de redoxstatus van de eerste elektronenacceptor van PS II (d.w.z. Q_A). De absorptieverandering in het nabij-infrarood zijn gerelateerd aan de redoxstatus van het PSI-reactiecentrum (d.w.z. P700). En de absorptieveranderingen in het zichtbare (groene) zijn gerelateerd aan de protonmotiefkracht die op thylakoïd niveau wordt gegenereerd.

Summary

I conducted my PhD within a multidisciplinary project that investigated the physiological causes and potential underlying genes responsible for the high rates of leaf area carbon assimilation among various Brassicaceae species. Specifically, the project research focused on *Hirschfeldia incana*, a plant species which exhibits exceptionally high rates of carbon assimilation for a C3 plant ($\sim$ 50 µmol m^{-2} s^{-1}), and compared it to other Brassicaceae species with more typical carbon assimilation rates. My research primarily centered on physiological aspects; I utilized various spectroscopic techniques to analyze photosynthetic light-use efficiency and morphological changes at the leaf level. Additionally, I developed specific instrumentation to enable certain aspects of the research.

In the second chapter, I developed a device to regulate the intensity of the light setup in the growth chambers. This "intelligent dimmer", composed of a micro-controller and an interface, allowed light intensity to be programmatically controlled. The device was used in all subsequent experiments conducted for the thesis and allowed the cultivation of plants under divergent light conditions.

In the third chapter, I explored the hypothesis that the elevated rates of light-use efficiency observed in certain Brassicaceae species as *H. incana* could stem from a reduction in PSII functional antenna size (σ_f(PSII)). To measure the σ_f(PSII) I utilized two independent spectroscopic techniques based on fluorescence rise and ultra-fast fluorescence decay. The results indicate that σ_f(PSII) is regulated in response to light intensities, even within a single leaf. Additionally, a linear correlation between σ_f(PSII) and maximum PSII quantum yield (F_v/F_m) was observed. I discuss whether the correlation is due to high-intensity quenching taking place in the PSII antenna or due to the improved trapping efficiency caused by the reduced optical cross-section (i.e. higher RC/LHCs ratio).

In the fourth chapter, I investigated the hypothesis that high rates of photosynthesis could be due to a different chloroplast size across plant species. I used a multiphoton microscope to acquire 3D images of chloroplasts within a leaf section exploiting the auto-fluorescence of chlorophyll *a*. Using image analysis based on machine learning I focused my analysis on possible changes of volume and surface at the level of single chloroplasts. I observed that some plant species adjust the chloroplast volume in response to irradiance, while other plant species maintain the same chloroplast volume. The species that show a response to irradiance, have also different chloroplast volume depending on

whether the chloroplasts are in cells located on the adaxial side or the abaxial side of the leaf.

In the last chapter, I detail the development of an open-source instrument aimed to further investigate the physiology behind high photosynthetic capacity. The instrument can measure up to five different fluorescence or absorbance change signals sequentially within a time window of half a millisecond. The instrument was designed to measure fluorescence signals to probe the redox state of the photosystem II first electron acceptor (i.e. Q_A), combined with absorbance changes in the near-infrared to measure the redox state of the PSI reaction center (i.e. P700), along with absorbance changes in the visible (green) to derive the proton motive force generated at the thylakoid level.

Acknowledgments

Writing the acknowledgment section is arguably the most challenging part of the thesis, especially considering that, if the reader is anything like me, these few pages will likely be the only part of the thesis to be read. The work presented in this thesis is the result of collaboration and the contributions of many people. I am grateful to everyone who has directly or indirectly taught me something and supported me, making these PhD years enjoyable, stimulating, and fun.

The first words go to my supervisors **Jeremy** and **Herbert**, thanks for having selected a student in environmental science for a PhD in biophysics. Jeremy, I value the freedom you gave me during these years, allowing me to pursue my interests in electronics and introducing me to the world of custom-built spectroscopes. I still remember the first time we assembled one of your devices; it was thrilling to see a signal change when the actinic light was applied to a leaf. Herbert, I appreciate your insightful questions, which pushed me to think deeper and better understand the measurements I was collecting. You have a keen eye for spotting inconsistencies in data, and I hope to become as skilled as you in solving "Fermi's problems" one day. Thank you also for steering me back on the right track when my interests were drifting a bit too far.

During this PhD journey, I also had an unplanned additional supervisor, **John**, you supported me and taught me most of my current knowledge of electronics. When I first saw your workspace I got very excited and I felt that I would learn a lot during my time at the Laboratory of Biophysics. Thank you for taking the time not only to design and assemble some of the circuits but also to explain how they work.

Parmi mes encadrants, une mention spéciale revient à **Bernard**. Ta supervision a été formidable et m'a poussé à approfondir ma compréhension des mécanismes de

séparation de charge. Le troisième chapitre te doit beaucoup, et je te remercie de m'avoir appris à être un bon fleuriste et j'espère, un meilleur biophysicien. Un mot vas aussi à **Léo**, merci de m'avoir accueilli et supporté pendant mon séjour à Cadarache.

The work reported in this thesis was part of a broader consortium project that involved multiple talented researchers ranging from the field of genetics to modeling, **Francesco**, **Sofia**, **Nam**, and **Moges**. It was a pleasure working with you, and fun to team up to try to unravel the mechanisms behind the high photosynthetic capacity of those Brassicaceae. Thanks also to all the people involved in the project **Dick**, **Xinyou**, **Paul**, **Sandra**, **Eric**, **Mark**, and **Steven**, your participation and thoughts contributed enormously to this work. I would also like to extend a word of gratitude to the Supervisory Board for their critical review and to the founders of the project who enabled it.

Max, we did some fun work together, like building multiplexed weighing scales to measure plant water use, and some less fun work, like annotating countless stomata and chloroplasts to feed the detection algorithm. Some nights, I can still see the shape of stomata when I close my eyes.

I would like to thank all the staff of the Laboratory of Biophysics, that extensively supported me during my research. Thank you **Arjen** for introducing me to the world of spectroscopy and for your patience in the case I ended up misaligning something by putting my finger where I should not have. **Cor** it was very fun doing together the Biophotonics practical, and thanks for all your help in ordering electronic components. **Brenda** thank you for your help with all the administrative-related matters, a good university depends as much on its technical capacity as on its administration. **Frank** having you as an opponent would be as stressful as it would result in great questions that would improve this thesis. **Ian**, it was a lot of fun to discuss DIY project together and see your skills in 3D printing. **Annelies** thanks for the great plays of Saboteur and other board games. Also thanks to the "old guards"; **Netty** for having supported me administratively at the beginning of my journey in the Netherlands. **Rob**, I am grateful that I had you as a mentor when introduced to the wonders of the streak-camera and introduced me to the concept "*Leef met vlag en wimpel, maar hou het simpel*".

I am grateful to have met a lot of nice and fun people during my time in Biophysics. **Ahmad** thanks for your support at the beginning of my journey. **Christo** thanks for teaching me alot about research and for finding the name "Fludometer". **Peter** your Veluweloop organization skills are unmatchable and thank you with **Mariska** for being

untirable spinning companions. **Jarne**, my lunch schedule is completely messed up since we are not in the same office. **Emilie**, it is a real pleasure working with you and I am looking forward to the next work. **Lavanyaa** hopes to prepare many more puri together. **Lennart** was super nice working with you and the streak. **Yuxi**, **Ben** and **David**, thanks for the good time spent at work or at the basket and football field. **Camilla**, thanks for answering politely when I asked "*Can you measure hydrogen with NMR?*". **Cleo** and **Dana** thanks for supporting my rants about Glotaring. **Johannes**, thank you for lending me a laser when I needed it and for the fun runs during the Veluweloop. **Sam** thanks for the fun time with **Martijn** playing klaverjassen, looking forward to more cycling in the Veluwe with **Cleo**. **Suyeon**, thanks for being my main provider of photosynthetic material with your desk plant and the fun times. **Abbas**, thanks for your perennial smile and the good moments spent together. **Francesco**, thanks for the good chats, and for letting me be the second favorite Italian. **Morwarid**, thanks to you I started driving faster than 90 km/h on the highway, **Mattia**, oltre ad avermi insegnato molto sui metodi classici, ti ringrazio anche per essere un caro amico..

I am grateful to the staff of Unifarm for their teamwork, which allows us to work as one. **Gerrit** and **Ferdinand** thanks for your support and the trust you gave me when implementing modified light fixtures. Thanks to **David**, **Jannik**, and **Dieke** for your advice on how to grow plants and for the general fun of working together.

WUR is full of technically skilled people who taught me a lot. **Maarten**, Chapter 5 owes a lot to the first prototype that you developed, it is a pleasure to work and chat with you about measuring systems. **Norbert**, your knowledge of sample preparation for microscopy improved a lot the work detailed in Chapter 4.

Marcel and **Ingi**, thank you for your continuous enthusiasm during the sports lessons, nothing is more important than a mens sana in corpore sano.

My journey in the Netherlands would not have started without a series of people who introduced me to research and supported my will to continue it.
Gerardo, grazie per essere stato non solo un eccellente supervisore, ma anche un caro amico. **Roberto**, ho imparato molto dal tuo sguardo critico sui numeri; grazie per avermi introdotto al mondo della ricerca. Prof. **Visco**, grazie per avermi guidato durante i miei primi passi incerti nello sviluppo di elettronica per la sensoristica. **Pino** e **Roberto**, grazie per avermi lasciato un ricordo fantastico di quegli anni a Chimica Nuova.
Adrian, **Fatima**, **Melissa**, **Joel**, **Jose**, **José Luís**, **Omar**, **Luisa** y **Shawn** ha sido un gran

placer trabajar en el Integrative Crop Ecophysiology Group de la UB. Con vosotros, descubrí cuánta satisfacción puede brindar el fatigoso trabajo de fenotipización en campo. Estoy agradecido a **Josep** de les Camps Experimentals por haberme dado la oportunidad de desarrollar mis primeros sistemas de iluminación para el crecimiento vegetal en un rincón del almacén.
Les amis d'enfance **Marc** et **Cécile**, les d'improbable soirée de pêche dans le Tibre, au voyage ensemble, merci d'être présent même lorsque les occasions de se voir sont parfois restreinte. **Andrea** e **Lele**, la vostra amicizia percorsa tra scampagnate per frasche e spiaggi invernali mi riempie il cuore. **Gabbo**, **Alban**, **Ilaria**, **Enrichetto**, **Dario**, **Adriano**, **Lorenzo**, **Gino**, **Sami**, **Catarina** e tutto il Settimo Cielo, i pranzetti domenicali, il salotto dirimpettàio e il vostro buon cuore mi hanno insegnato molto e sono grato che le nostre vie si siano incrociate.

And to the friends found here, the years since I first cycled on the Haarweg have flown by with you by my side. I'm not too fond of impersonal lists of names, but as my friend, I hope you'll forgive me as I'm writing these few lines in much less time than you deserve.
I never thought I would come to see that old grey building, the water/firehouse, as a warm and welcoming home. **Ahmed**, **Antonio**, **Berte**, **Canan**, **Dmitry**, **Elisa**, **Guy**, **Jiaqi**, **Khalid**, **Lisanne**, **Melania**, **Natassa**, **Nuran**, **Ömer**, **Ragavendra**, **Simen**, **Wali** and all the beautiful souls inhabiting the number 10/10A. Time passed so quickly between the endless repetitions of exercises on a debatably clean floor, the countless potlucks where I quickly discovered that most non-Italians could teach me how to cook dishes from my homeland, and the contortions we went through to squeeze through a too-small window to enjoy the first sunshine.
Amber, **Bea**, **Chandan**, **Charlotte**, **Corrie**, **Domi**, **Filip**, **Julian**, **Ketan**, **Klaudia**, **Martijn**, **Mites**, **Riccardo**, **Taylor** - I feel lucky that after these years in the Netherlands, I didn't just get a piece of paper, but also shared so many bike rides, runs, climbs, travels and wonderful experience with you.
Sanne and **Hugo** travelling across Europe with you on a bike is effortless.

Vincent and **Keshav**, thank you for agreeing to be my paranymphs during my thesis defense, and above all, for being such dear friends.

Elien, *la mia altra metà*, finding each other during this journey is a stroke of luck that's difficult to express in words.

I am grateful to my family for the care I received, and the endless discussions that questioned everything and helped me develop a critical spirit; with you, I know that I will always follow *la buona stella*.

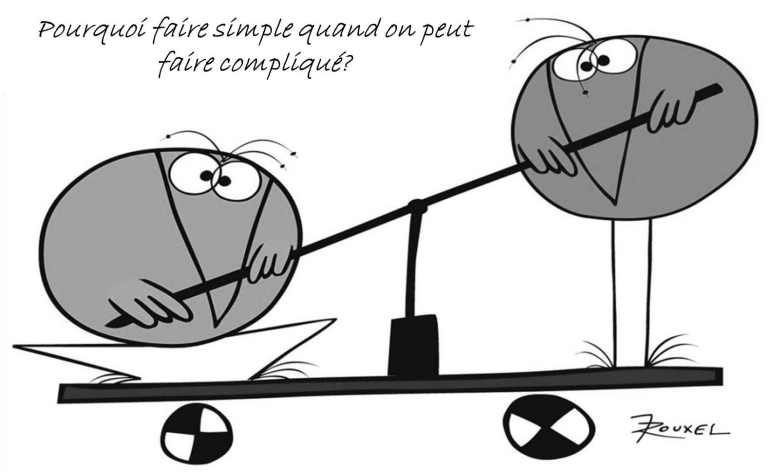

Colophon

The research presented in this thesis was performed at the Laboratory of Biophysics, Wageningen University & research, The Netherlands, and was financially supported by the "Stichting Photosynthesis 2.0" research fund.

Financial support from the Laboratory of Biophysics for printing this thesis is gratefully acknowledged.

Cover design by Elien Versteegen.

Printed by Ridderprint